5-2016

The Puzzling Bulge to Disk Nova Ratio in the Andromeda Galaxy (M31)

Amanpreet Kaur
Clemson University, akaur@g.clemson.edu

THE PUZZLING BULGE TO DISK NOVA RATIO IN THE ANDROMEDA GALAXY (M31)

A Dissertation
Presented to
the Graduate School of
Clemson University

In Partial Fulfillment
of the Requirements for the Degree
Doctor of Philosophy
Physics

---

by
Amanpreet Kaur
May 2016

Accepted by:
Dr. Dieter H. Hartmann, Committee Chair
Dr. Mark D. Leising
Dr. Sean D. Brittain
Dr. Joan P. Marler

Abstract

Novae in M31 are often associated with the bulge component of the light from this galaxy, i.e., more novae are assumed to be produced in the bulge of M31. But examining this from a population synthesis approach, one expects that evolved binaries in the disk should produce more novae. We strive to understand this bulge to disk nova ratio (R_{bd}) puzzle in M31 by exploring two scenarios. The nova rate normalized to the K-band luminosity for different galaxy Hubble types is approximately constant. We utilize this observed correlation to model the bulge and disk nova distribution. However, the decomposition of K light into bulge and disk does not yield a good match to the observed spatial distribution of novae in M31. Therefore, we conclude that the assumption that the nova rate follows total K light is too simple to explain the actual distribution of novae in this galaxy.

Second, we examine the role of dust in the disk of M31 in extinction novae, possibly more so in the disk, which would increase the relative number of observed bulge novae compared to those in the disk. We construct a three dimensional multi-component dust model (uniform background, 10 kpc ring, 2 logarithmic spirals) and apply it to novae in the bulge and the disk of M31. With model parameters calibrated from infrared emission models, this results in hiding only $\sim$ 1% of the novae in the disk and 0.3-0.4% in the bulge. We, therefore conclude that dust in M31 does not play a significant role in shrouding novae in the disk. In fact, the effect of the dust is not much higher for disk novae in comparison to bulge novae. Therefore, we conclude that the common assumption that "novae trace the

K-band light" is not supported by the detailed spatial models of novae in M31, and that extinction by dust is insufficient to resolve the puzzle of the relative scarcity of disk novae in M31.

Dedication

To my family, who let me explore the universe to follow my dreams ...

Acknowledgments

First of all, my deep gratitude goes to my advisor, Dr. Dieter H. Hartmann for giving me the freedom to work on my desired project, but at the same time providing his complete support and encouragement for the successful completion of this work. Many thanks goes to my committee members, Dr. Mark D. Leising, Dr. Sean D. Brittain and Dr. Joan P. Marler for their suggestions and comments, which immensely benefited this work. I would like to acknowledge the love and support of all my friends at Clemson, who made my stay here extremely fun and easy. I owe a lot of thankfulness to the staff at the Department of Physics and Astronomy, Clemson for their cheerful smiles and help they provided in every aspect. Last but not the least, I am greatly indebted to my family for their unconditional support at every aspect. This work would not have been possible without your encouragement.

Table of Contents

List of Tables

List of Figures

Chapter 1

Novae

1.1 Introduction

"Nova" is derived from the word $stella\ nova$, which translates into $new\ star$. The exact origin of this word is not very clear, but it was originated sometime around AD 75 (Bode and Evans, 2008). Novae can be divided into classical (CNe), recurrent (RNe), dwarf (DNe) and nova like variables (NL). DNe outbursts are believed to be the result of the gravitational energy release due to the sudden increased flow of mass to the primary. The detailed information of DNe and NLs is presented in Warner (2003). In the context of this work, we focus on CNe and RNe and hence the usage of the term "novae" would be used for these two subdivisions of novae.

The underlying mechanism for CNe and RNe is the thermonuclear runaway on the surface of a white dwarf (primary) accreting material from a main sequence or a red giant star (secondary), in a binary system (Starrfield et al., 1972). These two subclasses differ on the basis of their frequency of occurrence and the mass of the primary in the binary system. The white dwarfs in RNe are believed to be massive as compared to the ones in CNe (Webbink et al., 1987). Classical nova outbursts are expected to repeat over a time span

of 1000- 100,000 years, whereas the recurrent ones repeat over smaller time scales i.e. $\sim$ few months to 25 years. A complete review of classical and recurrent novae is presented in Bode (2010). The thermonuclear runaway leads to an ejection of accreted matter in the form of an expanding shell, releasing energy in the range 10^{44} - 10^{45} erg (Yaron et al., 2005). The peak magnitude at the optical maximum varies from $M_V \simeq$ -6 to -9 during this outburst, which corresponds to $\sim 1.5 \times 10^4$ $L_\odot$ in the optical- infrared regime as compared to $\sim$ 1 $L_\odot$ in quiescence. The typical mass of ejecta is $10^{-5} < m_{ej} < 10^{-4} M_\odot$ (Yaron et al., 2005). In a broad prospective, all novae follow a similar trend during the evolution. They show a pre-maximum halt before reaching the maximum optical brightness, which could take 1-2 days or several weeks. A schematic of the optical light curve evolution is presented in Fig. 1.1. During this evolution, as the ejecta expands, it exhibits different spectroscopic stages (McLaughlin, 1946; Bode and Evans, 2008).The details of light curve evolution and spectroscopic stages are discussed later in this chapter.

1.2 Historical Perspective

Pre-telescopic novae observations were recorded as early as 200 B.C. by Chinese, Japanese and Korean astronomers and the details of these observations till 14th century are listed in Table 1.1. in Bode and Evans (2008). All these observations were limited to our own galaxy. Until the 20^{th} century, the terms, novae and supernovae were interchanged, since the observational data were not abundant. The discovery of T Aur in 1892 marked the commencement of the regular monitoring of these objects via photographic techniques. The spectroscopic studies of this object hinted at the underlying close binary system responsible for the outburst (Snijders et al., 1984). During this time, there was a big debate between astronomers regarding the existence of extragalactic nebulae i.e. other galaxies, which made this distinction even more difficult. The discovery of S Andromedae (the first

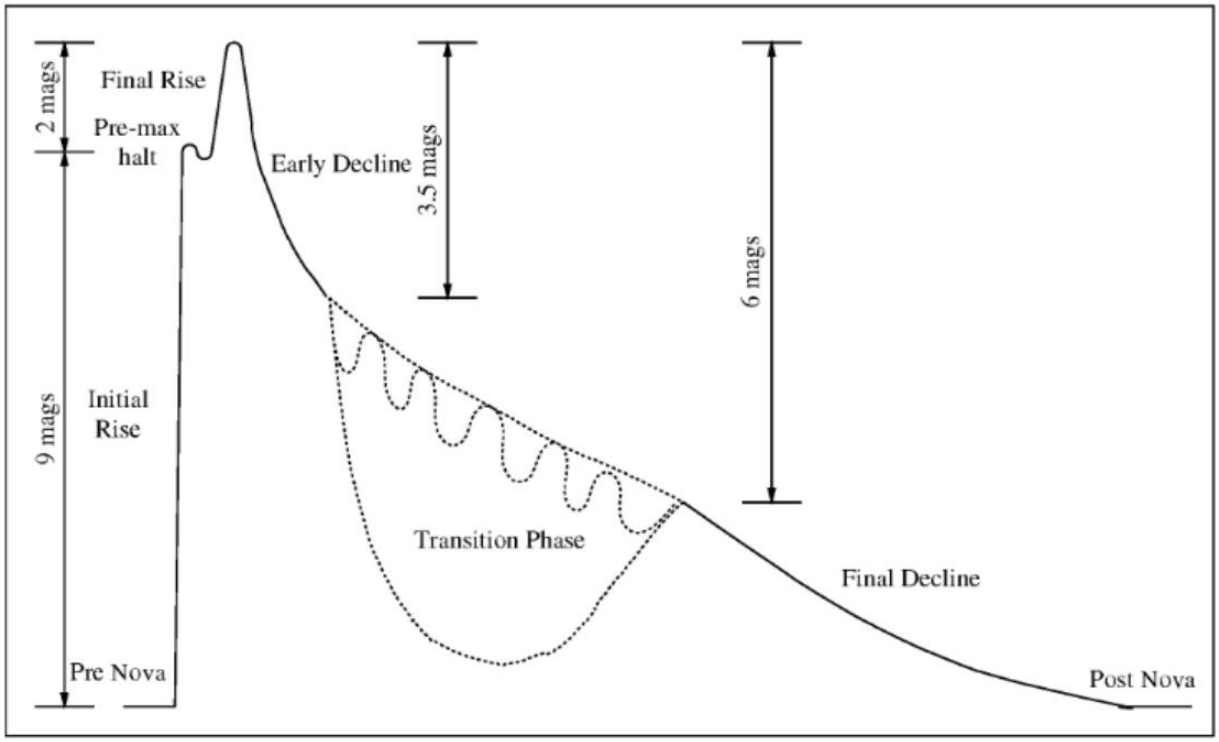

Figure 1.1 A schematic of nova optical light curve adapted from Bode and Evans (2008).

supernova in M31, wrongly classified as nova then), which rivaled the whole galaxy in its brightness changed the perspective of astronomers. Many other novae found in Andromeda were very faint as compared to S And and this lead to a division of "novae" into two magnitude classes, such that the supernovae were called the *upper class novae* (Lundmark, 1927), *exceptional novae* (Hubble, 1929) and finally *supernovae* by Baade and Zwicky (1934). Lundmark (1935) firmly established the difference between supernovae and novae. The author differentiated these two phenomenon on the basis of peak magnitude (-15 for super novae and -7 for novae) and their respective frequencies i.e. 1 per 50 years for supernovae and 50 per year for novae in Milky Way. A very early nova catalog can be found in Hagen (1921), but the classical work of Gaposchkin (1957) was a major breakthrough in this field. Since last two decades, nova monitoring has been taken over by

amateur astronomers, in particular for Milky Way and Andromeda. The most recent and updated nova observations are cataloged in General Catalog of Variable Stars (GCVS)[1]. In particular, nova specific finding catalogs with finding charts could be found in Duerbeck (1987), and Downes and Shara (1993); Downes et al. (2001).

1.3 Classification

Classical and Recurrent Novae can be classified on their photometric and spectroscopic evolution in the optical regime as described below.

1.3.1 Photometric

1.3.1.1 Speed Class

Although, the overall optical light curve evolution for all novae is similar, but the time span for the decline in the brightness from its peak to quiescence varies from a few months to years. This property of novae lead various astronomers to divide novae into different speed classes e.g. McLaughlin (1945) divided 100 galactic novae into "very fast", "fast", "average" and "slow" types. This classification was defined by the time these transients took to decline by 2 and 3 magnitudes i.e. t_2 and t_3, respectively. Gaposchkin (1957) followed a very similar schematic for the speed class, but the definitions of "fast" and "slow" were quite different from the previous author. The Table 1.1 displays the speed wise classification of novae.

[1] http://www.sai.msu.su/groups/cluster/gcvs/gcvs/

Table 1.1. Speed Class of Novae

Speed Class	t_2^* (days)	$t_3^\dagger$ (days)
McLaughlin (1945)		
Very Fast	< 7	10
Fast	8-24	30
Average	25-49	70
Slow	50-250	200
Gaposchkin (1957)		
Very Fast	< 10	< 20
Fast	11-25	21-49
Moderately Fast	26-80	50-140
Slow	81-150	141-264
Very Slow	151-250	265-440

*Time taken to decline by 2 magnitudes from the optical peak

†Time taken to decline by 3 magnitudes from the optical peak

1.3.1.2 Light Curve Class

The overall evolution of a nova outburst follows the trend shown in Fig. 1.1, but a more thorough classification utilizing the real novae light curves was presented by (Duerbeck, 1981) using 100 galactic novae. Loosely based on this scheme, more recently, Strope et al. (2010) characterized nova light curves based on their shape by categorizing the light curves into seven different classes: "S"- smooth light curve, "P" - plateaus, "D" - dust dips, "C" - cusp-shaped secondary maxima, "O" - quasi-sinusoidal oscillations, "F"- flat topped, "J" - jitters/flares as displayed in Fig. 1.2. The possible underlying mechanism for each type of light is explained below:

S : Typical nova light curve; radiative transfer mechanism in the expanding shell.

P : Extended supersoft source illuminating the accretion disk, uniquely from RNe.

D : Formation of dust particles in the expanding shell.

C : Secondary maxima with accelerating rise in brightness to a sudden drop.

O : Oscillations during the transition phase which could last from 5-25 cycles.

F : Interval of constant magnitude at the peak for 2-8 months.

J : Sudden isolated brightening at irregular intervals.

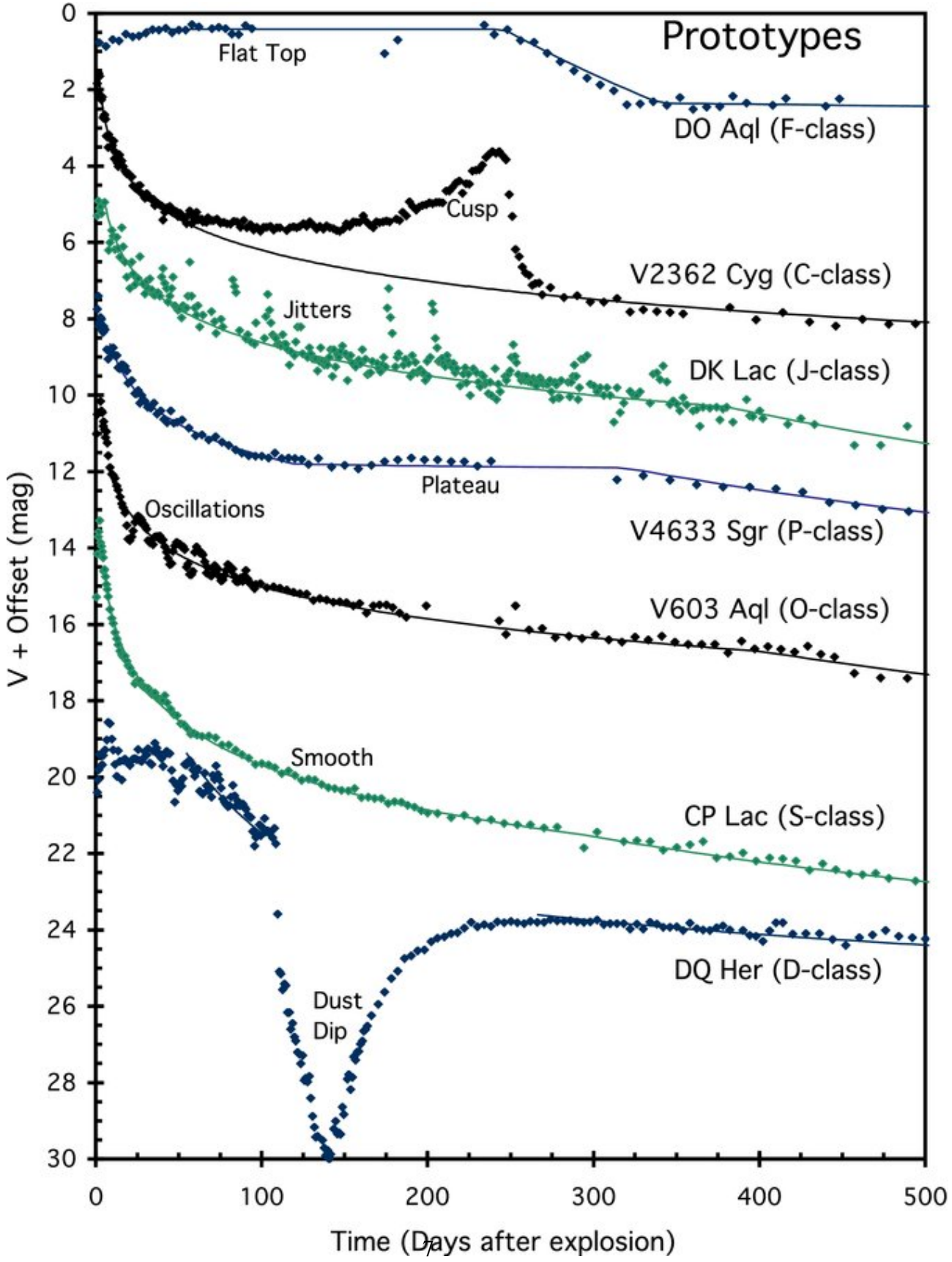

Figure 1.2 Morphology of example light curves from Strope et al. (2010)

1.3.2 Spectroscopic

After the nova outburst, the expanding shell exhibits different spectroscopic stages due to the evolution of photosphere, winds on the surface of the white dwarf and nucleosynthesis processes in the binary system. Various authors divided these objects into different spectral phases based on different properties. Some of these schemes are briedfly discussed below:

McLaughlin (1960)'s classification :

This author made the first attempt to broadly classify novae into different spectral stages, which are described below.

Pre-maximum spectrum : This phase represents the expanding optically thick shell of a nova outburst. It is characterized by strong continuum and blue-shifted absorption lines.

Principal spectrum : This type of spectrum is visible during the optical (visual) maximum. Strong absorption lines broader than the pre-maximum stage are seen during this phase. Emission lines of Fe II or He/N other than Balmer lines are seen as the strongest ones in this stage. Moreover, emission lines of [O I] suggest presence of neutral zone.

Diffuse enhanced spectrum : The absorption lines overlapping the broad emission component displays P-Cygni profile in this phase. The absorption lines broaden even more than the previous state, exhibiting velocities almost twice as much as in the principal spectrum.

Orion Spectrum : The previous spectral state comprises of the principal spectrum overlapped with diffused enhanced spectrum. Orion stage adds another absorption system with additional diffused absorption lines. During this phase, a nova enters the transition phase

and NIII (4640 Å) absorption line appears. The ionization levels increase and the emergence of higher ionization emission lines start to appear as the strength of the absorption component declines.

Nebular Spectrum : This is the final stage of the nova outburst before it reaches quiescence. The nova ejecta is optically thin at this stage, which leads the "photosphere" of the ejecta to move inwards, thereby increasing the ionization levels in the ejecta. Forbidden and higher ionization emission lines are seen in this phase of the nova evolution.

Williams et al. (1991)'s classification :

This author introduced a spectral classification which was defined based on the characteristics of the stronger emission lines. This classification scheme is referred to as the Tololo Classification System. The classification criteria is presented below:

Phase C (coronal) : If the line strength of [Fe X] (6374 Å) is stronger than [Fe VII] (6087 Å), the spectrum is classified as coronal.

Phase P (permitted) : If a spectrum does not exhibit coronal C phase, it is categorized as permitted. This is further divided into two categories i.e P_{fe} and P_n, provided the non-Balmer strong emission lines are Fe II or nitrogen, respectively.

Phase A (auroral) : If any auroral forbidden line exhibits higher flux than the strongest Balmer lines, the spectrum is designated as auroral in Phase A.

Phase N (nebular) : If the nova spectrum does not exhibit C or A phase, it is called nebular in nature. The strongest non-Balmer lines in this stage are forbidden.

^{o} If the neutral O I (8446 Å) is stronger than the Hβ, the spectrum is designated with a superscript 'o', which could be combined with any of the above mentioned phases.

Shore (2012)'s classification :

Shore (2012) presented a more detailed multi- wavelength perspective of the spectroscopic evolution and redefined the phases utilizing the most recent understanding of novae phenomenon. Briefly explained below are the different stages exhibited by novae and the possible physical explanation for these stages.

The Fireball Phase: The expanding envelope is almost opaque at this stage and very rarely observed. The expansion velocity is extremely high so that the loss of energy via radiation is minimal, i.e., adiabatic expansion. The temperature of this expanding shell decreases since the expansion time scale is shorter than the radiation diffusion time. This decreasing temperature (T$\approx$ 1-2 $\times$ 10^4 K) leads to the recombination process in the expanding envelope.

The Iron Curtain: This stage is seen as a result of the recombination process (line absorption by low ionization species e.g. Fe II and continuum absorption by CNO), which leads to the increase in the opacity in the UV regime. The flux is thus redistributed to the less opaque high wavelength regime i.e. optical and Fe II emission lines appear in the spectrum. The suppression of the UV flux due to the accelerated recombination process producing Fe II emission lines in the optical spectrum is called the Iron Curtain phase.

The Lifting of the Iron Curtain: The further expansion of the envelope exposes its inner regions i.e. moving the pseudo-photosphere inwards, which decreases the UV opacity. Consequently, the recombination rate decreases and this lifts the Iron Curtain. Since

the radiation temperature increases in this stage (receding photosphere), the increase in ionization shifts the flux peak from the optical to the UV regime.

The Transition Stage: The transition stage marks the appearance of the nebular lines (forbidden) e.g. OIII, NII etc. At this stage, the pseudo-photosphere recedes to almost the surface of the underlying white dwarf. The extremely low densities in the expanding envelope allows the forbidden transitions (no collisional de-excitation), thereby producing emission from the OIII, NII etc in the optical regime.

The Nebular and Coronal Spectra: This is the last stage of a nova spectrum before it returns to its quiescent stage. The highly ionized nebular and coronal lines (Ne VII, FeVII-FeXIV) appear since the photosphere in this stage corresponds to the surface of the white dwarf and everything is ionized at this point.

1.3.3 Emission Lines Based Spectral Classification :

The presence of Fe II and He/N spectral features, detected shortly after the outburst, distinguishes between two spectral types (Williams, 1992). Some novae have been seen transitioning from one spectral type to another e.g. T Pyx (Williams, 2012), these are classified as "hybrid" novae. The observations of novae revealed that the temporal evolution of the He/N class novae is very rapid as compared to the Fe II class and the former class is brighter near optical peak than the latter. The properties of these two spectral classes of novae are tabulated in Table 1.2.

Association of Fe II and He/N with Disks and Bulges :

In the Milky Way, Fe II novae have a broader latitude distribution ($\sim$ 1 kpc), whereas He/N novae are more concentrated towards the thin disk plane Della Valle and

Table 1.2. Fe II vs He/N type

Parameter	Fe II type	He/N type
Velocity (km/s)	< 2500	$\sim$ 3000 - 10,000
P-Cygni	yes	no
Evolution	slow	fast
Brightness	faint	bright
White Dwarf	CO	ONeMg
Nebular Stage	[Ne III] present	Coronal lines not necessarily present
Spatial position	near center	extended to the disk

Livio (1998). Extragalactic studies e. g. in Andromeda galaxy, Fe II novae appear more concentrated towards the inner region ("bulge") of the galaxy, whereas the He/N novae are slightly extended farther in the Galactic plane ("disk"), although the radial dependence of spectral class can neither be accepted nor ruled out, as suggested by Shafter et al. (2011). This could be understood as a consequence of smaller sample size, especially He/N class, which comprises only 12% of the total 89 spectroscopically identified novae in M31. Later, studies of novae in M33 by Williams and Shafter (2004), which is a bulge-less galaxy revealed more He/N novae than Fe II type, which is against the norm i.e. Fe II type novae are usually more abundant (85% in M31). The scarcity of Fe II type novae in M33, which are normally associated with the bulge population could be explained by the missing bulge in this galaxy. Overall, if trusted, the implication of this bimodal split suggests the association of two spectral types with two distinct populations of the host galaxy, which was suggested by various authors e.g. Duerbeck (1990). It was proposed that the Fe II novae, which are fainter and slower, are consistent with an older stellar population (in bulge) as compared to brighter and faster He/N novae. Therefore, it is crucial to understand the properties of novae in disks and bulges of galaxies to uncover the question of distinct populations. In order to solve this puzzle, we need to first understand the intrinsic bulge to disk nova ratio

of that galaxy. In the Milky Way, the high extinction in the mid- plane hinders our ability to find novae in the disk, thereby making it almost impossible to measure the bulge vs disk nova rates. We, therefore move to our nearest neighbor to explore this puzzle of bulge vs disk novae. The detailed introduction to this bulge/disk nova rate problem is provided in the next chapter.

Chapter 2

The Puzzle of the Bulge to Disk Nova Ratio in M31

2.1 Novae in Andromeda

2.1.1 Why Andromeda ?

Since our work involves study of novae as a population instead of a single source, it requires a statistically significant sample size based on an unbiased survey, which is very hard to achieve in the Milky Way, as the extinction in the galactic plane hinders one's ability to collect sufficient data. Therefore the Milky Way is not an appropriate candidate to conduct our research. M31, being the nearest galaxy with a substantially high global nova rate ~ 50 yr^{-1} (Shafter and Irby, 2001) emerges as the best candidate for this work.

2.1.2 Observational History

The very first nova observations in M31 were reported in Hubble (1929). The author reported a total of 85 novae and estimated a nova rate ~ 30 yr^{-1}. The author also pointed that these transients were frequently observed near the nuclear region and that the luminosities of these sources were independent of their position in the galaxy. Three decades later, Arp (1956) published work regarding novae in Andromeda, which was conducted through two years of observations discovering 30 new novae. A nova rate = ~ 26 yr^{-1} was derived from these observations by taking into account the survey bias. Moreover, the author found the correlations between their duration, rate of decline and maximum magnitudes, i.e., *novae with brighter peak magnitude decline faster* and vice-versa. These relations were earlier implied by Zwicky (1936) and McLaughlin (1945) in their respective analysis of known novae. Rosino (1964) extended this work by finding 46 novae over a period of 8 years of observations with Asiago observatory [1]. The author agreed with the earlier claim of correlations between different parameters of novae as well as the nova rate determined by Arp (1956) and Hubble (1929). In a continued effort to increase the sample size of novae from M31, Rosino (1973) published 44 new novae discovered over a span of 7 years, which contained the very first two recurrent novae in this galaxy. Capaccioli et al. (1989) combined the complete sample of novae in M31 and derived a nova rate ~ 29 yr^{-1}, which was in agreement with the previous observations. Most of these observations were confined to the inner regions of this galaxy, whereas Sharov and Alksnis (1991) conducted survey of M31 with wide field telescopes at Crimean Station of the Sternberg Astronomical Institute and at the Radioastrophysical Observatory in Baldone near Riga, Latvia and discovered novae up to 20 kpc away from the nucleus. This observational work added 21 new novae to the sample. The most recent H-alpha survey conducted by Shafter and Irby (2001) added

[1] http://archive.oapd.inaf.it/asiago/

$\sim$ 90 more novae to the growing sample in M31 and they suggested a global nova rate $\sim$ 50 yr^{-1}. In the recent years, most of the novae in M31 are discovered by many amateur astronomers and the sample size of these transients in this big spiral is $>$ 1000 at present. The most complete catalog of all the optical observations of these objects can be found at the following link: `http://www.mpe.mpg.de/~m31novae/opt/m31/index.php`.

2.2 Bulge vs Disk Nova Rate

Ciardullo et al. (1987) conducted the H-alpha survey of M31 discovering 44 novae and reanalyzed the already discovered novae from Arp (1956) and Rosino (1964, 1973). They deduced that the novae in M31 follow B light in the inner regions (bulge) and the nova rate falls off faster than the B light towards the outer disk regions. In order to determine the separate nova rates attributed to the disk and the bulge of the galaxy, the authors utilized a maximum likelihood technique to deduce the bulge to disk nova rate. They compared the observed spatial distribution of novae to a variety of modeled distributions by matching the observed bulge to disk luminosity ratio. This technique allowed these authors to determine $R_{db} = \frac{\rho_{disk}}{\rho_{bulge}} \leqslant 0.1$ (by number) . Two years later, Capaccioli et al. (1989) combined the total observations of novae in M31, finding that 85% of the novae belonged to the bulge population and also derived an upper limit on the disk to bulge nova rate, $R_{db} < 0.15$. One of the most recent bulge to disk nova rate in M31 was suggested by a more complete sample of novae using H-alpha observations by Shafter and Irby (2001) following the same maximum likelihood technique as Ciardullo et al. (1987). These authors derived the $R_{db} \sim$ 0.41. The most recent observations of M31 by Darnley et al. (2006) using the POINT-AGAPE microlensing survey[2] observed a higher nova rate $\sim$ 65 yr^{-1} in comparison to all the previous measurements and also derived a bulge and disk nova rate $\sim$ 38 yr^{-1} and $\sim$

[2]http://www.ing.iac.es/PR/SH/SH2006/agape.html

27 yr^{-1}, respectively.

2.3 The Controversy of the Bulge to Disk Nova Ratio

Although, as stated above, the novae had been associated with the bulge population by many authors as mentioned above, yet the extragalactic studies of galaxies by della Valle et al. (1994), which conducted a survey of different hubble type of galaxies, concluded that the late hubble type galaxies are more nova prolific producers, implying younger populations, i.e., disks should be producing more novae than the bulges. In addition, confirming the observational results of these authors, Hatano et al. (1997) modeled the nova distribution suggesting that most of the novae seen as bulge novae in projection of M31 are actually disk novae, i.e., disk produces more novae. These studies were later supported by the theoretical modeling of evolution of the underlying binary system for novae by Yungelson et al. (1997). This study suggested that the younger stellar populations (mainly disk) should produce more novae than the older populations. Recent observations of many hubble type galaxies by Shafter et al. (2000) did not find any strong correlation between the hubble type and the nova rate of a galaxy. This discrepancy between the observations and theoretical results has not been resolved yet. Moreover, the regular association of spectral class of novae with the bulge (Fe II type) or disk (He/N type) population has also been called into a question. Recent observations of novae in the Milky Way revealed 5 sources which underwent a spectral transformation from He/N to Fe II type calling the "bimodal population" into question (Williams, 2012). One such case has also been reported in Andromeda by Shafter et al. (2011). Therefore, the underlying nature of nova distribution is not very clear yet. In order to understand the true novae spatial distribution, we probe the intrinsic bulge to disk nova rate in M31 by investigating two hypotheses which could possibly explain the observed distribution of novae.

2.4 Addressing the Issue

We address the above mentioned issue by exploring two scenarios. First, we model the nova distribution imitating the K light in the bulge and the disk of Andromeda. This model is based on the known constant luminosity specific nova rate per unit K luminosity for galaxies, which is introduced in the next chapter. Second, we explore the effects of dust on the observed nova distribution in the disk of M31 by constructing a multi-component model, which could be the reason for hiding novae from the disk and thereby causing the discrepancy in the predicted and the observed disk nova rate.

In addition, there are several factors which are very critical to completely understand the open question of bulge vs disk nova rate e.g. the observational bias due to the large size of Andromeda on the sky, and the revision of the population synthesis models regarding the underlying binary populations.

Chapter 3

Do Novae Follow K Light in M31 ?

As already discussed in the previous chapter that most studies of novae in M31 (e.g. Ciardullo et al. (1987); Capaccioli et al. (1989); Shafter and Irby (2001)), have suggested their association with the bulge light based on the observed distribution, but Hatano et al. (1997) modeled the nova distribution suggesting that most of the novae seen as bulge novae in projection of M31 are actually disk novae, i.e., the disk produces more novae. The theoretical modeling of the underlying binaries by Yungelson et al. (1997) suggested that the younger populations should have a higher nova production rate. This issue of nova population from disk vs. bulge is a mystery, which is still not completely solved. In this chapter, we investigate this bulge-disk nova problem by probing the "Novae follow light"scenario. In order to understand whether novae follow light in M31, we employ the information from the Luminosity Specific Nova Rate per unit K band luminosity, which is seen as a constant irrespective of the Hubble types as discussed in various studies e.g. Ciardullo et al. (1990), Shafter et al. (2000) and Shafter et al. (2014). The nova rate as a function of K band luminosity is illustrated in Fig. 3.1 and Fig. 3.2

We utilize this information to model a nova distribution based on the K light in M31.

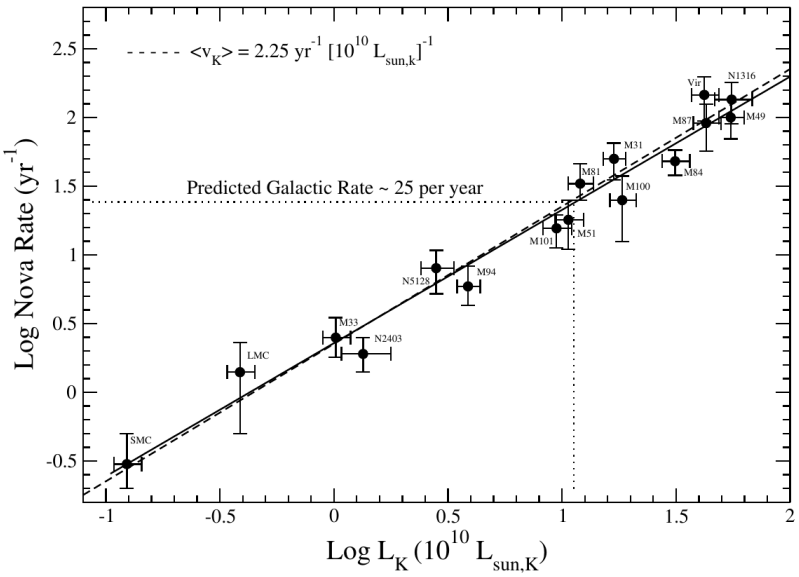

Figure 3.1 Nova rate correlation with the K luminosity in different Hubble types (Shafter et al., 2014)

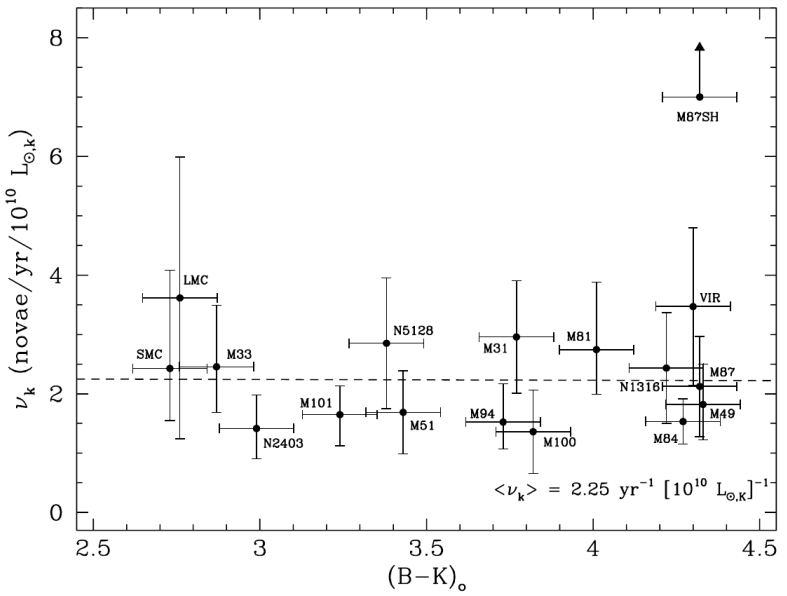

Figure 3.2 Luminosity Specific Nova Rate per unit K luminosity (LSNR) vs the (B-K) color index. Source: Shafter et al. (2014).

3.1 Spatial Distribution Model for Bulge and Disk Novae in M31

The foremost assumption for our model is drawn from the fact that since the progenitors of novae are drawn from an older population of evolved stars and such stars are part of both bulge and the disk, therefore if novae trace light in M31, it would be a combination of both the bulge and the disk light. We construct a 3-dimensional model for novae in M31 based on the disk and bulge K light distribution, assuming a mass to light ratio, $\Upsilon = 1$ (in solar units). The decomposition of this relative contribution to the nova rate for these two components, to first order, follows from its bulge to disk ratio (luminosity), which was determined to be 0.41, (Courteau et al., 2011). The 3D model was inclined by an inclination angle, i=77°. Here we sample the axi-symmetric double exponential disk component (luminosity) given by:

$$\rho(r, z) \propto e^{-r/R_r} e^{-z/R_z} \tag{3.1}$$

For the bulge distribution, we assume a spherically symmetric density profile following a spatial density profile (luminosity) given by Terzić and Graham (2005) and Widrow (2008) as follows:

$$\rho_b(r) \propto \left(\frac{r}{R_e}\right)^{-p} e^{-b(r/R_e)^{1/n}} \tag{3.2}$$

The projection (on the sky) of these distributions yield an exponential profile and a Sersic profile (Sérsic, 1963),

$$I = I_e\Big[e^{-b_n}\Big(\frac{R}{R_e}\Big)^{\frac{1}{n}} - 1\Big] \tag{3.3}$$

where $b = 1.992n - 0.3271$ (Capaccioli et al., 1989). for the surface brightness profile for the disk and the bulge, respectively. The parameters, R_r, R_z, b and n are obtained

from the most recent photometric survey of M31 (Courteau et al., 2011). The parameter , p is analytically determined as function of the Sersic Index, n as described in Terzić and Graham (2005):

$$p = 1.0 - \frac{0.6097}{n} - \frac{0.05563}{n^2} \tag{3.4}$$

We generate our nova sample from Monte Carlo realizations of these density profiles, which yields 29 % percent of the events from the bulge and the remainder (71%) attributed to the disk. All the parameters employed in this model are listed in the Table 3.1.

Parameter	Value
Bulge Radius, r_b	5 kpc
Disk Radius, r_d	15 kpc
Disk Scale Length, R_r	4.71 kpc
Disk Scale Height, R_z	0.1 kpc
Bulge effective Radius, R_e	1.0 kpc
Sersic Index, n	2.2
Bulge to Disk Ratio, BDR	0.41

Table 3.1 K band light parameters for M31 adopted from Courteau et al. (2011) for our nova spatial distribution model.

3.2 Comparison with Shafter's Sample

The resulting projected distribution for novae in the bulge and the disk from our model is presented in Fig. 3.3 (*top*). In general, bulge novae are associated with the slow FeII type novae and the He/N fast type are seen extended more in the disk. We utilize the

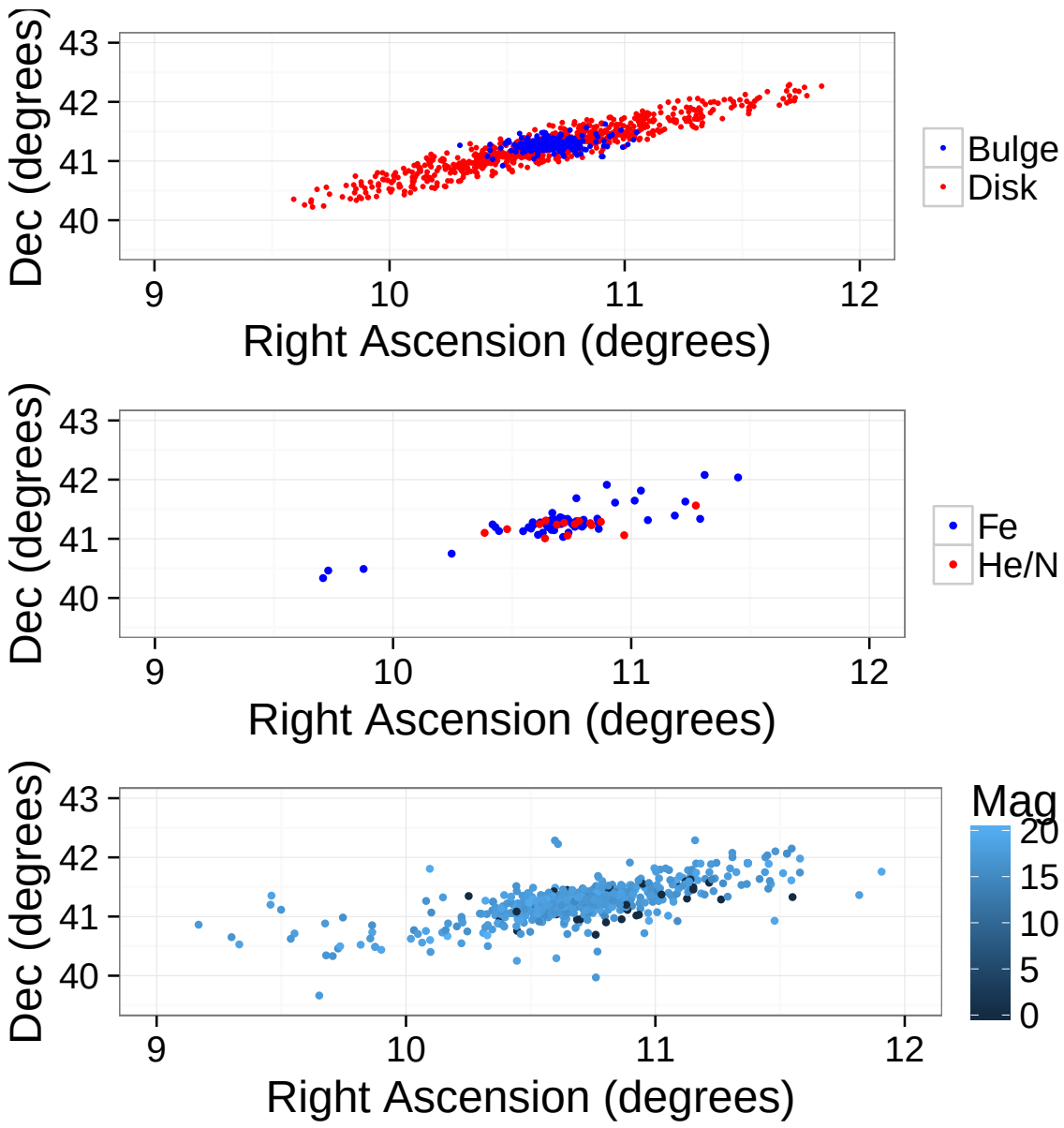

Figure 3.3 This figure shows the projected model distribution of novae following the K light in M31 (*top*). The *middle* figure shows the observed 89 novae in M31 with known spectral information as illustrated in the figure These data were obtained from Shafter et al. (2011). The *bottom* panel shows the total observed novae seen till date in M31. This sample has been obtained from `http://www.mpe.mpg.de/~m31novae/opt/m31/index.php`. The color scheme displays the magnitude at which each nova was observed. The "0" value for magnitude implies missing information.

spectroscopic information of 89 novae as presented in Shafter et al. (2011) (see Fig. 3.3 $(middle)$) to compare our model distribution of bulge and disk novae. It is clearly seen from the figure that our model and Shafter's sample are not a good match, especially in the outer disk region. A 2D K$-$S test applied on this observed vs the modeled distribution yields a very small probability $\sim 0.02\%$ for these two distributions to be similar, i.e., indicating almost no match as shown in Fig. 3.4. Moreover, the correlation of spectroscopic classification with bulge and disk populations is not very clear from the observed sample (see Fig. 3.3 $(middle)$). Although, He/N seem to be more extended as compared to the Fe II type, the latter type are not confined to only the bulge region of galaxy. In addition, the number of He/N type novae are even smaller (11) in number as compared to (78) Fe II novae, which would prohibit us to draw any robust conclusions regarding either the overall distribution of novae or association of different spectroscopic types with the bulge/disk regions. Overall, comparing our light nova model with a very small sample size could play a significant role in the observed statistical outcome of the model-data comparison. If we intend to compare the overall distribution of novae irrespective of their spectroscopic type, we should be able to utilize a larger nova sample from all the observations conducted for M31. We conduct this experiment by collecting a more complete nova sample of M31, which is described in the following section.

3.3 Comparison with the Complete Nova Sample

The complete sample size of novae discovered in M31 is available at the following website:
`http://www.mpe.mpg.de/~m31novae/opt/m31/index.php`. The latest nova sample size is 1002 and the projected distribution of all these novae can be seen in Fig. 3.3. We compare our model with this sample and perform the K-S test to check whether the

observed and the model novae are drawn from the same distribution. The results of our 2-sample KS test are shown in Fig. 3.5 and clearly these two distributions do not match, yielding a probability of near 0%, thereby proving that the observed sample of novae do not follow K light. In particular, the decomposition of K light into bulge and disk does not explain the observed spatial distribution of novae in M31, although the overall nova rate is proportional to the total integrated luminosity of M31 in K band.

3.4 Summary

Since the "Novae trace light" approach in our model does not fit well with either the observed distribution of the complete M31 nova sample or a subset of novae with known spectroscopic information, we conclude that the "novae trace light" approach should be reconsidered. Moreover, it seems that although the total nova rate is a function of overall integrated K band luminosity, the decomposition into bulge and disk light does not explain the overall distribution of novae in Andromeda. Indeed, the nova population in the bulge and the disk of Andromeda could be different, which could be a result of the independent evolution of bulge and disk in the galaxy. Therefore, understanding novae as a population in any galaxy is quite a complicated problem, which can not be explained by a simple light based model. It is quite evident that many factors are involved in fully understanding the nova population in M31 e.g. role of dust, star formation histories of bulge and disk, metallicities, observational bias etc.

In the next chapter, we probe the role of dust in extincting the novae in the disk. In an attempt to explore this role, we construct a 3-dimensional dust model for M31 and investigate whether dust plays a crucial part by hiding the novae in the disk leading to the observed more concentrated nova population. We will also investigate if the nova distribution follows K light in reality, but the dust extinction in the disk causes the biased observed distribution,

thereby causing the discrepancy between our light model and the observations.

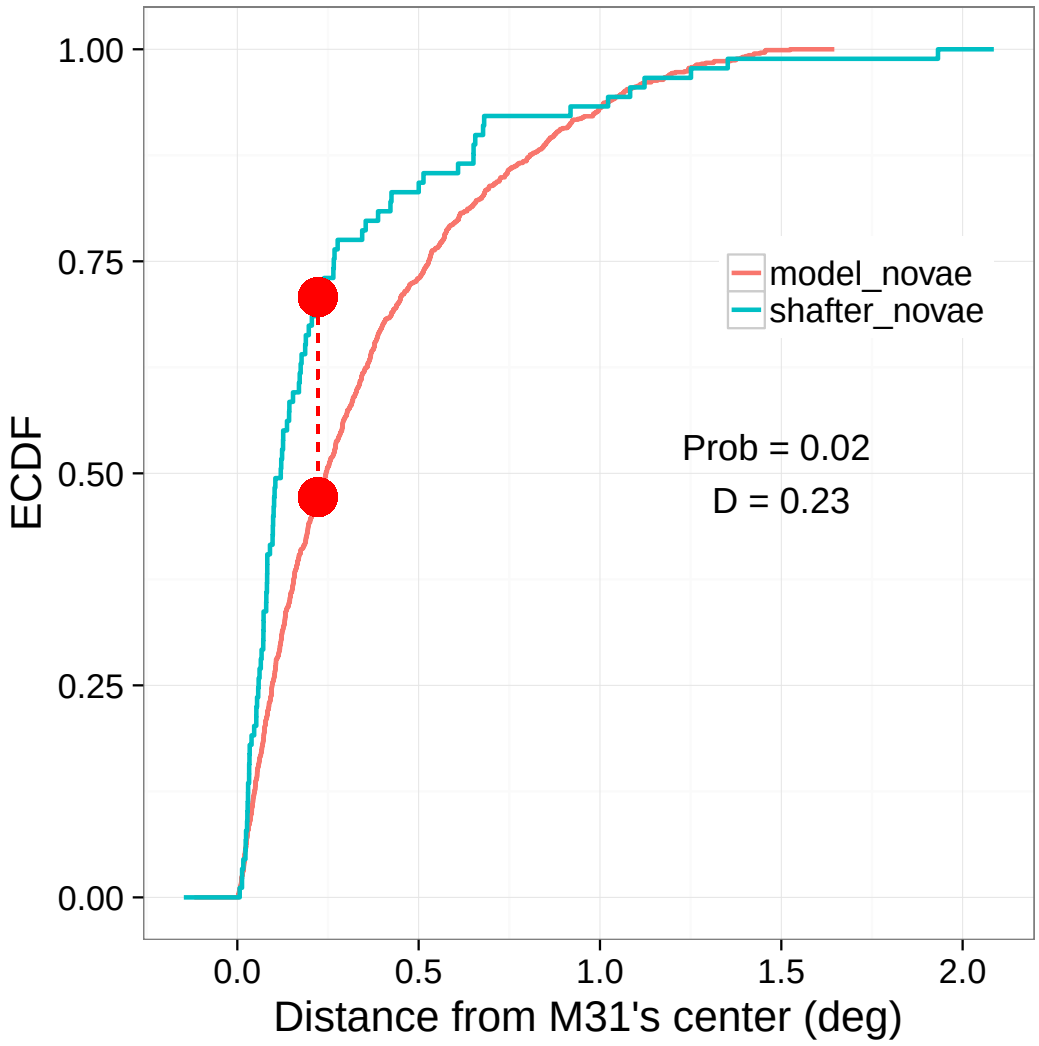

Figure 3.4 The Empirical Cumulative Distribution Function (ECDF) plotted for the K light based nova distribution model (*red*) overplotted with the ECDF for the spectroscopic sample obtained from Shafter et al. (2011) (*blue*). The *dashed* vertical line represents the maximum distance between these two distributions, denoted by D = 0.23. The K-S test yielded a probability of 0.02% that these two data are drawn from same distributions. This figure clearly shows no match between our work and the observed sample of novae in M31.

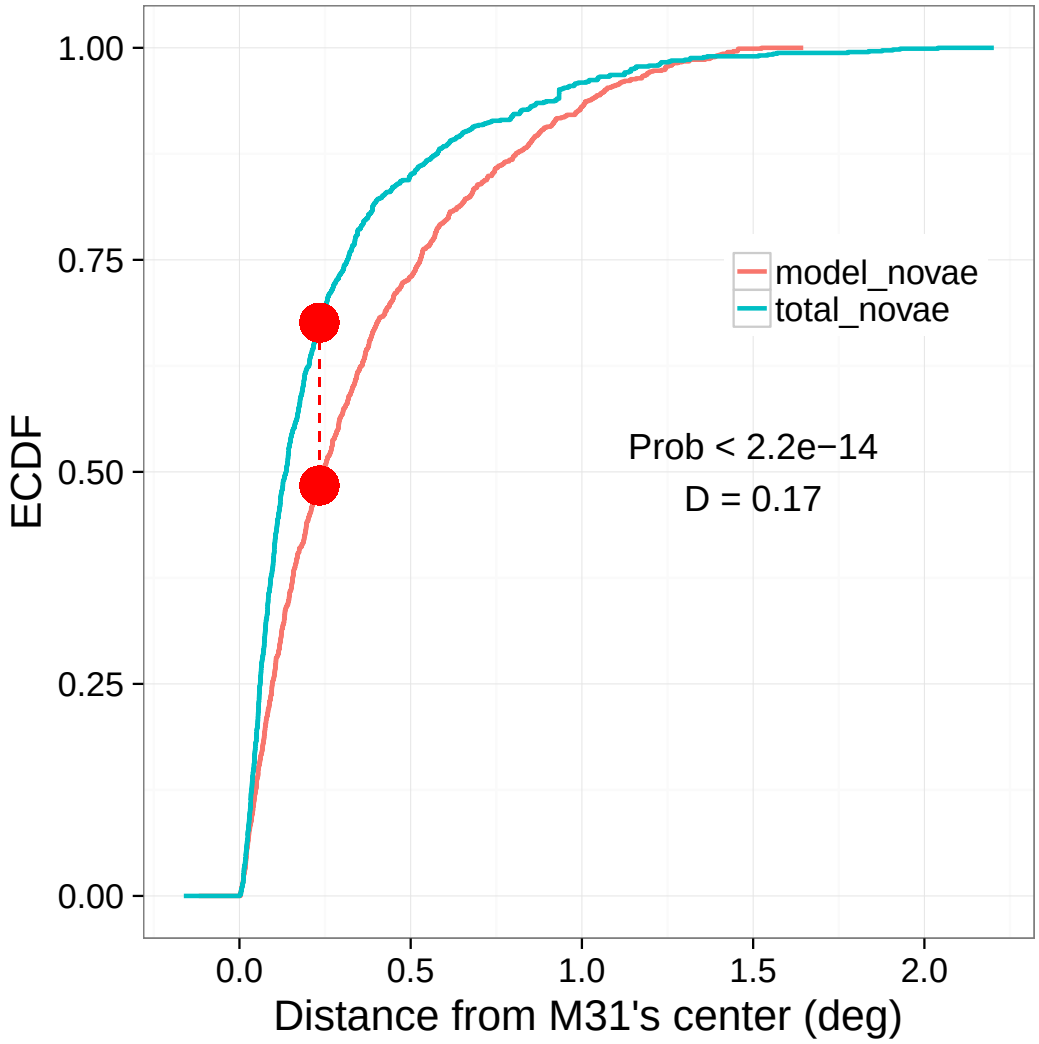

Figure 3.5 The Empirical Cumulative Distribution Function (ECDF) plotted for our K light based nova distribution model (red) overplotted with the ECDF for all the novae observed in M31 till date ($blue$). The $dashed$ vertical line represents the maximum distance between these two distributions, denoted by D = 0.17. The K-S test yielded a probability of $\sim$0.0% that these two data are drawn from same distributions.

Chapter 4

Modeling Dust in M31

4.1 History of Observations of Dust in M31

Andromeda, being the nearest spiral galaxy to our home, Milky Way has been extensively studied to explore the dust properties in order to compare these two galaxies. One of the very first detailed dust explorations in Andromeda was conducted by Xu and Helou (1996). These authors employed IRAS (Infrared Astronomical Satellite) in conjunction with the optical, UBV and HI maps to study the diffuse emission in M31. They utilized the radiative transfer method to calculate the mean optical depth (τ_ν) from center to 14 kpc of the galaxy. Their calculations suggested τ_ν = 0.7 at $\sim$ 2 kpc increasing to peak value $\sim$ 1.6 at 10 kpc. They inferred the dust mass, $M_d \approx 2.2 \times 10^7 M_\odot$. Two years later, Haas et al. (1998) utilized emission maps from ISO (Infrared Space Observatory) to study the cold dust in Andromeda. They concluded the dust mass to be $M_d \approx 3.5 \times 10^7$ $M_\odot$. With the advent of modern day infrared astronomy, telescopes like Spitzer and Herschel were exploited by various authors (e.g. Gordon et al. (2006), Fritz et al. (2012), Smith et al. (2012)) to infer the behavior of dust in M31. Draine et al. (2014) used the data from both these telescopes along with the dust model (Draine and Li, 2007) and studied the dust

properties in a very detailed manner and suggested $M_d \approx 5.4 \times 10^7$ $M_\odot$ within the 25 kpc in radius of the galaxy. These authors also concluded that the maximum optical depth (as seen in the V band) within M31 from us ~ 8. Dalcanton et al. (2015) used Hubble Space Telescope to construct a color magnitude diagram for the red giants and finding their optical depth results to be 2.5 times smaller than the values provided in Draine et al. (2014). We apply this wealth of dust information collected from these various studies to construct a multi-component dust model for the Andromeda galaxy. The main objective of this model is to understand the effects of dust on the observed spatial nova distribution and infer the intrinsic bulge to disk nova ratio.

This chapter first introduces the dust size distribution and properties adopted for our extinction work. This is followed by describing the concept of optical depth to measure extinction. The components of our dust model and their underlying assumptions are explained in the following section.

4.2 Adopted Dust Properties

We assume that the dust particles are spherical in nature and the composition is silicates only such that the density of silicate dust particle, ρ = 3.1 g/cm^3. The underlying grain size distribution is assumed to be Mathis-Rumpl-Nordsieck (MRN), which for the dust number density, n and grain size, a, is described as follows:

$$dn = Ca^{-\alpha}da$$

where C can be calculated, such that

$$C \int_{a_{min}}^{a_{max}} a^{-\alpha} da = 1$$

This yields

$$C = \frac{\alpha - 1}{a_{min}^{1-\alpha} - a_{max}^{1-\alpha}}$$

For the MRN distribution: $a_{min} = 0.005\mu m$, $a_{max} = .25\mu m$ and $\alpha = 3.5$.

Therefore, **Average size** of a dust particle can be calculated as follows :

$$< a >= \int_{a_{min}}^{a_{max}} C a^{-3.5} a da$$

yielding

$$< a >= \frac{5}{3} \times \frac{a_{min}^{-1.5} - a_{max}^{-1.5}}{a_{min}^{-2.5} - a_{max}^{-2.5}}$$

or

$$\boxed{< a >= 0.008\mu m} \tag{4.1}$$

Average mass of a dust particle can be calculated as follows :

$$< m >= \frac{20\pi\rho}{3} \times \frac{a_{max}^{0.5} - a_{min}^{0.5}}{a_{min}^{-2.5} - a_{max}^{-2.5}}$$

$$\boxed{m_d =< m >= 4.927 \times 10^{-17} g} \tag{4.2}$$

where ρ = 3.1 g/cm^2

In general,

$$< a^t >= \int_{a_{min}}^{a_{max}} C a^{-\alpha} a^t da$$

This integral can be calculated as :

$$\boxed{< a^t >= \frac{C}{t-\alpha+1}[a_{max}^{t-\alpha+1} - a_{min}^{t-\alpha+1}]} \tag{4.3}$$

These calculated properties are incorporated in our extinction model.

4.3 Extinction Calculation Method

The optical depth, τ_λ is a quantity which measures the amount of absorption that radiation experiences while passing through an absorbing medium, i.e., dust in the context of this work. In terms of the dust's cross-section (absorption + scattering), $\sigma(a, \lambda)$, distance along our line of sight, s and number density of dust particles, $n(s)$, the optical depth is defined as follows :

$$\tau_\lambda = \int n(s)\sigma(a, \lambda)ds$$

Assuming that the dust follows a certain distribution, ϕ(s) within a medium, we can rewrite the number density as :

$$n(s) = n_{d,0}\phi(s)$$

where $n_{d,0}$ is the number density normalization factor which depends on the distribution of dust in the absorbing medium. Therefore,

$$\boxed{\tau_\lambda = n_{d,0} \int \phi(s)\sigma(a, \lambda)ds} \tag{4.4}$$

Calculation of $n_{d,0}$:

For the total dust mass, M_d in a medium with volume, V, each dust particle of mass, m_d, the following equation can be employed to calculate $n_{d,0}$:

$$\boxed{M_d = m_d \times n_{d,0} \times \iiint_V \phi(s)\, dV} \tag{4.5}$$

This equation can be rearranged to solve for $n_{d,0}$, provided all the other parameters are known.

Calculation of $\sigma(a, \lambda)$:

The cross-section for a dust particle is a very complex parameter and it depends on the grain size and the wavelength of the radiation. In general, the average cross section for a dust grain is :

$$< \sigma >= (Q_{abs} + Q_{sca})\sigma_{geom}$$

where $\sigma_{geom} = \pi < a^2 >$ is the geometrical cross section for a spherical dust particle. Q_{abs} and Q_{sca} are the efficiencies for absorption and scattering phenomenon, which are dependent on the size of a dust particle and the wavelength of the incident radiation. Laor and Draine (1993) described that the properties of a dust grain are formulated by the dielectric constants, $\epsilon = \epsilon_1 + i\epsilon_2$ which are related to refractive indices, $m = n + ik$, i.e., defining the absorbing and scattering properties of the material. The relationships between the dielectric constants and refractive indices are as follows:

$$\epsilon = m^2,\ \epsilon_1 = n^2 - k^2,\ \epsilon_2 = 2nk$$

For silicates only in the Rayleigh-Gans approximation limit, these quantities can be

simplified to the following forms (Bohren and Huffman, 1983) :

$$Q_{abs} = \frac{8}{3}\mathrm{Im}(m)x$$

$$Q_{sca} = \frac{32|m-1|^2x^4}{27+16x^2}$$

where $x = \frac{2\pi a}{\lambda}$

Therefore, for the MRN distribution, the effective cross section could be written as :

$$< \sigma >= \Big(\frac{8}{3}\mathrm{Im}(m)x + \frac{32|m-1|^2x^4}{27+16x^2}\Big)(\pi a^2)$$

or

$$< \sigma >= \Big\langle \frac{16\pi^2}{3\lambda}\mathrm{Im}(m)a^3 \Big\rangle + \Big\langle \frac{512\pi^5|m-1|^2a^6}{\lambda^2(27\lambda^2+64\pi^2a^2)} \Big\rangle$$

or

$$< \sigma >= \frac{16\pi^2}{3\lambda}\mathrm{Im}(m) < a^3 > + C\int_{a_{min}}^{a_{max}} \frac{512\pi^5|m-1|^2a^6}{\lambda^2(27\lambda^2+64\pi^2a^2)}a^{-3.5}da$$

where

$$C\int_{a_{min}}^{a_{max}} \frac{512\pi^5|m-1|^2a^6}{\lambda^2(27\lambda^2+64\pi^2a^2)}a^{-3.5}da = C\frac{512\pi^3|m-1|^2}{64\lambda^2}\int_{a_{min}}^{a_{max}} \frac{a^{2.5}}{a^2+\frac{27\lambda^2}{64\pi^2}}da$$

Since, we would like to understand the dust properties in the optical wavelength regime, we utilize the information about the silicates and their dielectric properties for $\lambda = 0.55\mu m$ from Draine (1985). For our calculated average grain size and silicates only

composition, this authors provides $\epsilon_1 = 2.95, \epsilon_2 = 0.101$ such that

$$n = \frac{(\epsilon_1^2 + \epsilon_2^2)^{0.5} + \epsilon_1)^{0.5}}{\sqrt{2}}$$

, and

$$k = \frac{(\epsilon_1^2 + \epsilon_2^2)^{0.5} - \epsilon_1)^{0.5}}{\sqrt{2}}$$

Therefore, after substituting all these values, we conclude that

$$< \sigma >= 1.053 \times 10^{-5} + C\frac{512\pi^3|m-1|^2}{64\lambda^2} \times 0.0129$$

$$< \sigma >= (1.058 + 9.323) \times 10^{-13} cm^2$$

or

$$\boxed{< \sigma >= 1.038 \times 10^{-12} cm^2} \tag{4.6}$$

For a given distribution function, $\phi(s)$, equation 4.2, 4.4 and 4.5 can now be employed to calculate the optical depth, from which the extinction in any particular wavelength regime can be calculated.

4.4 Components of the Dust Extinction Model:

Recent infrared observations by Gordon et al. (2006) (at 24 μm, 70 μm and 160 μm) using *Spitzer*-MIPS were explained by a simple population - dust grain model as explained in the Marleau et al. (2006) to fit the Spectral Energy Distribution of M31 shown in Fig. 4.1, which showed that > 99 % ($M_d = 4 \times 10^7 M_\odot$) of the dust mass in M31 is traced by 160

μm observations. We therefore construct our spatial extinction model for M31 based on the dust distribution as seen in the 160 μm image (see Fig. 4.2) obtained by Spitzer as follows :

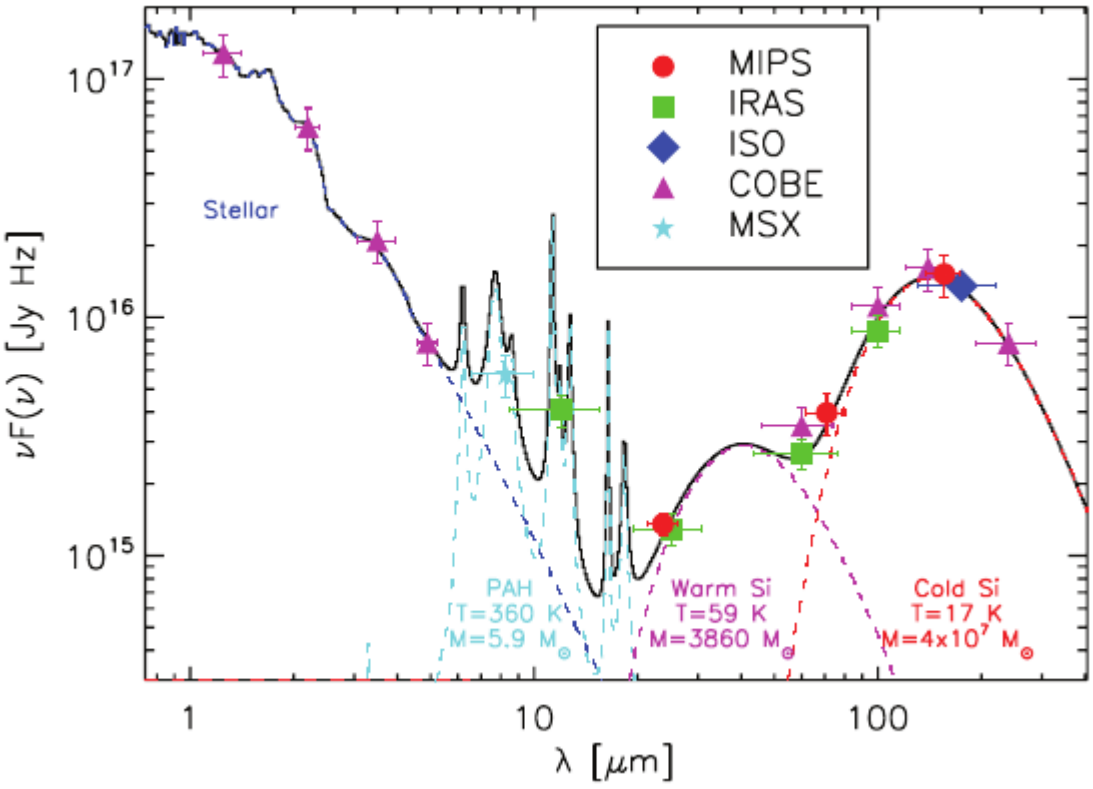

Figure 4.1 M31 global fluxes, plotted along with previous measurements from IRAS, COBE, ISO and MSX. Marleau et al. (2006)'s dust grain plus stellar population model has been fitted to the data. (Source: Gordon et al. (2006)

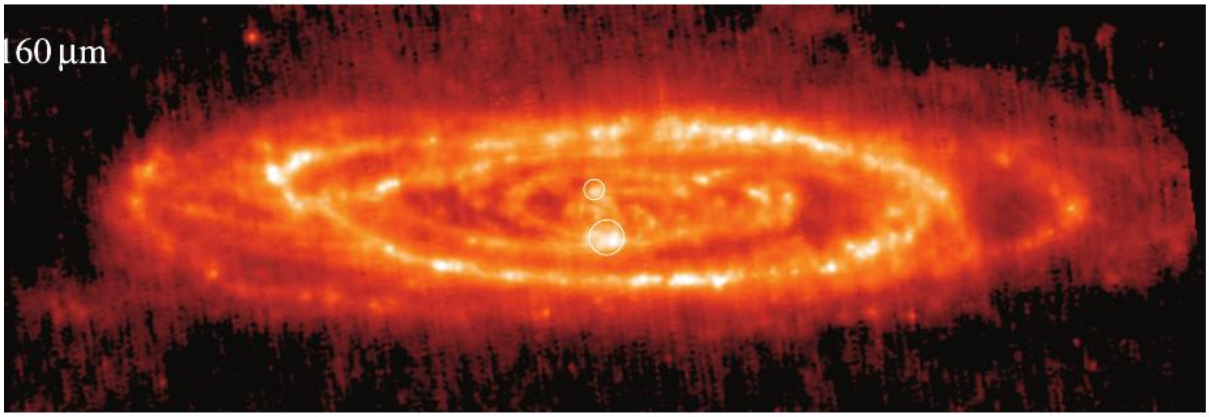

Figure 4.2 M31 image at 160 μm obtained with Spitzer-MIPS (Source: Gordon et al. (2006)

The bulge of M31 is assumed to be dust-free and the extended disk region is a combination of the following components :

- A smooth background component - uniform disk
- A circular ring at 10 kpc
- Two logarithmic spiral arms

4.4.1 Dust Mass in Each Component:

The total dust mass in Andromeda is divided into 3 components such that the calculate surface density for each component is calibrated against the observed dust mass surface density in these regions as shown in Fig. 3(b) in Draine et al. (2014). These calibrations require the total dust mass (Total Dust Mass, $M_{total} = 4 \times 10^7 M_\odot$) to be divided into different components as the following :

- Dust mass in the disk, $M_{disk} = 0.68 \times 10^7 M_\odot$
- Dust mass in the ring, $M_{ring} = 1.28 \times 10^7 M_\odot$
- Dust mass in each spiral, $M_{spiral} = 1.02 \times 10^7 M_\odot$

4.4.2 Dust Distribution Parameters in the Uniform Disk:

Based on the infrared studies of M31 by Smith et al. (2012); Fritz et al. (2012); Draine et al. (2014), we note that there is negligible amount of dust within the 3 kpc radius of M31. We, therefore distribute the dust uniformly within the disk of M31 from r_{min}=3.0 kpc and r_{max}=15 kpc, in the radial direction. The vertical extent of the dust distribution is assumed to be 100 pc, which is adopted from the Milky way dust properties (Drimmel and Spergel, 2001), corresponding to z_c=0.05 kpc above and below the galactic plane.

- Total dust mass in the disk, $M_{d,disk} = 0.68 \times 10^7 M_\odot$
- Radial extent $= 3.0 < r < 15.0$ (kpc)
- Vertical extent $= -0.05 < z_c < 0.05$ (kpc), above & below the plane)
- Distribution Function, $\phi_{disk}(r, \theta, z) =$ Uniform in radial and vertical direction

In order to calculate the optical depth along any line of sight, s through and beyond M31, we can rewrite equation 4.4:

$$\boxed{\tau_\lambda = n_{d,0,disk} \int \phi_{disk}(s)\sigma(a,\lambda)ds}$$

We would first need the following equation to calculate $n_{d,0}$, employing the following equation 4.5, which is rewritten here for the disk component:

$$\boxed{M_{d,disk} = m_d \times n_{d,0,disk} \times \iiint_V \phi_{disk}(r,\theta,z)\, r dr\, d\theta\, dz}$$

Evaluating the integral :

$$\iiint_V \phi_{disk}(r,\theta,z)\, r dr\, d\theta\, dz$$

$$= 2\pi \int_{r_{min}}^{r_{max}} r dr \int_{-z_c}^{z_c} dz$$

$$= \pi \times (r_{max}^2 - r_{min}^2) \times 2z_c$$

$$= 2\pi z_c (r_{max}^2 - r_{min}^2) = 67.86\, kpc^3$$

Substituting all the known parameters, we can find that

$$\boxed{n_{d,0,disk} \simeq 1.399 \times 10^{-10} \text{cm}^{-3}}$$

The procedure to calculate the optical depth corresponding to the disk region of M31 along different lines of sight is described in appendix A.

4.4.3 Dust Distribution Parameters in the Ring at 10 kpc:

- Total dust mass in the ring, $M_{d,ring} = 1.28 \times 10^7 M_\odot$
- Radial extent $= 9.0 < r < 11.0$ (kpc)
- Vertical extent $= -0.5 < z_c < 0.5$ (kpc) (above and below the plane)
- Distribution function, $\phi_{ring}(r, \theta, z)$ = Gaussian like Probability distribution

$$\phi(r, \theta, z) = \frac{1}{2\pi} e^{\frac{-(r-r_c)^2}{2r_0^2}} e^{\frac{-z^2}{2z_0^2}}$$

- Scale length, $r_0 = 1.0$ (kpc) (variance in the radial component)
- Scale height, $z_0 = 0.1$ (kpc) (variance in the vertical component)

Following the similar steps, as in the case of the disk, the optical depth could be written as follows:

$$\boxed{\tau_\lambda = n_{d,0,ring} \int \phi_{ring}(s)\sigma(a, \lambda)ds}$$

where $n_{d,0,ring}$ can be calculated using the following relationship:

$$\boxed{M_{d,ring} = m_d \times n_{d,0,ring} \times \iiint_V \phi_{ring}(r, \theta, z)\, r dr\, d\theta\, dz}$$

For the ring centered at $r_c = 10$ kpc, the following integral can be evaluated as follows :

$$\iiint_V \phi(r, \theta, z)\, r dr\, d\theta\, dz$$

$$= 2\pi \frac{1}{2\pi} \int_{r_{min}}^{r_{max}} r e^{-\frac{(r-r_c)^2}{2r_0^2}} dr \int_{-z_c}^{z_c} e^{-z^2/2z_0^2} dz$$

The following exponential integrals will be employed in the calculation of above integral :

$$\boxed{\int e^{-ct^2} dt = \sqrt{\frac{\pi}{4c}} \text{erf}(\sqrt{c}t)} \quad \boxed{\int t e^{-ct^2} dt = \frac{-1}{2c} e^{-ct^2}}$$

In this case,

$$\int_{-z_c}^{z_c} e^{-z^2/2z_0^2} dz = 2 \int_0^{z_c} e^{-z^2/2z_0^2} dz,$$

since the integrand is an even function in this case. Therefore,

$$\boxed{\int_{-z_c}^{z_c} e^{-z^2/2z_0^2} dz = \sqrt{2\pi z_0^2}\ \text{erf}\left(\frac{z_c/z_0}{\sqrt{2}}\right)}$$

and

$$\boxed{\int_{r_{min}}^{r_{max}} r e^{-\frac{(r-r_c)^2}{2r_0^2}} dr = r_0^2 \Big(e^{\frac{-(r_{min}-r_c)^2}{2r_0^2}} - e^{\frac{-(r_{max}-r_c)^2}{2r_0^2}} \Big) + r_0 r_c \sqrt{\frac{\pi}{2}} \Big[\text{ erf } \left(\frac{r_{max}-r_c}{\sqrt{2r_0^2}}\right) - \text{ erf } \left(\frac{r_{min}-r_c}{\sqrt{2r_0^2}}\right) \Big]}$$

Proceeding to the calculation of $n_{d,0,ring}$ with $r_{min} = 9.0$ and $r_{max} = 11.0$ kpc, we find that:

$$\boxed{n_{d,0,ring} \simeq 4.16 \times 10^{-9}\ \text{cm}^{-3}}$$

The procedure for evaluating the optical depth of M31 in this ring is described in Appendix A.

4.4.4 Dust Distribution Parameters in the Logarithmic Spirals

In general, a logarithmic spiral is defined as follows :

$$r = ae^{b\theta}$$

where b = tan(pitch angle (ϕ_p))

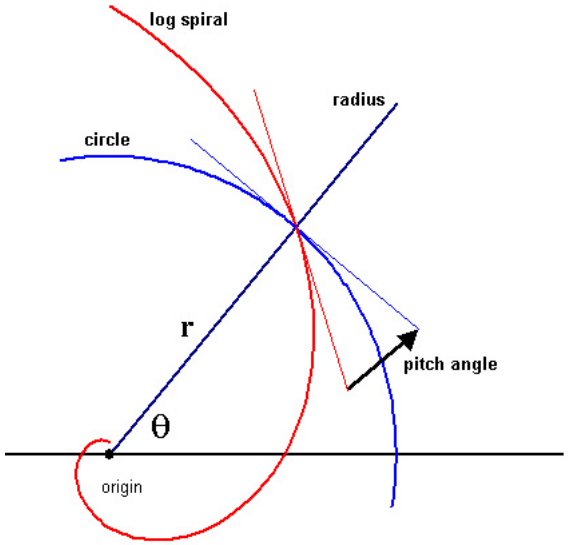

- Total dust mass in each spiral, $M_{d,sp1} = 1.02 \times 10^7 M_\odot$
- Radial extent $= 0.0 < r < 15.0$ (kpc)
- Vertical extent $= -0.5 < z < 0.5$ (kpc) (above and below the plane)
- Scale length, $r_0 = 0.5$ (kpc) (variance in the radial component)
- Scale height, $z_0 = 0.05$ (kpc) (variance in the vertical component)
- Minimum radius at the first turn, $a = 5.0$ kpc

- Pitch angle, $\phi_p = 9.5^\circ$
- Distribution function = Gaussian Probability distribution

Since, the distribution of the dust is assumed to be Gaussian in radial and vertical direction. Therefore, the following integral :

$$\iiint_V \phi(r,\theta,z)\, r dr\, d\theta\, dz$$

from the equation

$$\boxed{M_{d,spiral} = m_d \times n_{d,0,spiral} \times \iiint_V \phi_{spiral}(r,\theta,z)\, r dr\, d\theta\, dz}$$

$$= \frac{1}{2\pi}\int_{\theta_1}^{\theta_2}\left(\int_{ae^{b\theta}-r_{sp}}^{ae^{b\theta}+r_{sp}} re^{-\frac{(r-ae^{b\theta})^2}{2r_0^2}} dr\right)d\theta \int_{-z_c}^{z_c} e^{-z^2/2z_0^2} dz$$

where r_{sp} is the half width of the spiral.

As derived in the case of the ring:

$$\boxed{\frac{1}{2\pi}\int_{-z_c}^{z_c} e^{-z^2/2z_0^2} dz = \sqrt{z_0^2/(2\pi)}\ \text{erf}\left(\frac{z_c/z_0}{\sqrt{2}}\right)}$$

Now,

$$\int_{ae^{b\theta}-r_{sp}}^{ae^{b\theta}+r_{sp}} re^{-\frac{(r-ae^{b\theta})^2}{2r_0^2}} dr =$$

$$2r_0^2\ \sinh(r_{sp}/(2r_0^2)) + ar_0e^{b\theta}\sqrt{0.5\pi}\left(\text{erf}\left(\frac{r_{sp}}{\sqrt{2r_0}}\right) - \text{erf}\left(\frac{-r_{sp}}{\sqrt{2r_0}}\right)\right)$$

which implies :

$$\int_{\theta_1}^{\theta_2}\left(\int_{ae^{b\theta}-r_{sp}}^{ae^{b\theta}+r_{sp}} re^{-\frac{(r-ae^{b\theta})^2}{2r_0^2}} dr\right)d\theta =$$

$$2r_0^2(\theta_2-\theta_1)\,\sinh(r_{sp}/(2r_0^2))+ar_0\sqrt{0.5\pi}\left(\text{erf}\left(\frac{r_{sp}}{\sqrt{2r_0}}\right)-\text{erf}\left(\frac{-r_{sp}}{\sqrt{2r_0}}\right)\right)\int_{\theta 1}^{\theta_2}e^{b\theta}d\theta$$

For $\theta_1 = 0$,

$$V_{disk}=\left[2r_0^2\theta_2\,\sinh(r_{sp}/(2r_0^2))+(ar_0)\sqrt{0.5\pi/b^2}\left(\text{erf}\left(\frac{r_{sp}}{\sqrt{2r_0}}\right)-\text{erf}\left(\frac{-r_{sp}}{\sqrt{2r_0}}\right)\right)(e^{b\theta_2}-1)\right]$$

$$\times\sqrt{z_0^2/(2\pi)}\;\text{erf}\left(\frac{z_c/z_0}{\sqrt{2}}\right)$$

The implies a number density,

$$\boxed{n_{d,0,sp1}\simeq 3.48\times 10^{-9}\text{cm}^{-3}}$$

The procedure to calculate τ_λ is explained in Appendix A.

4.5 Composite Extinction Map for M31

We executed Monte Carlo simulations to generate 1 million lines of sight on the Celestial Sphere spanning the whole area of M31. We then integrated through M31 to the Sun and calculated the optical depth along each line of sight to generate the extinction map for each component. The exact procedure and details of these calculations are described in Appendix A. The resulting extinction maps (displayed in terms of A_V) and dust surface mass density maps ($M_\odot/pc^2$) are shown below for each component in Fig. 4.3 - 4.10. We can clearly see that novae present in the 10 kpc ring region would suffer the maximum amount of extinction as compared to other regions. The overall background uniform disk component does not contribute much to the opacity of the galaxy. This transparency of the background disk component seems to imply that the dust probably does not have a huge role to play in extincting the novae in Andromeda. We will discuss this in detail in the next

section by applying our calibrated extinction model to novae in Andromeda galaxy.

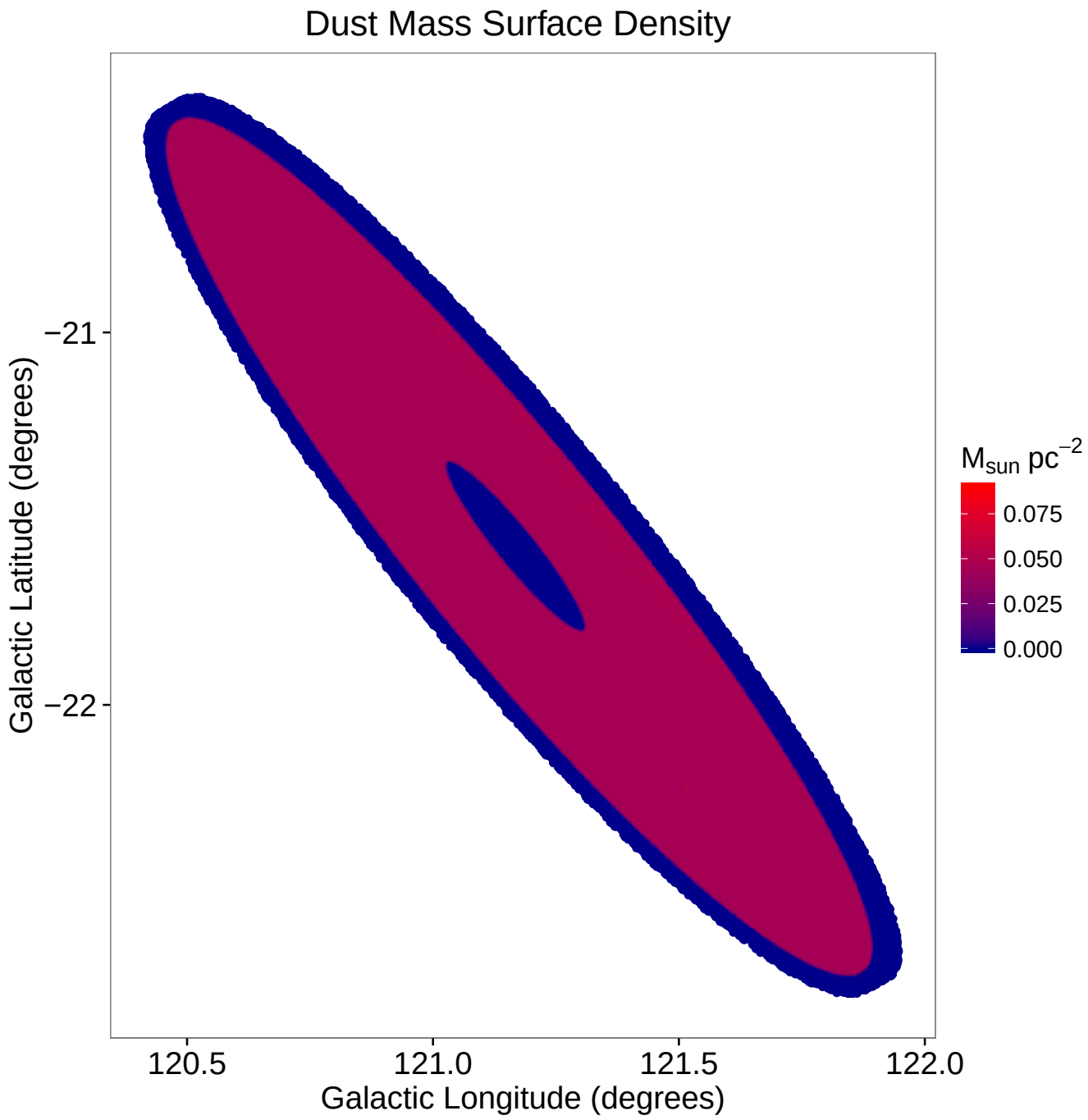

Figure 4.3 Dust Mass Surface Density Map : Uniform Disk

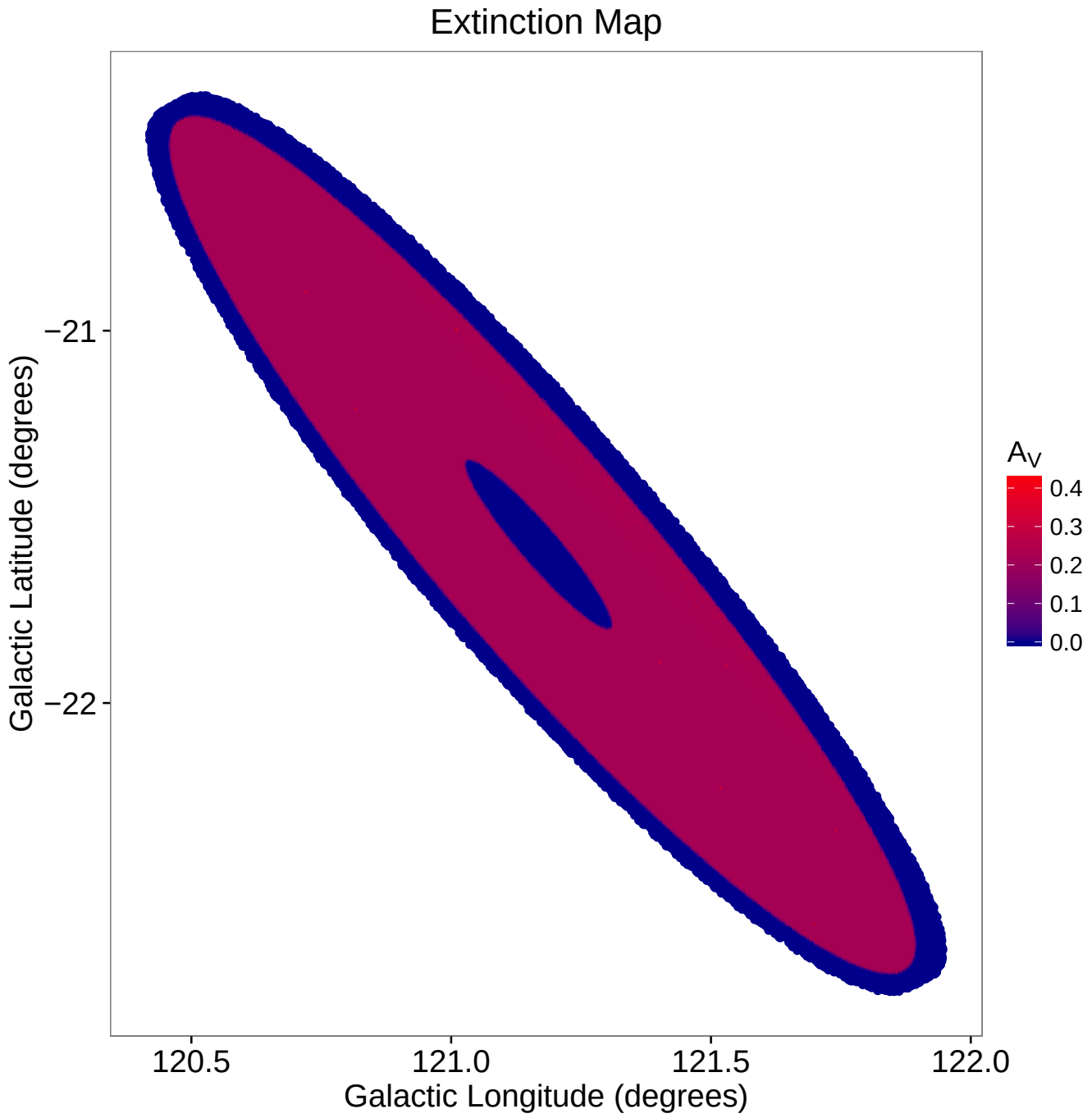

Figure 4.4 Extinction map : Uniform Disk

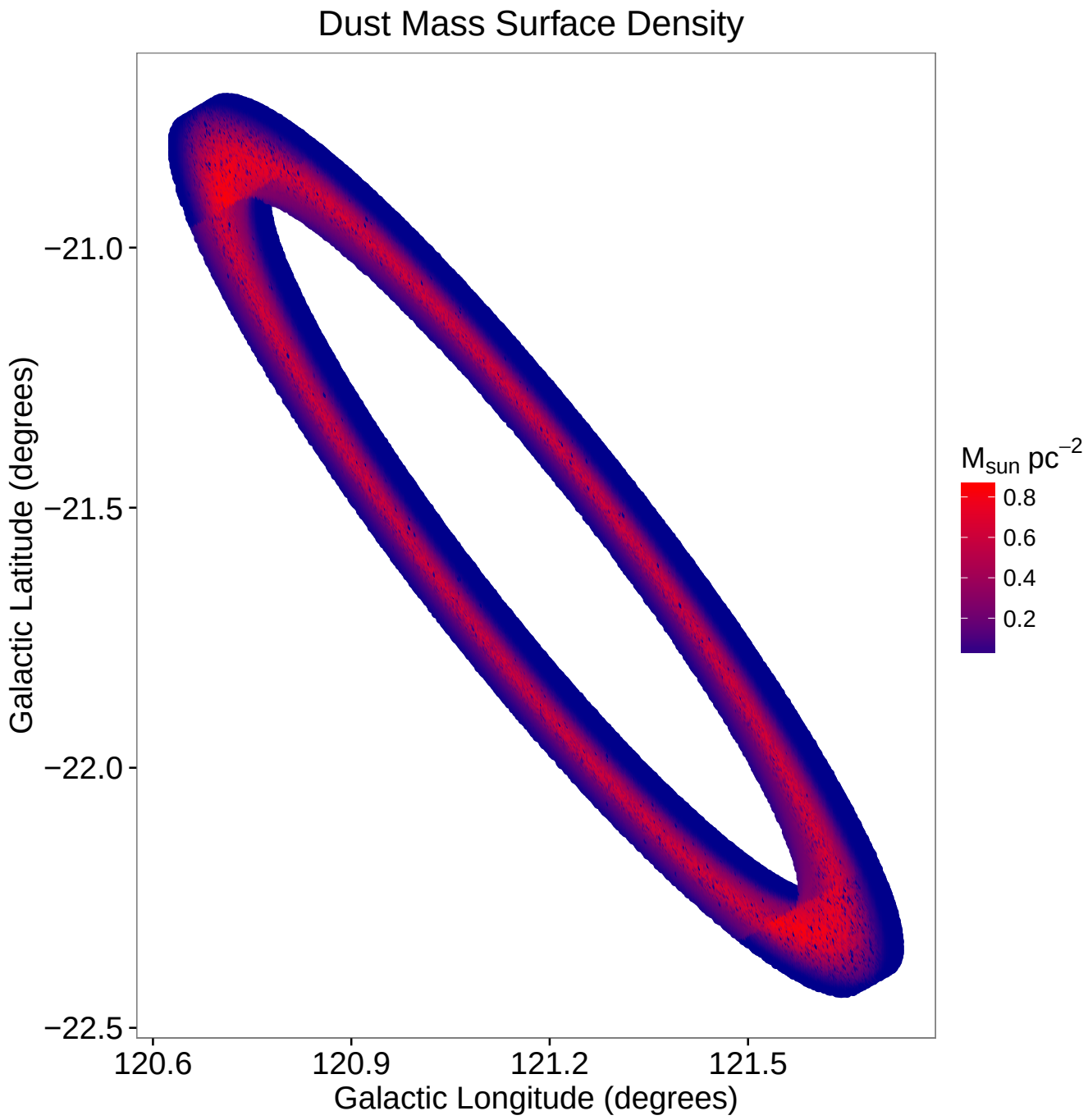

Figure 4.5 Dust Mass Surface Density Map : 10kpc Ring

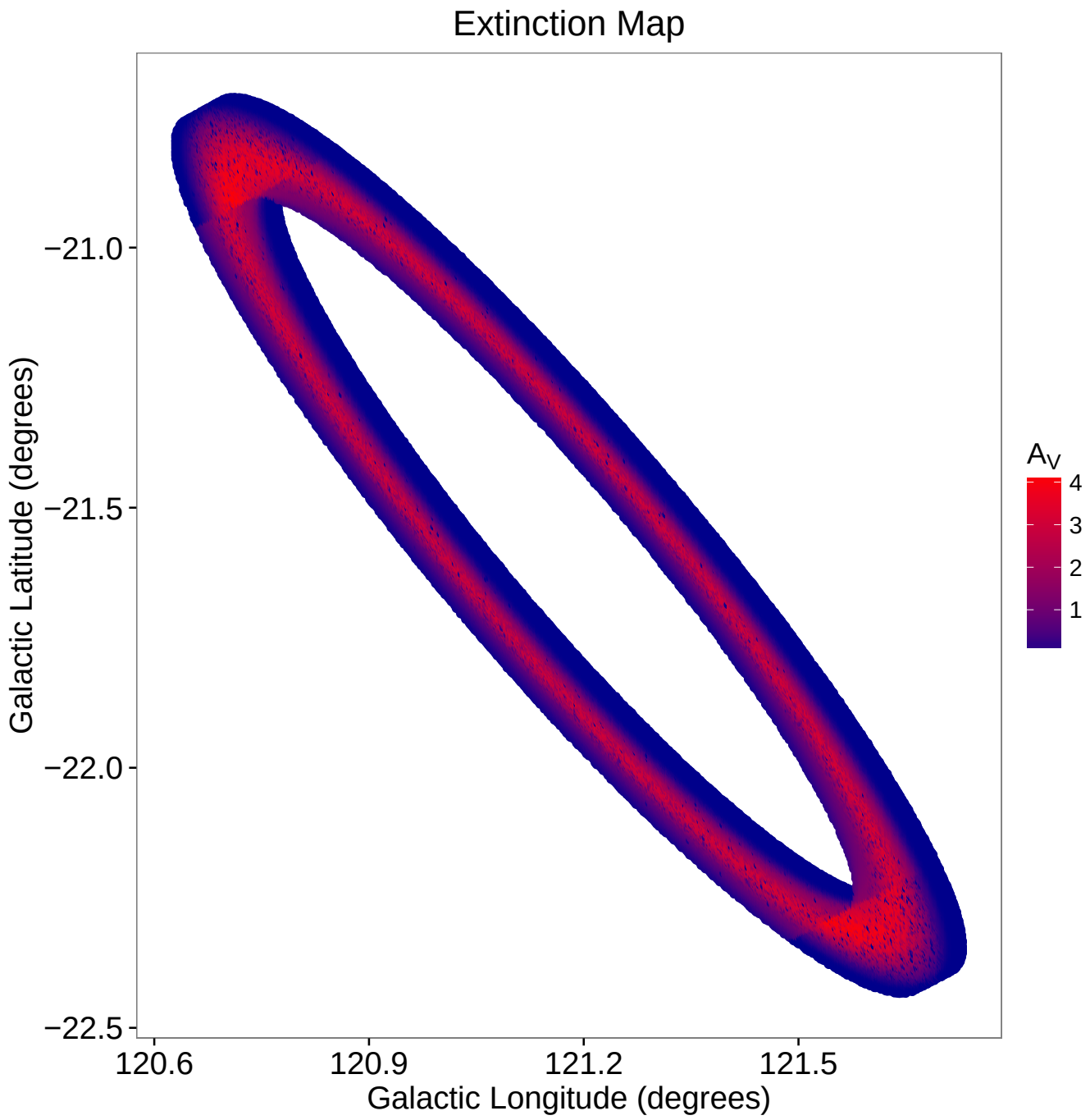

Figure 4.6 Extinction map : Ring

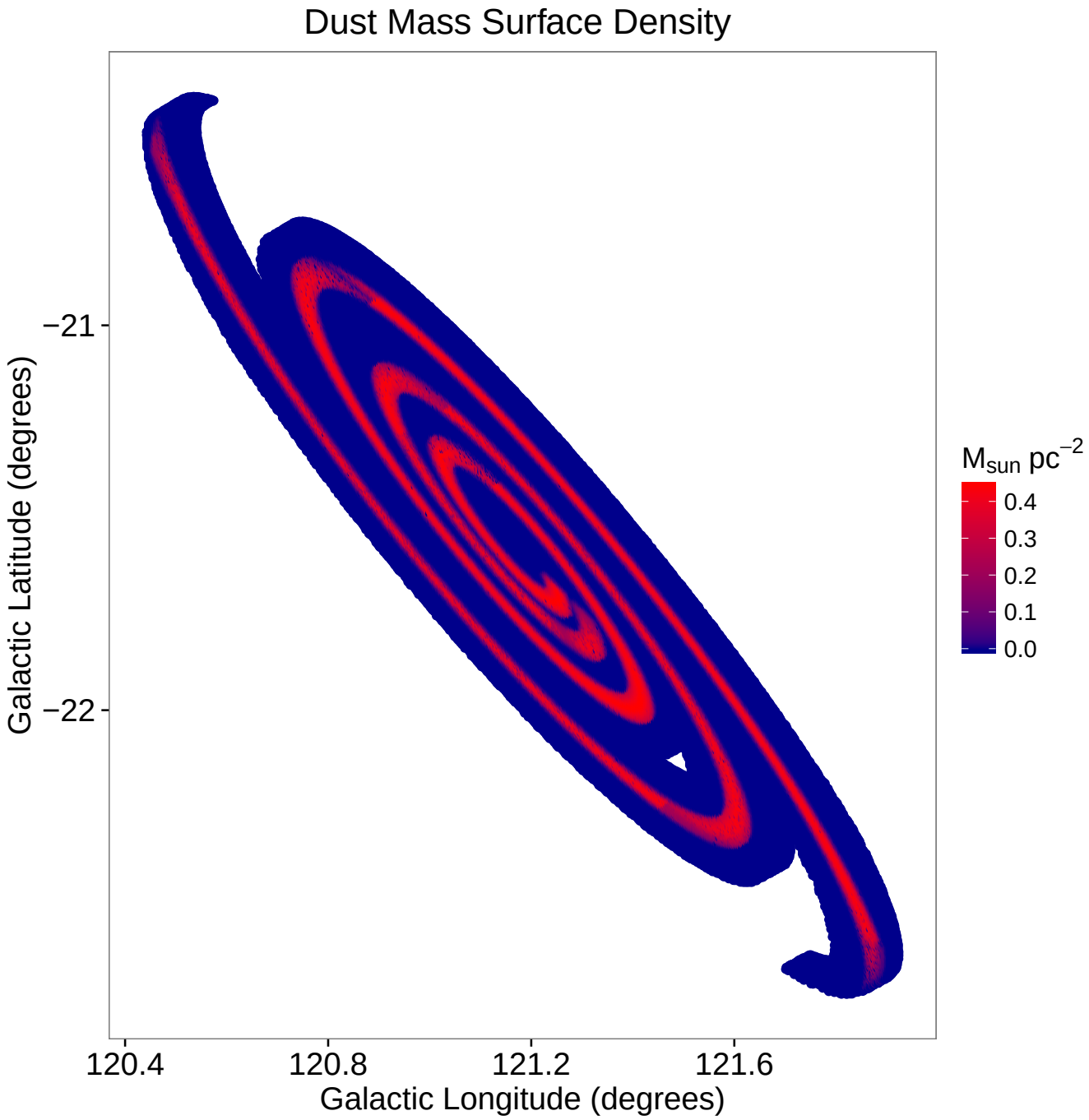

Figure 4.7 Dust Mass Surface Density Map : Two Logarithmic Spirals

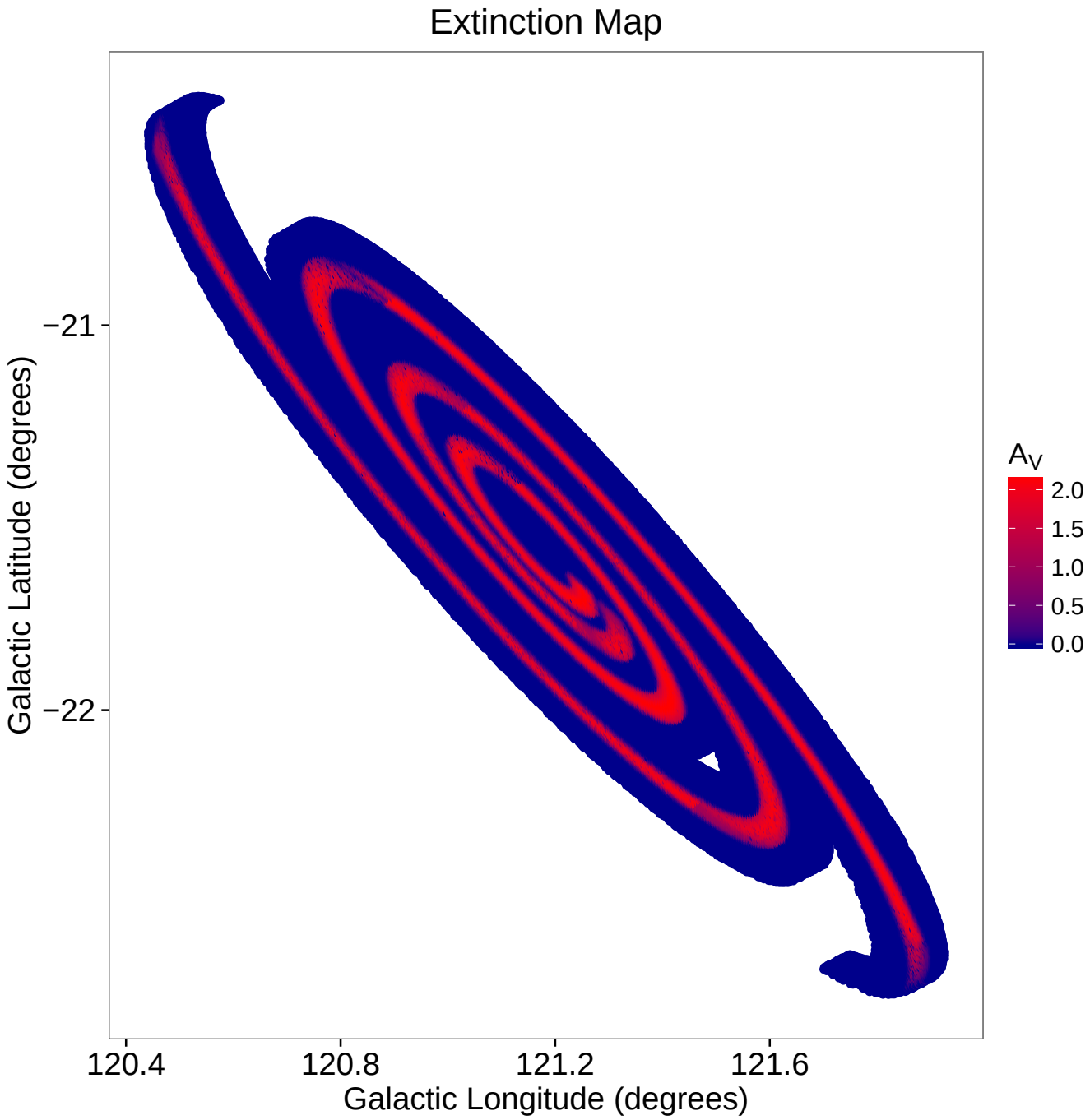

Figure 4.8 Extinction map : Two Logarithmic Spirals

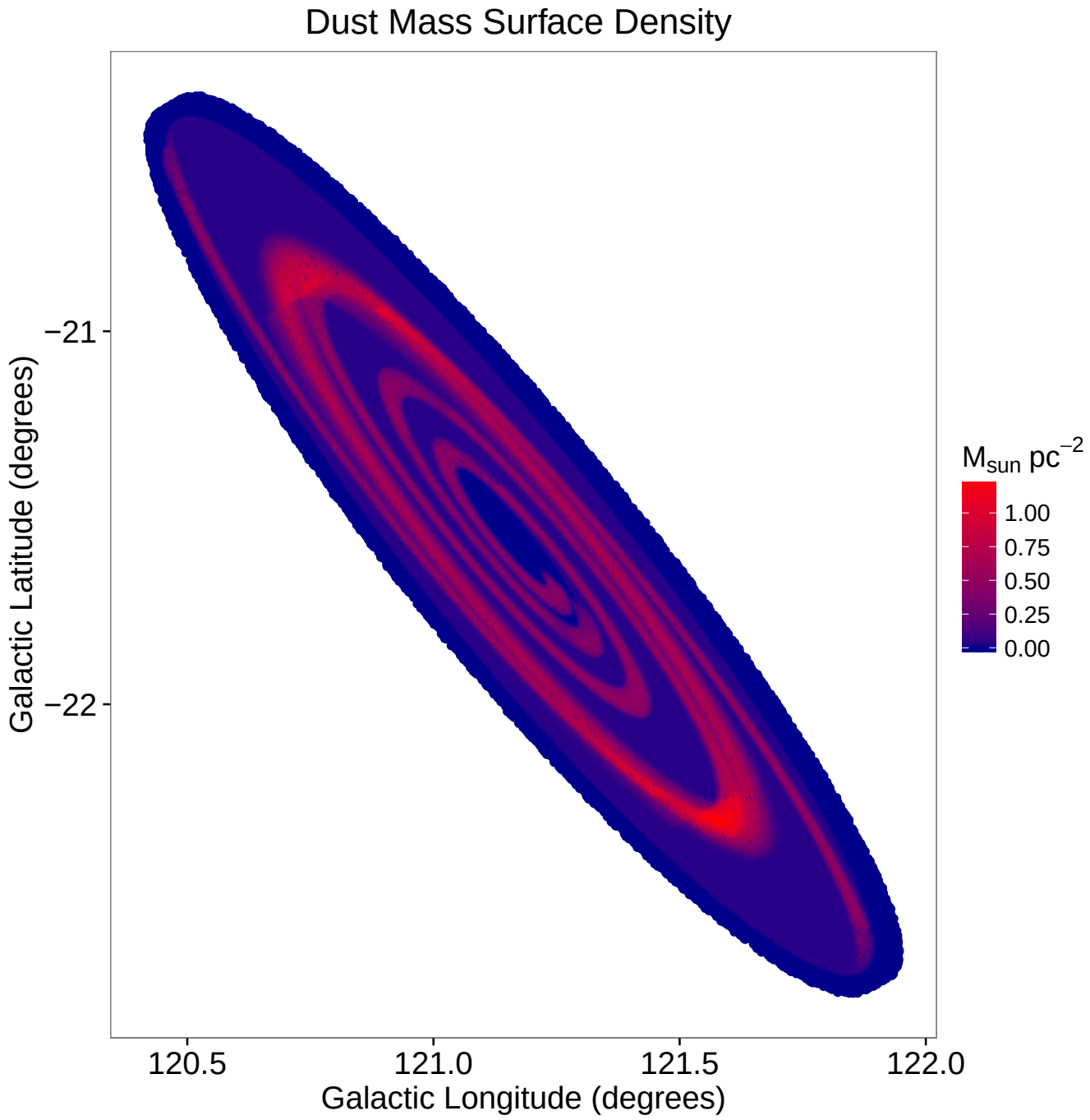

Figure 4.9 Dust Mass Surface Density Map : Composite

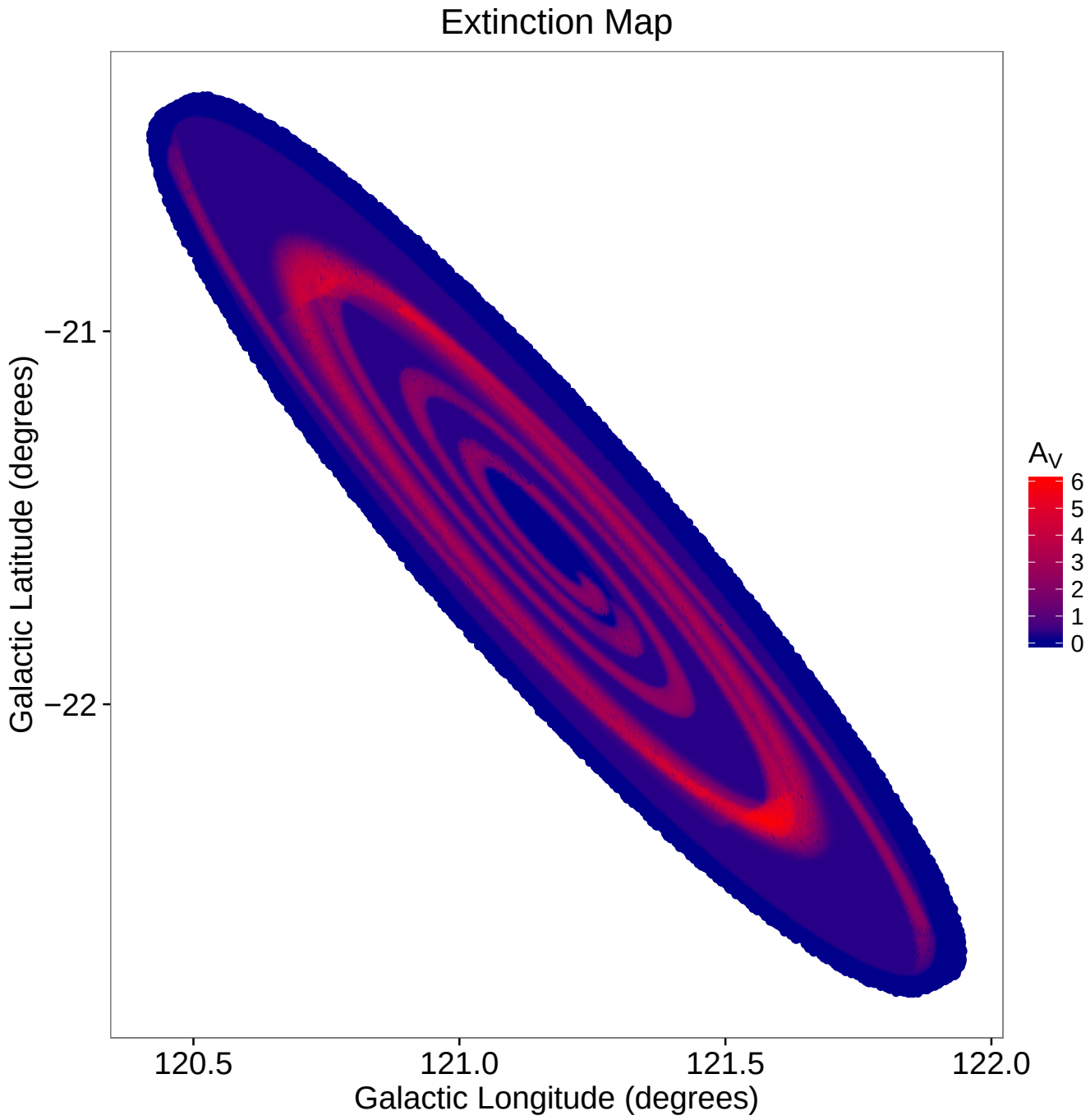

Figure 4.10 Extinction map : Composite

4.6 Summary

This dust model yields maximum extinction, $A_V \sim 6$, which corresponds to the ring region in the galaxy. This value falls in between the Draine et al. (2014)'s value ($A_V \sim 7$), yielded by their model and Dalcanton et al. (2015)'s estimate of $A_V \sim 3.2$, which was obtained using the red giant stars in M31. Since, our model yielded the observed dust surface mass density profiles for all the different components, we assume that if possible, the extinction measurements yielded by our model should be smaller, based on the observations. In the context of this work, we will explore the effects of extinction employing our dust model on varying nova distributions and study its effects on the observed bulge to disk nova ratio. This work is described in the next chapter.

Chapter 5

The Effect of Dust Extinction in M31 on the Observed Bulge to Disk Nova Ratio

In this chapter, we apply our multi-component dust model on novae in Andromeda and study its effect on the bulge and disk populations of these sources. Since the spatial distribution of novae in M31 (bulge and disk) is not well understood, we assume two kinds of distributions to study the effect of dust on novae in the bulge and the disk. The assumed distributions are :

- Uniform Nova Distribution in the Disk and the Bulge
- K light like Nova Distribution (details in Chapter 3)

In both these cases, the assumed bulge to disk nova ratio is 0.41, which is described in Courteau et al. (2011). We will discuss the effects of application of our extinction map to these as two distributions as explained below. The foreground extinction towards the direction of Andromeda is added as a constant value, A_V = 0.17 mag (Schlafly and Finkbeiner, 2011) [1] to the extinction values obtained within the galaxy. The apparent V magnitudes at

[1] https://ned.ipac.caltech.edu/forms/calculator.html

which novae in M31 are observed vary from $\sim$ 14 to 20, as shown in Fig. 5.1 (`The data were obtained from http://www.mpe.mpg.de/ m31novae/opt/m31/index.php`). Based on these observations, we define the limiting magnitude for M31 novae to be 20, i.e., any nova fainter than 20 magnitude in the visual band would not be detected by our telescopes.

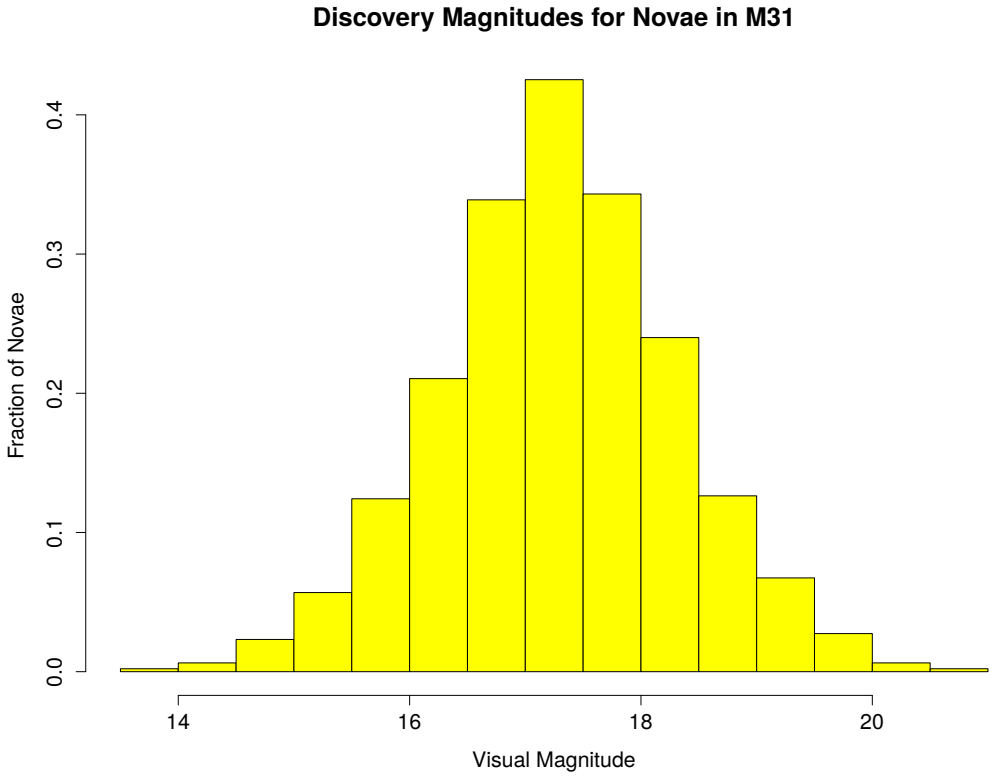

Figure 5.1 A histogram for the observed visual magnitudes for novae in M31. This distribution can be fit with a gaussian with mean and standard deviation 17.34 and 1.02, respectively.

5.0.1 Construction of the Intrinsic Nova Magnitude Distribution

Since the observed nova magnitude distribution in M31 can be explained with a gaussian fit, we therefore generate random magnitudes for the modeled novae following a

gaussian distribution. The adopted mean and the standard deviation for this function are such that when the modeled extinction correction is applied, this distribution matches the observed distribution. This fit is shown in Fig. 5.2. For the example shown in Fig. 5.2, the

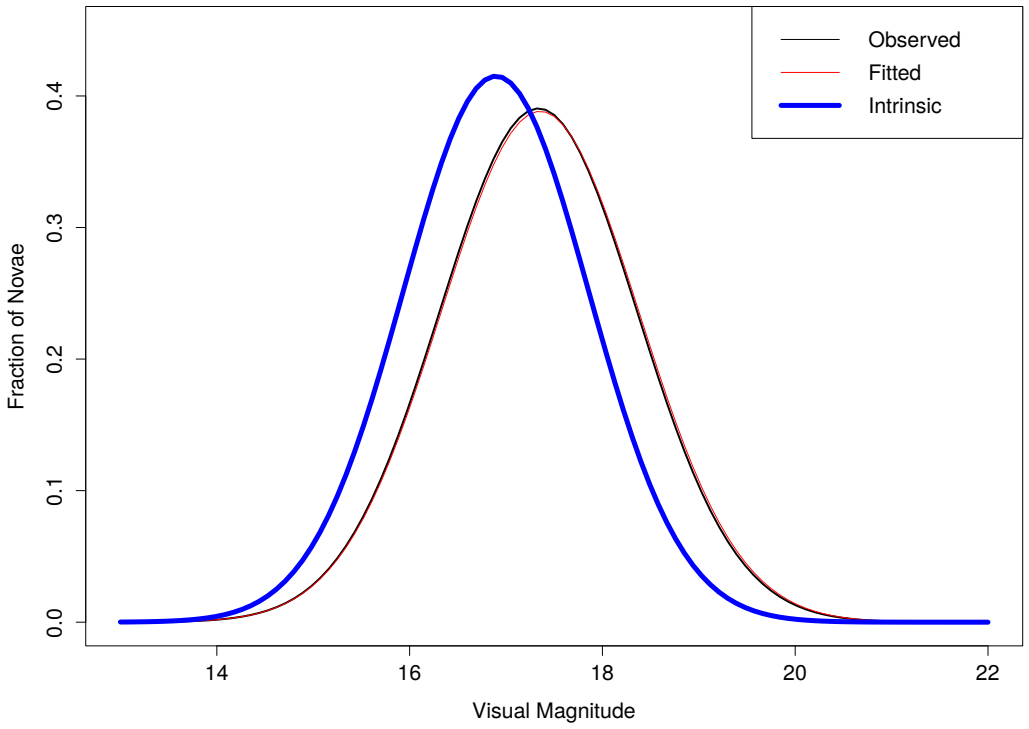

Figure 5.2 The fitted gaussian for the observed magnitudes is shown in black color. The blue curve corresponds to the artificially generated gaussian distribution, i.e., intrinsic magnitude distribution, such that when the extinction correction is applied, the resulting fit (red) matches the observed distribution.

adopted mean and standard deviation for the generated (intrinsic) magnitude distribution are 16.89 and 0.96, respectively. After applying the extinction correction to this data, the mean and standard deviation change to 17.35 and 1.02, respectively, closely matching the observed distribution (mean = 17.33 and standard deviation = 1.02). This example is shown for novae distributed according to the K light, but this procedure is repeated to obtain the "intrinsic" magnitude distribution, when the underlying novae are distributed uniformly in

the disk and the bulge.

5.1 Extinction for the Uniform Nova Distribution

Bulge novae follow spherically symmetric uniform distribution and are confined to 5 kpc in all directions. Disk novae are distributed uniformly along the radial direction and the vertical direction. The extent of the radial direction is 15 kpc, whereas the thickness of the underlying disk distribution has been varied between thick (`2kpc`), medium (`1 kpc`), thin (`500 pc`) and almost infinitely thin (`10 pc`)to understand the effects of dust with the varying thickness of our source distribution. A sample of 10000 novae along different lines of sights were simulated according to the above defined combined distributions and the optical depths for all the lines of sights were calculated. The resulting cumulative distribution function for the novae in the bulge and the disk are shown in Fig. 5.3 and Fig. 5.4, respectively. These results for each component are discussed in the following sections.

5.1.1 Dust's effect on bulge novae

The bulge novae, which are distributed uniformly in a spherical symmetric system, experience extinction in the range, A_V = 0.0 to 2.22 as shown in Fig. 5.3. The percentage of novae with $A_V > 2$ are only 0.07 %, which is significantly small. Almost 60% of the novae are unaffected by the dust in Andromeda, i.e., they experience only the foreground extinction due to the Milky Way, whereas rest of the novae experience dust due to a combination of the ring, spiral arms and the underlying background disk. We will compare this result with the extinct novae in the disk and estimate the observed bulge to disk nova rate.

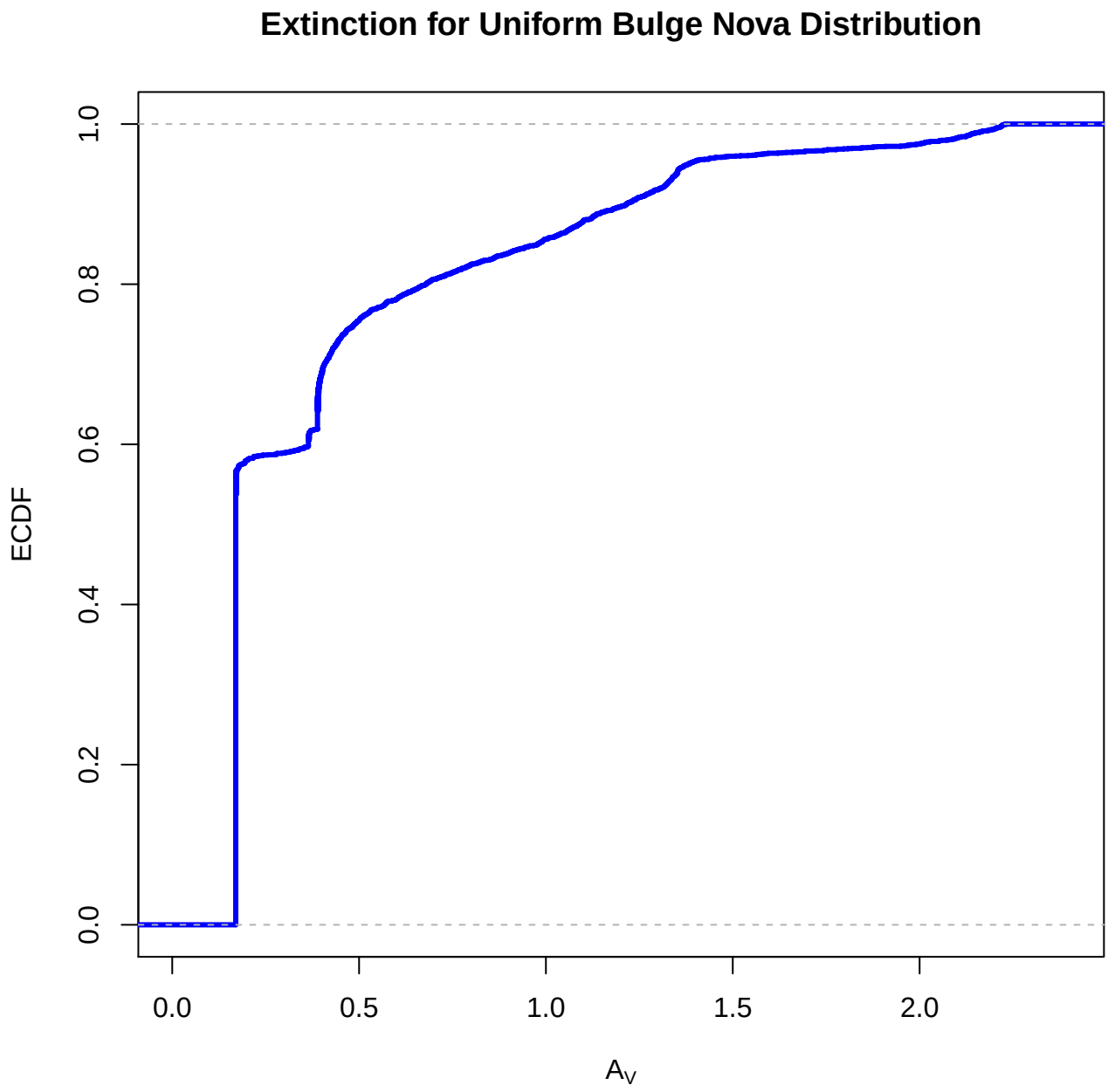

Figure 5.3 The ECDF for the A_V values for the bulge novae in M31.

5.1.2 Dust's effect on disk novae

Since the disk distribution of novae has been imparted varied vertical heights, i.e., `2 kpc`, `1 kpc`, `500 pc` and `10 pc`, we study the variation of the effects of dust on novae as shown in the Fig. 5.4. The broader distributions, i.e., `2 kpc` and `1 kpc` show very similar behavior, which can be explained by the fact that the main extinction component responsible for extincting novae is the ring, whose thickness is 1 kpc in vertical direction and nova distributed across 1 kpc or greater vertical distribution will experience similar amount of extinction. Atleast half of the novae which are distributed on the far side of M31 will encounter more dust along our line of sight as compared to the ones which are relatively closer to us. This effect is quite visible in Fig. 5.4 for these thick distributions. These distributions exhibit a wide range in terms of the extinction of novae as compared to the infinitely thin nova distribution. In this case, all the novae are almost in the same plane and therefore experience very similar amount of extinction, making the range of Av_V is narrower. Therefore, this model yields that the number of novae experiencing $Av_V > 2$ increases with the thickness of the distribution. The quantitative results are presented in the next section.

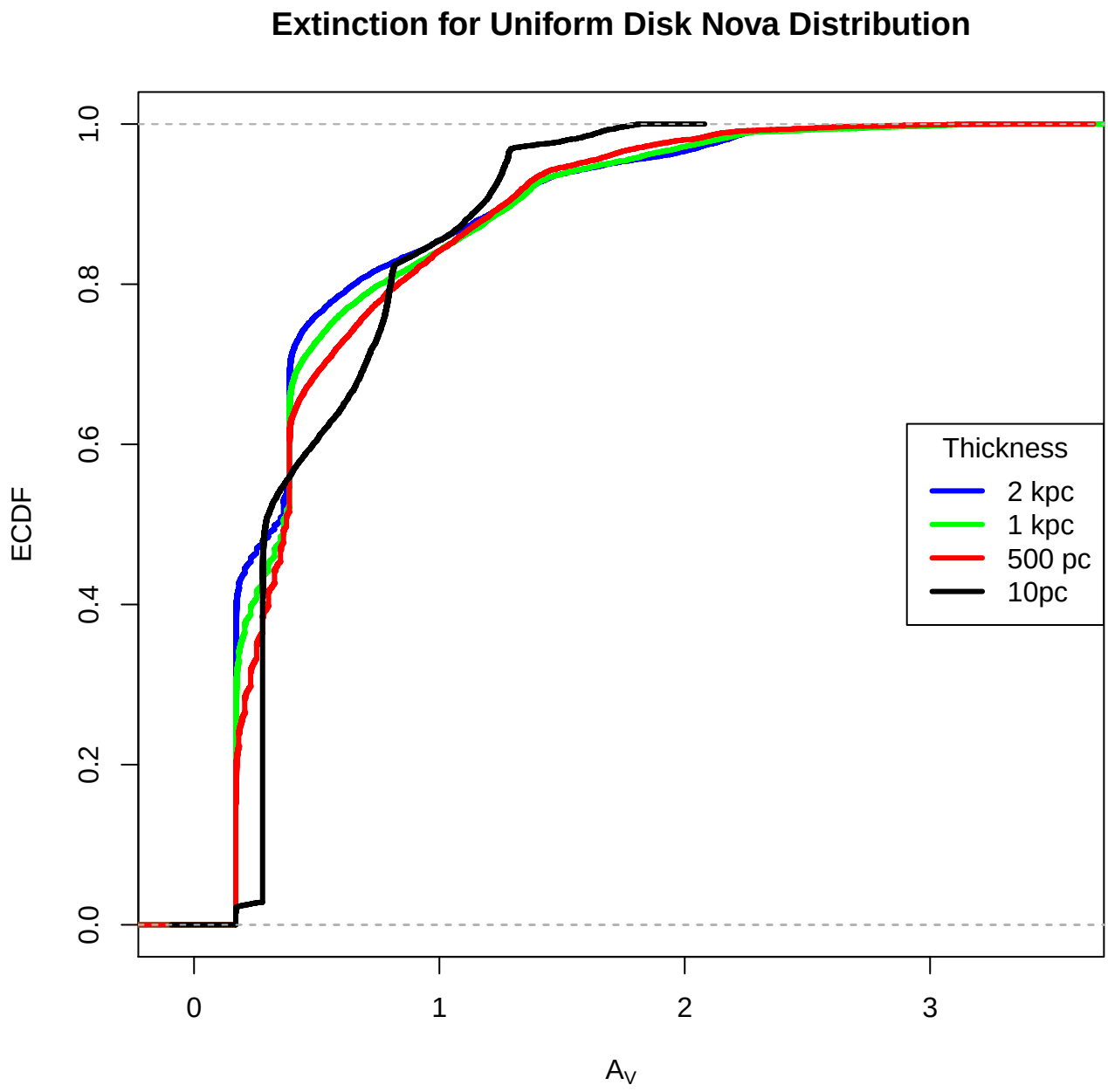

Figure 5.4 The ECDF for the A_V values for the disk novae in M31.

5.1.3 Intrinsic vs Observed Bulge to Disk Nova Ratio

In our model, we assumed a bulge to disk nova ratio $\sim 41\%$, which was derived from the light model of novae. We calculate the optical depths for all these novae in the bulge and the disk, independently. The number of novae experiencing $m_V > 20$ are assumed to be extinct and utilizing this information, we calculate the observed bulge to disk nova ratio as shown in the Table 5.1.

Disk thickness for nova distribution	Observed Bulge/Disk Nova Ratio	Disk Novae with $m_V > 20$
2 kpc	.41	1.0%
1 kpc	.41	1.0%
500 pc	.41	0.95%
10 pc	.41	0.6%

Table 5.1 The observed R_{bd} nova ratio due to the dust distributions of different thicknesses, assuming the theoretical ratio .41. Novae in the bulge with $m_V > 20 \sim 0.3$ %

5.2 Extinction for the K band like Nova Distribution

The nova distribution is assumed to follow K light. All the model parameters in this distribution are derived from the nova light model as described in Chapter 3. We repeat the exact same procedure to calculate the consequences of dust on novae in the bulge and the disk, if they follow K light in both the bulge and the disk and the results are shown in Fig. 5.5. It is quite evident from this figure that the number of novae

almost no extinction within M31 are quite high ($\sim 70\%$) in number in the bulge as compared to the disk ($\sim 10\%$). Using the intrinsic nova magnitude distribution as explained earlier, we obtain that the total number of novae experiencing total extinction in the bulge

and the disk are 0.4% and 0.6%, respectively. We, therefore conclude that the dust in M31 does not favor either the bulge or the disk component for hiding novae. Moreover, the effects of dust, although minimal, have a similar effect on both these components of M31. This result implies that the underlying assumed distribution has a big role to play in the outcome of extincted novae. Since this model assumes almost no extinction near the nuclear region, but places most of the novae (bulge novae and the double exponential declining nova distribution away from the center of M31) near the nuclear region. Therefore, it is evident that the actual number of novae in the outer regions, where the ring and the spirals are present are very few in number and hence the outcome of our extinct nova number is very small, irrespective of its disk or bulge nature. The results of this model are presented in the next section.

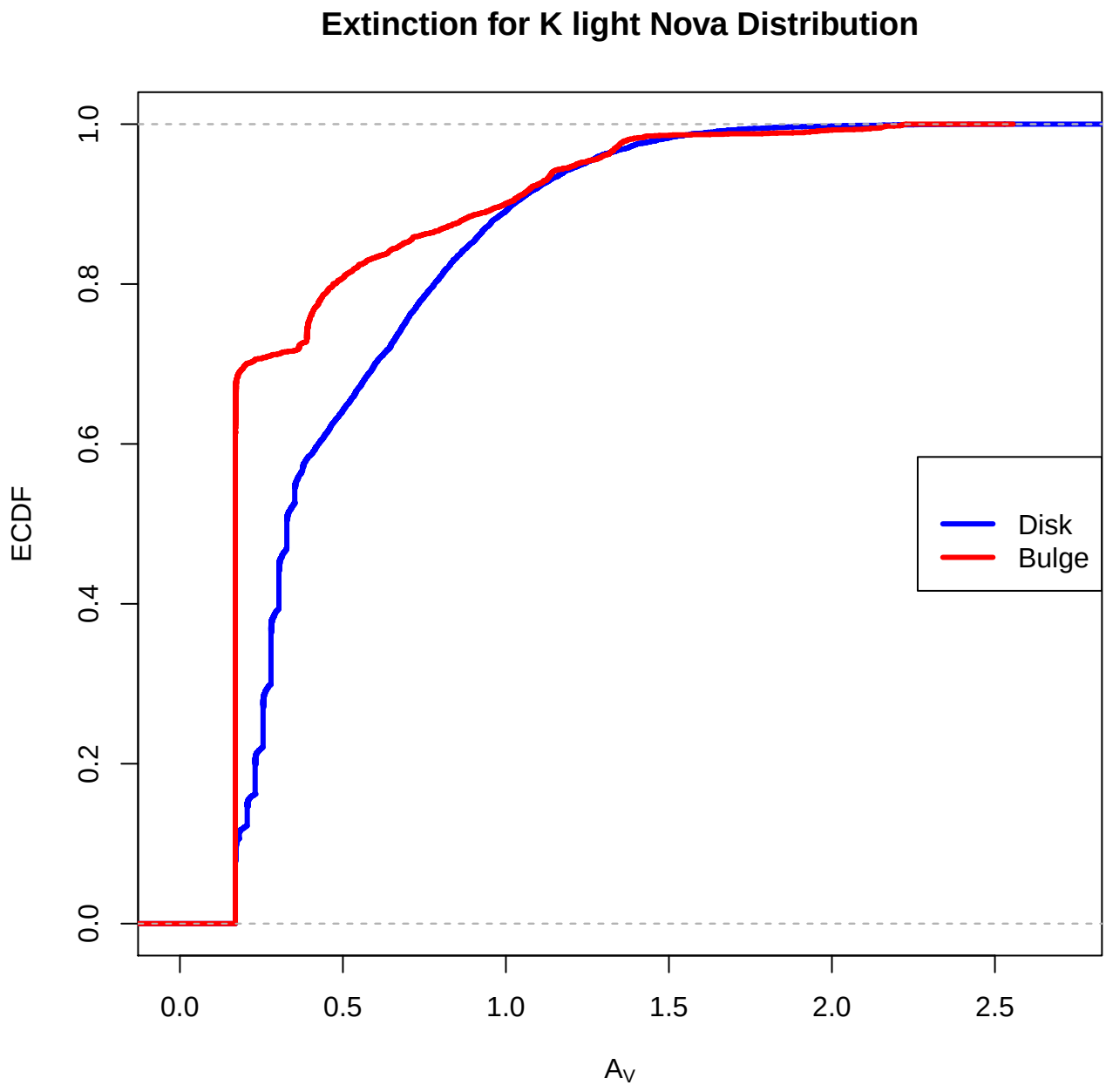

Figure 5.5 The ECDFs for the A_V values for the K light bulge and disk novae

5.2.1 Intrinsic vs Observed Bulge to Disk Nova Ratio

For a theoretical R_{bd} nova ratio equal 0.41, the observed values yield a R_{bd} ratio = 0.411, which is not much different from the adopted intrinsic ratio. This includes removing novae experiencing $m_V > 20$ (apparent magnitude in V band) from our model. This results implied that the dust does not affect the actual bulge to disk nova ratio. We note that the number of $m_V > 20$ novae in the bulge and the disk are very similar, i.e., $< 1\%$, which is not a huge effect on novae in either component of the galaxy. If we fit these filtered nova data to the observed distribution, it would not extinct novae particularly from the disk only, rather the effect of dust is quite similar and small on the bulge and the disk. This could be explained based on the fact that the ring in Andromeda is the main dust contributor and since both the bulge and the disk are affected by it, the effects on extinction should be quite similar in both the regions.

5.3 Summary

Dust in Andromeda had been cited as one of the possible contributing factor in the "missing" disk novae from M31 by many authors e.g. Arp (1956), Capaccioli et al. (1989), Ciardullo et al. (1990), Shafter and Irby (2001). We tested this hypothesis by constructing a 3-dimensional 3 component model utilizing the information about dust in Andromeda. Our dust model when applied to different nova distributions does not particularly extinct a huge amount of novae in the disk. Although our model is simplistic in nature, the observational and modeling results of dust in Andromeda hinted at a maximum of $A_V \sim 4$ (Dalcanton et al., 2015) - or $A_V \sim 7$ (Draine et al., 2014). Both of these authors agree that the highest amount of extinction would occur in the 10 kpc ring structure and which is what we also observe in our work. However, we conclude that the dust in M31 does not play a major role

in hiding the disk novae. Moreover, the effect of the dust is very similar on novae in both the components. This suggests that other factors e.g. the population synthesis approach for understanding the underlying population for both the components of M31, may play a larger role. Other factors that could be responsible for the observed nova distribution are briefly discussed in the next chapter.

Chapter 6

Results and Discussion

6.1 Puzzle of Bulge to Disk Nova Ratio Solved yet ?

Extragalactic nova studies are important in the context of understanding the stellar population distribution in various galaxies. Moreover, if the location of nova population in these galaxies are completely understood, the comparison with the SNe-Ia location could yield important results regarding the nova-Supernova Ia connection, since novae have been cited as the possible progenitors of SNe-Ia e.g. Starrfield et al. (1988), Yungelson et al. (1997), Hachisu and Kato (2001). Therefore, knowledge of the spatial distribution of novae in different galaxies is of great value, but it is quite a challenging task. In our neighbor spiral galaxy, Andromeda, nova monitoring campaigns by Hubble (1929), Arp (1956), Rosino (1964, 1973) and Ciardullo et al. (1987) established their association with the bulge population of the galaxy. The problem with this association lies in the fact that the evolved population of stellar progenitor systems in the disk should of course also produce novae, which seems inconsistent with the observations and this question was first brought into focus by Capaccioli et al. (1989). The dearth of nova samples in different galaxies for comparison restricted these authors to draw any particular conclusion regarding the absence of

novae in the disk of Andromeda. Ciardullo et al. (1990) compared the LSNR (Luminosity Specific Nova Rate), i.e., nova rate normalized to the K band luminosity of the galaxy to different Hubble types of galaxies and found no trend between these two quantities, which implies a nova rate K-light correlation. Some years later, della Valle et al. (1994) compared the nova rate in galaxies of different Hubble types and concluded that the late Hubble types are more prolific nova producers. The nova rate per unit K luminosity was higher for M33 than M31, which implied that the disk dominated populations produce more novae than the bulge populations. The reason for the discrepancy between these two publications was the different normalization factors for different galaxies. With the most observations of different galaxies, Shafter et al. (2000) repeated this study and came to the same conclusions drawn by Ciardullo et al. (1990), thereby suggesting no correlation between Hubble type and the specific nova rate in that galaxy. The LSNR is a constant; ~ 2 per year per K-band luminosity in units of $(10^{10} M_{\odot})$. In other words, novae follow K light in all galaxies.

Here, we test this scenario by constructing a surface photometry based model for the nova distribution in the bulge and the disk of the Andromeda galaxy. Under the assumption that novae follow K light, we decompose novae into bulge and disk populations and utilize the observed K band surface brightness to generate the 3D nova distributions for these two components of M31. The bulge novae follow a distribution such that the projected density matches a standard Sersic profile with index 2.2. The novae in the disk are assumed to follow the double exponential distribution. All parameters associated with these two components were derived from Courteau et al. (2011). The resulting modeled nova distribution does not match the observed radial distribution, indicating that the "Novae follow light" hypothesis requires some modification. Although, the observed global nova rate per unit K luminosity of M31 is consistent with the relation established by the larger sample of spirals, the decomposition into two separate components does not match the observed spatial distribution.

Dust in the disks of spirals has been suggested by various authors e.g. Arp (1956), Hatano et al. (1997), Shafter et al. (2000), Shafter and Irby (2001) as one of the possible factors hiding novae in this extended component of spiral galaxies. Hatano et al. (1997) constructed a model for novae in M31 by dividing novae into bulge and disk class based on their magnitudes (bright in the disk and faint in the bulge) concluding that the majority of novae in M31 seen as bulge novae due to the projection of the galaxy are actually disk novae. These authors, for the first time also studied the effects of dust extinction in the disk. Since detailed information about dust in M31 was not widely available at the time, these authors did not draw any strong conclusions in this regard. Fortunately, the space-based telescopes Spitzer and Herschel, enabled detailed IR studies of M31, revealing its dust properties (total amount, temperature and angular distribution). We use the observations reported in Gordon et al. (2006) and Draine et al. (2014) to create a 3D dust extinction model in which the bulge is assumed to be dust free, but the disk has three distinct components: a uniform disk component, a ring at 10 kpc, and two logarithmic spiral arms. This composite extinction model is then applied to the novae in M31. We find that bulge and the disk novae experience very similar amount of dust extinction, and generally brightness reductions by less than one magnitude (in the V band). The dust in Andromeda hides (assumed to apply when m_V exceeds 20) at most 1% of novae in the disk and 0.4% - 0.6% novae in the bulge. The role of dust in extincting novae from the extended disk region of M31 is thus almost negligible, and can not be invoked to resolve the puzzling fact that the bulge overproduces novae in comparison to the disk. One needs to explore other factors that might explain the observed nova spatial distribution.

To summarize, we conclude that novae do not follow K light in M31, when decomposed into its established bulge and disk components. Therefore, the intrinsic bulge to disk

nova ratio can not be derived from the K light distribution. In addition, the dust in the disk component of the galaxy does not extinct enough light to explain the missing novae in this component. In fact, the dust affects about equally to novae in the bulge and in the disk. Therefore the observed bulge to disk ratio would not be very different from the intrinsic ratio, if dust effects are included.

In order to finally resolve the Bulge/Disk ratio puzzle, more factors must be investigated. The evolution of the underlying binaries by treating the bulge and the disk star formation histories, separately, could be essential for a clearer understanding of this puzzle. Recently, modeling of novae populations using a hybrid binary population synthesis approach by Chen et al. (2016) concluded that novae in spiral galaxies host high mass white dwarfs and are more luminous than the ones in the ellipticals. In addition, the white dwarfs associated with novae in ellipticals are less massive than the ones in spirals. If the bulge and the disk of M31 hosts different populations in these two components such that the bulge resembles isolated elliptical galaxies, then it is clearly necessary to treat these two components separately in the population synthesis models. Further aspects of this intriguing puzzle could evolve metallicity of the underlying progenitor populations, and dust in the vicinity of novae, such as dusty wind-blown bubbles which might be preferentially associated with novae in the disk. The bulge-disk decomposition of novae in galaxies requires further study. In this thesis we conclude that the basic paradigm ”novae trace K-light” is not supported by detailed observations of M31, and that dust does not offer a remedy by hiding most novae in the disk.

Appendices

Appendix A Calculation of the Optical Depth

A monte carlo approach was employed to generate one million lines of sight within M31 (inclined at 77° at a distance = 785 kpc from the Sun) uniformly distributed within a radius of 15 kpc. The adopted height for the distribution was 1 kpc. The effective optical depth along each line of sight, utilizing these points was calculated for each component of the dust model of M31.

Revisiting the definition of optical depth (equation 4.4) from Chapter 4, we can write,

$$\boxed{\tau_\lambda = n_{d,0}\, \sigma(a,\lambda) \int \phi(s) ds} \tag{1}$$

Since we already described the procedure to calculate $n_{d,0}$ and $\sigma(a,\lambda)$, we will describe how to calculate $\int \phi(s) ds$, this section.

A.1 Calculating the $\int \phi(s) ds$ for the uniformly distributed dust in the disk:

The total effective distance is calculated provided the radial and vertical conditions are met while moving from the source to the Sun (l.o.s). i.e. in the case of the disk. The composite trapezoidal rule was employed in these calculations. As shown in Fig. A.1 :

- `x_comp, y_comp, z_comp` : Components of the position vector from the source to our line of sight.
- `nx, ny, nz` : Components of the unit vector from the source to the sun.
- `xn, yn, zn` : Position of the source within M31
- `s` : Ideally, the distance of the source from the sun, since the dusty disk is limited to 15 kpc, we limit this distance to 50 kpc.

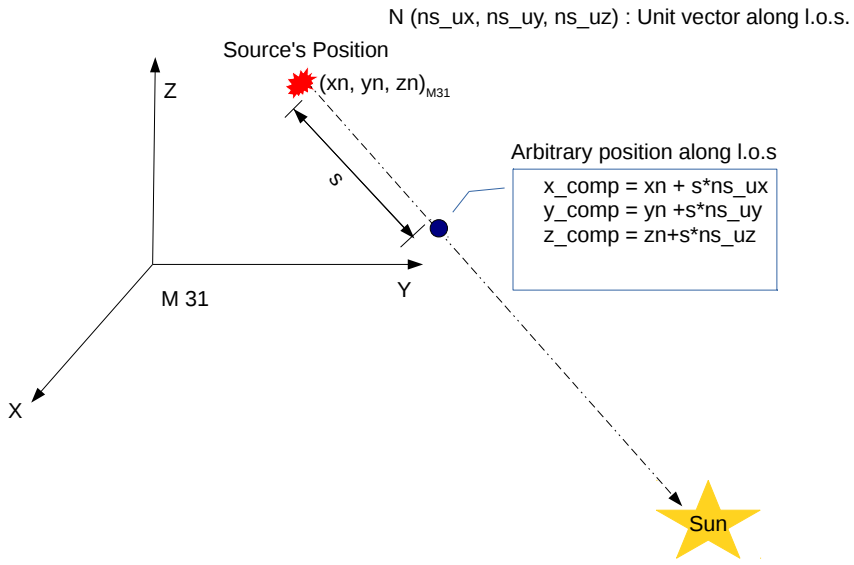

Figure A.1 An arbitrary source's position in M31 along our line of sight.

Our program computes the effective distance from the source to the Sun by estimating the radial and vertical components of the line of sight vector, providing the l.o.s. passes through the dusty disk i.e. radial and vertical components' conditions are met with the dust distribution as shown below.

```
// Calculate extinction along our line of sight from the source to the Sun
// Uniform Disk
#include <stdio.h>
#include <math.h>
#include <stdlib.h>
#include <stdbool.h>
#define PI 3.142
#define number 1000000
```

```
float y(float x, float xn, float yn, float zn, float ns_ux, float ns_uy,
     float ns_uz, float l, float b, float ns){
      float z_c=0.05;// half of the disk width
      float r_max=15.;// kpc maximum radius
      float r_min = 3 ; //kpc ; minimum radius
      float x_comp=xn+x*ns_ux;
      float y_comp=yn+x*ns_uy;
      float z_comp=zn+x*ns_uz;
      float radial=pow((x_comp*x_comp+y_comp*y_comp),0.5); // radial component
   if (radial <=r_max && radial >=r_min && z_comp<=z_c && z_comp >=-z_c){
      return 1.;
            } else {
                        return 0;
              }
   }
int main(){
      FILE *fp=NULL;
   fp=fopen("Av_disk.txt","w"); // store tau and l,b
   float x0,step;
   double s, int_val, tau; /* s = distance from the source to the "sun"*/
   int i,n, u, k;
   float sigma = 1.038e-12;
   float m_dust=4.9e-17;
   float M_d=0.68e7 ;//M_solar
   float constant = 3.08e21 ;// kpc to cm
```

```
/* Calculation of number density as described in the Chapter 4 */
double n_0_den=m_dust*pow(constant,3)*2*PI*z_c*r_min*r_min
      *(pow((r_max/r_min),2)-1);
double n_0_num=2.e33*M_d;
double n_0= n_0_num/n_0_den;
/* Calculation of the effective distance through the dust */
printf("Enter x0, xf, no. of subintervals: ");
/* x0=0 (initial position of the position vector from the source to the sun) */
/* xf=50 (final position of the position vector from the source to the sun) */
scanf("%f%f%d",&x0, &xf,&n);
FILE* val= NULL;
printf("k xn yn   zn    int_val     tau \n");
val=fopen("novae_uniform_unitvectors.txt", "r");
for(u=0;u<=(number-1);u++){
      fscanf(val,"%f %f %f %f %f %f %f %f %f", &xn[u], &yn[u], &zn[u],
           &ns_ux[u], &ns_uy[u], &ns_uz[u], &l[u], &b[u], &ns[u]);
      }
for(k=0;k<=(number-1);k++){
step = (xf-x0)/n;
s = y(x0,xn[k],yn[k], zn[k]...) + y(xf,xn[k],yn[k], zn[k]...);
for(i = 1; i < n; i++){
  s += 2*y(x0+i*step,xn[k],yn[k], zn[k]...);
      }
  int_val = s*step/2;
  tau = int_val*sigma*n_0*constant;
  fprintf(fp,"%f\t%f\t%1.7f\t%f\n",l[k],b[k],fabs(tau),ns[k]);
}
```

```
fclose(fp);
return 0;
}
```

Similarly, by inverting the direction of the unit vector, we calculate the effective distance along the same line of sight from the source to opposite direction of the Sun i.e. by inverting the direction of the unit vector. In the end, we add these two components, which yields the total extinction map due to the dust in the disk.

A.2 Calculating the $\int \phi(s)ds$ for the Gaussian Like Distribution of Dust in the Ring:

The dust distribution parameters for this component have been explained in Chapter 4. In this section, the steps taken to calculate the $\int \phi(s)ds$ are described as follows :

- The initial and the final points of intersection of l.o.s with the ring ($s_i(x_i, y_i, z_i)$ and $s_f(x_f, y_f, z_f)$) are stored. It has been taken into account in our program in case the source passes through the ring twice i.e. on the far side and the near side as shown below.

```
#include <stdio.h>
#include <math.h>
#include <stdlib.h>
#include <stdbool.h>
#define PI 3.142
#define number 1000000

int main(){
bool change=true;
FILE *fp=NULL;
```

```
fp=fopen("Av_ring.txt","w");
FILE *fp1=NULL;
fp1=fopen("ring_lb_r1.txt","w");

int k;
float r_min=9; // minimum ring's radius (kpc)
float r_max=11; // maximum ring's radius (kpc)
float step=0.01;
float u_max=30;
float z_c = 0.5; // half the height of the ring
static float ns_ux[number],ns_uy[number],ns_uz[number],....;
FILE* val= NULL;
val=fopen("novae_uniform_unitvectors.txt", "r");
for(k=0;k<=(number-1);k++){
  fscanf(val,"%f %f %f %f %f %f %f %f %f", &xn[k], &yn[k], &zn[k]...);
  float u=0.;
  int i=0.;
  for (u=0.;u<=u_max;u=u+step){
     i=i+1;
/* calculating the x_comp w.r.t the center C when stepped by 'u'
units from the source along the l.o.s. */
     x_comp=xn[k]+u*ns_ux[k];
     y_comp=yn[k]+u*ns_uy[k];
     radial[i]=pow((x_comp*x_comp+y_comp*y_comp),0.5);
     if (radial[i] >=r_min && radial[i] <=r_max){
        z_comp[i]=zn[k]+u*ns_uz[k];
        if(z_comp[i] >=-z_c && z_comp[i] <= z_c){
```

```
            if(change) {
            fprintf(fp,"%f\t%f\t%f\t%f\t%f\t%f\t%f\t%f\t%f\t%f\t",
            x_comp,y_comp,z_comp[i],l[k],b[k],ns[k],ns_ux[k],ns_uy[k],ns_uz[k],
            pow((radial[i]*radial[i]+z_comp[i]*z_comp[i]),0.5));
            // storing the initial s and final s
            fprintf(fp1,"%f\t%f\t%f\t%f\n",
            pow((xn[k]*xn[k]+yn[k]*yn[k]+zn[k]*zn[k]),0.5),l[k],b[k],ns[k]);
                change=!change;
                      }}}          // radial condition
else { // if the condition of radial and z_comp is not met
      if(!change){
  fprintf(fp,"%f\n",pow((radial[i-1]*radial[i-1]
  +z_comp[i-1]*z_comp[i-1]),0.5));
            change=!change;
}}}}
return 0.;
}
```

- Steps are taken along our l.o.s using the following equations

$$x_{comp} = x_i + (s_f - s_i) \times nx$$

$$y_{comp} = y_i + (s_f - s_i) \times ny$$

$$z_{comp} = z_i + (s_f - s_i) \times nz$$

to calculate the Gaussian function at every step and sum up all the values to calculate the effective distance, when our l.o.s. passes through the ring. The composite

trapezoidal rule was employed in this summation (integration) as shown below:

```
/* calculate extinction due to the dust ring from the source to the Sun */
#include <stdio.h>
#include <math.h>
#include <stdlib.h>
#include <stdbool.h>
#define MAX_FILE_NAME 100
#define PI 3.142
float y(float x, float xn, float yn, float zn,
     float l, float b, float ns, float ns_ux,
     float ns_uy, float ns_uz, float int_s, float fin_s){
float r_0=1.0; //kpc (scale length)
float z_0=0.1; //kpc (scale height)
float r_ring=10.; //kpc (center)
float x_comp=xn+x*ns_ux;
float y_comp=yn+x*ns_uy;
float z=zn+x*ns_uz;
float radial=pow((x_comp*x_comp+y_comp*y_comp),0.5);
      return (1/(2.*PI))*exp(-(radial-r_ring)*(radial-r_ring)/(2*r_0*r_0))
      *exp(-z*z/(2.*z_0*z_0));
      }
int main(){
FILE *fp=NULL;
fp=fopen("Av_ring_sum.txt","w");
float x0,xf,step;
double tau;
int i, m, k;
```

```
/* to read the number of lines in the previous file */
FILE *fp1;
int number = 0; // Line counter (result)
char filename[MAX_FILE_NAME];
char c; // To store a character read from file
fp1 = fopen("Av_ring.txt", "r");
/* Extract characters from file and store in character c */
for (c = getc(fp1); c != EOF; c = getc(fp1))
if (c == '\n') // Increment count if this character is newline
number = number + 1;
fclose(fp1);
printf("The file %s has %d lines\n ", filename, number);

/* Calculating tau */
float *ns_ux, *ns_uy, *ns_uz, *xn, *yn,*zn,*l,*b,
    *ns, *int_s, *fin_s, *int_val, *fin_val ;
ns_ux=malloc(sizeof(float)*number);
ns_uy=malloc(sizeof(float)*number);
... (define all the parameters)
float s,tot_val;
float m_dust=4.9e-17; //g
float sigma= 1.038e-12 ; // cm2
float M_d= 1.02e7 ;//M_solar
float constant = 3.08e21 ;// kpc to cm
float z_c=0.5; // half the ring's vertical height
double n_0_den1=m_dust*pow(constant,3)*pow(2.0*PI*z_0*z_0,0.5)
*erf(pow(1./2,0.5)*z_c/z_0);
```

```
double n_0_den2=r_0*r_0*(exp(-(r_min-r_ring)*(r_min-r_ring)/
(2.*r_0*r_0))
-exp(-(r_max-r_ring)*(r_max-r_ring)/
(2.*r_0*r_0)));
double n_0_den3=r_0*r_ring*pow(PI/2.0,0.5)*(erf(pow(1./(2*r_0*r_0),0.5)
*(r_max-r_ring))-erf(pow(1./(2*r_0*r_0),0.5)
*(r_min-r_ring))) ;
double n_0_num=2.e33*M_d;
double n_0_den=n_0_den1*(n_0_den2+n_0_den3);
double n_0= n_0_num/n_0_den;
int n =1e4;
FILE* val= NULL;
val=fopen("Av_ring.txt", "r");
      for(m=0;m<=(number-1);m++){
      fscanf(val,"%f %f %f %f %f %f %f %f %f %f %f\n",
       &xn[m], &yn[m], &zn[m], &l[m], &b[m],
       &ns[m], &ns_ux[m], &ns_uy[m], &ns_uz[m],
       &int_s[m], &fin_s[m]);
                  }
for(k=0;k<=(number-1);k++){
      int_val[k]=int_s[k];
      fin_val[k]=fin_s[k];
      if (int_val[k] <= fin_val[k]){
      x0=int_val[k];
      xf=fin_val[k];
}
      else {
```

```
        xf=int_val[k];
        x0=fin_val[k];
        }
        xf=xf-x0;
        x0=0;
        step = (xf-x0)/n;
    s = y(x0,xn[k], yn[k], zn[k]...) + y(xf,xn[k], yn[k], zn[k] ...);
    for(i = 1; i < n; i++){
    s += 2*y(x0+i*step,xn[k], yn[k], zn[k]...);
        }
        tot_val = s*step/2;
    tau= tot_val*sigma*n_0*constant;
        fprintf(fp,"%f\t%f\t%1.7f\t%f\n",l[k],b[k]
        ,tau,ns[k]);
}
fclose(fp);
return 0;
}
```

- These steps are repeated by reversing the direction of the unit vector.

A.3 Calculating the $\int \phi(s)ds$ for the Gaussian Like Distribution of Dust in the Spirals:

The steps followed for the calculation of the effective distance are similar to those in the ring, except that here the same procedure is followed for every turn of the spiral.

```
/*Calculating the points of intersection of all the l.o.s with the dusty spiral
```

```
#include <stdio.h>
#include <math.h>
#include <stdlib.h>
#include <stdbool.h>
#define PI 3.142
#define number 1000000
int main(){
bool change=true;
FILE *fp=NULL;
fp=fopen("Av_spiral1_ini.txt","w");
FILE *fp1=NULL;
fp1=fopen("spiral1_lb_r.txt","w");
int k;
float z_c=0.5;
float a_sp = 5.0; // turning radius
float b_sp = tan(9.5*PI/180.);
static float ns_ux[number],ns_uy[number],ns_uz[number],
xn[number], yn[number],zn[number],
l[number],b[number],ns[number],x_comp,y_comp;
FILE* val= NULL;
val=fopen("novae_uniform_unitvectors.txt", "r");
for(k=0;k<=(number-1);k++){
fscanf(val,"%f %f %f %f %f %f %f %f %f", &xn[k],
 &yn[k], &zn[k], &ns_ux[k], &ns_uy[k],
  &ns_uz[k], &l[k], &b[k], &ns[k]);
```

```
float u_max=30;
float step=0.005;
float u=0.;
int m=0.;
static double radial[1000000]={0}, z_comp[1000000]={0};
for (u=0.;u<=u_max;u=u+step){
  m=m+1;
  x_comp=xn[k]+u*ns_ux[k];
  y_comp=yn[k]+u*ns_uy[k];
  radial[m]=pow((x_comp*x_comp+y_comp*y_comp),0.5);
  angle[m]= atan2f(y_comp, x_comp);
float dr=1.5; // width of a spiral
double r_sp=a_sp*exp(b_sp*angle[m]);
if ((fabs(r_sp*exp(b_sp*2*PI)-radial[m])<=dr ||
 fabs(r_sp-radial[m])<=dr ||
 fabs(r_sp*exp(b_sp*4*PI)-radial[m])<=dr)
 && radial[m] <=15.){

z_comp[m]=zn[k]+u*ns_uz[k];
if(z_comp[m] >=-z_c && z_comp[m] <= z_c){
if(change) {
fprintf(fp,"%f\t%f\t%f\t%f\t%f\t%f\t%f\t%f\t%f\t%f\t",
x_comp,y_comp,z_comp[m],l[k],b[k],ns[k],
ns_ux[k],ns_uy[k],ns_uz[k],
pow((radial[m]*radial[m]+z_comp[m]*z_comp[m]),0.5));
fprintf(fp1,"%f\t%f\t%f\t%f\n",
pow((xn[k]*xn[k]+yn[k]*yn[k]+zn[k]*zn[k]),0.5),
```

```
l[k],b[k],ns[k]);
change=!change;
 }}}
else if(!change){
   fprintf(fp,"%f\n",pow((radial[m-1]*radial[m-1]
   +z_comp[m-1]*z_comp[m-1]),0.5));
      change=!change;
      }}}
return 0.;
}
```

```
/* Calculating extinction due to the dusty spiral */
#include <stdio.h>
#include <math.h>
#include <stdlib.h>
#include <stdbool.h>
#define MAX_FILE_NAME 100
#define PI 3.142
float y(float x, float xn, float yn, float zn, float l, float b,
float ns, float ns_ux, float ns_uy, float ns_uz,
float int_s, float fin_s){
float x_comp=xn+x*ns_ux;
float y_comp=yn+x*ns_uy;
float z=zn+x*ns_uz; // using z_comp later
float b_sp = tan(9.5*PI/180.);
float radial=pow((x_comp*x_comp+y_comp*y_comp),0.5);
```

```
float theta_comp=atan2f(y_comp, x_comp);
float a_sp = 5.0;
float r_0=0.5;
float z_0=0.05;
if (fabs(radial-a_sp*exp(b_sp*theta_comp)) <= 0.5){
return exp(-(radial-a_sp*exp(b_sp*theta_comp))*
(radial-a_sp*exp(b_sp*theta_comp))/
(2.*r_0*r_0))* exp(-z*z/(2.*z_0*z_0))/(2*PI);
}
else if (fabs(radial-a_sp*exp(b_sp*
(theta_comp+2*PI))) <= 0.5){
return exp(-(radial-a_sp*exp(b_sp*(theta_comp+2*PI)))
*(radial-a_sp*exp(b_sp*(theta_comp+2*PI)))/
(2.*r_0*r_0))* exp(-z*z/(2.*z_0*z_0))/(2*PI);
}
else if (fabs(radial-a_sp*exp(b_sp*(theta_comp+4*PI))) <= 0.5){
return exp(-(radial-a_sp*exp(b_sp*(theta_comp+4*PI)))
*(radial-a_sp*exp(b_sp*(theta_comp+4*PI)))/
(2.*r_0*r_0))* exp(-z*z/(2.*z_0*z_0))/(2*PI);
}
else {
return 0.;
}}
int main(){
FILE *fp=NULL;
fp=fopen("Av_spiral1_sum.txt","w");
float x0,xf,step;
```

```
double tau;
int i, m, k;
/* to read the number of lines in the previous file */
FILE *fp1;
int number = 0; // Line counter (result)
char filename[MAX_FILE_NAME];
char c; // To store a character read from file
fp1 = fopen("Av_spiral1_ini.txt", "r");
for (c = getc(fp1); c != EOF; c = getc(fp1))
if (c == '\n')
number = number + 1;
fclose(fp1);
printf("The file %s has %d lines\n ", filename, number);
float *ns_ux, *ns_uy, *ns_uz,
 *xn, *yn,*zn,*l,*b, *ns,
 *int_val, *fin_val, *int_s, *fin_s ;
ns_ux=malloc(sizeof(float)*number);
ns_uy=malloc(sizeof(float)*number);
...

float s,tot_val;
float m_dust=4.9e-17;
float sigma= 1.038e-12 ;
float M_d=1.02e7 ;//M_solar
float constant = 3.08e21 ;// kpc to cm
float b_sp = tan(9.5*PI/180.);
float a_sp = 5.0;
```

```
float r_0=0.5;
float z_0=0.05;
float z_c=0.5;// arm height
float r_c=0.75; //half the width of one spiral
float theta_max=4*PI;
double n_0_den1=m_dust*pow(constant,3)*pow(z_0*z_0/(2*PI),0.5)
*(erf(z_c/pow(2*z_0*z_0,0.5)));;
 double n_0_den2=(2.*r_0*r_0*theta_max*sinh(r_c/(2*r_0*r_0)))
 +((a_sp/b_sp)*pow(0.5*PI*r_0*r_0,0.5)
 *(exp(b_sp*theta_max)-1)*
 (erf(r_c/pow(2*r_0,0.5))
 -erf(-r_c/pow(2*r_0,0.5))));
double n_0_den=n_0_den1*n_0_den2;
double n_0_num=2.e33*M_d;
double n_0= n_0_num/n_0_den;
printf("%e\t%e\n",n_0,n_0_num/(n_0*m_dust*pow(constant,3)));
int n =1e4;
FILE* val= NULL;
val=fopen("Av_spiral1_ini.txt", "r");
for(m=0;m<=(number-1);m++){
fscanf(val,"%f %f %f %f %f %f %f %f %f %f %f\n",
 &xn[m], &yn[m], &zn[m], &l[m], &b[m],
  &ns[m], &ns_ux[m], &ns_uy[m],
   &ns_uz[m], &int_s[m], &fin_s[m]);
}
for(k=0;k<=(number-1);k++){
int_val[k]=int_s[k];
```

```
fin_val[k]=fin_s[k];
if (int_val[k] <= fin_val[k]){
x0=int_val[k];
xf=fin_val[k];
}
else {
xf=int_val[k];
x0=fin_val[k];
}
xf=xf-x0;
x0=0;
step = (xf-x0)/n;
s = y(x0,xn[k], yn[k], zn[k], l[k], b[k],
 ns[k],ns_ux[k], ns_uy[k], ns_uz[k],
 int_s[k], fin_s[k]) + y(xf,xn[k], yn[k], zn[k],
  l[k], b[k], ns[k],ns_ux[k], ns_uy[k], ns_uz[k],int_s[k], fin_s[k]);
for(i = 1; i < n; i++){
   s += 2*y(x0+i*step,xn[k], yn[k], zn[k], l[k], b[k],ns[k],ns_ux[k], ns_uy[k],
}
tot_val = s*step/2;
tau= tot_val*sigma*n_0*constant;
fprintf(fp,"%f\t%f\t%1.7f\t%f\n",l[k],b[k],tau,ns[k]);
}
fclose(fp);
return 0;
}
```

These steps are repeated for another spiral by introducing the phase angle. In order to calculate the extinction map, all these steps are repeated by changing the signs of the unit vector.

A.4 Calculation of Dust Mass Surface Density

Employing the above steps for each component, we can derive the optical depth corresponding to wavelength, λ = 0.55 μm (V band). Defining the optical depth in terms of the number surface density of dust (N (cm^{-3})), we can rewrite,

$$\tau_V = N\sigma(a, \lambda)$$

or

$$N = \frac{\tau_V}{\sigma(a, \lambda)} \ pc^{-2}$$

The dust mass surface density, $\Sigma_{(M_\odot \ pc^{-2})}$ can be written as :

$$\Sigma_{(M_\odot \ pc^{-2})} = m_d \frac{\tau_V}{\sigma(a, \lambda)}$$

A.5 K Light like Nova Distribution

This following program generates the nova distribution yielding a double exponential profile for the disk and a sersic in projection for the bulge.

```
; for K light distribution model for novae
close,1,2,3,4,5, 10, 11, 12
s=12356
number=10000
nb= nint(number*41./141) ; bulge novae
```

```
nd=number-nb ; disk novae
max_bulge_rad=5.0 ; kpc
n=2.2 ; Sersic index
R_e=1.0 ; Courteau 2011
pi=acos(-1)
norm= 1/(4*pi)
M=1.
L=1.
b=1.9992*n-0.3271
p=1.0-(0.6097/n)-(0.05563/n^2)
H=0.1 ; scale height in kpc
R_h=4.71; Courteau et al 2011
pi=acos(-1)
deg=180/pi
ra_gc=266.405 ; galactic center
dec_gc=-28.9361724 ; galactic center
ra_ngp=192.85948 ; north galactic pole
dec_ngp=27.12825
l_ncp=122.9319186 ; north celestial pole
ra_m31=10.68468
dec_m31=41.26903
l_Mc=121.1744050 ; radians
b_Mc=-21.57 ; radians
D_M=785. ; Distance to M31
; cartesian coordinates of M31
Tx1=D_M*cos(l_Mc/deg)*cos(b_Mc/deg)
Ty1=D_M*sin(l_Mc/deg)*cos(b_Mc/deg)
```

```
Tz1=D_M*sin(b_Mc/deg)
Txx=Tx1/D_M
Tyy=Ty1/D_M
Tzz=Tz1/D_M
inc=(77.)/deg
; rotation angle in the cartesian coordinate system for i = 77 deg
u=atan2(-tzz*txx+(cos(inc)*sqrt(sin(inc)^2-Tyy^2)),(txx*txx-cos(inc)^2))
;center conversion of coordiantes gal to equatorial
t1_c=sin((l_ncp-l_Mc)/deg)*cos(b_Mc/deg)
t2_c=(cos(dec_ngp/deg)*sin(b_Mc/deg))-(sin(dec_ngp/deg)
*cos(b_Mc/deg)*cos((l_ncp-l_Mc)/deg))
ra_c=(deg*(atan(t1_c/t2_c)+(ra_ngp/deg)))-180.
dec_c=deg*(asin((sin(b_Mc/deg)*sin(dec_ngp/deg))+
(cos(b_Mc/deg)*cos(dec_ngp/deg)*cos((l_ncp-l_Mc)/deg))))
; ############ Disk ############
t=randomu(s,nd)*0.8
openw,1,'r_dist.txt'
for i=0, nd-1 do begin
r_in=R_h*sqrt(2.*t[i])
jump :f=1-((1+r_in/R_h)*exp(-r_in/R_h))-t[i]
f1=(r_in/R_h^2)*exp(-r_in/R_h)
r1=r_in-f/f1
a=abs(r_in-r1)
if (a le 1.e-4 and a ge 0.) then begin
print, i,r_in, r1
printf,1,r_in
endif else begin
```

```
r_in=r1
goto, jump
endelse
endfor
close,1
openr,1,'r_dist.txt'
r_in=fltarr(nd)
readf,1,r_in
print,"disk radii:", max(r_in), min(r_in)
; cylindrical
phi_d=randomu(s,nd)*2.*pi
x=r_in*cos(phi_d)
y=r_in*sin(phi_d)
z_ran=randomu(s,nd)*1.+randomu(s,nd)*(-1.)
z=H*asinh(z_ran/2)
R=sqrt(x^2+y^2+z^2)
x_sr=cos(u)*x+sin(u)*z
y_sr=y
z_sr=-sin(u)*x+cos(u)*z
; shift to M31
x_Mc=Tx1+x_sr
y_Mc=Ty1+y_sr
z_Mc=Tz1+z_sr
R_Mc=sqrt(x_Mc^2+y_Mc^2+z_Mc^2)
theta_Mc=acos(z_Mc/R_Mc)
phi_Mc=atan2(y_Mc,x_Mc)
```

```
l_M=(phi_Mc)*deg
b_M=(pi/2-theta_Mc)*deg

; l and b for disk to ra and cdec
t1=sin((l_ncp-l_M)/deg)*cos(b_M/deg)
t2=(cos(dec_ngp/deg)*sin(b_M/deg))-(sin(dec_ngp/deg)
*cos(b_M/deg)*cos((l_ncp-l_M)/deg))
;calculate ra and dec from l and b in 2000

ra=(deg*(atan(t1/t2)+(ra_ngp/deg)))-180.
dec=deg*(asin((sin(b_M/deg)*sin(dec_ngp/deg))+
(cos(b_M/deg)*cos(dec_ngp/deg)*cos((l_ncp-l_M)/deg))))


v=42./deg ; position angle rotation
netra=(ra-ra_c)/deg;for radians
netdec=(dec-dec_c)/deg
; counterclockwise
ra_rot=cos(v)*(netra)+sin(v)*(netdec)
dec_rot=-sin(v)*(netra)+cos(v)*(netdec)
ra_n=ra_rot*deg+ra_c ; this is in degrees
dec_n=dec_rot*deg+dec_c ; this is in degrees

; Recalculating the l and b coordinates
glactc, ra_n,dec_n,2000,l_m,b_m, 1,/degree
glactc, rab_n,decb_n,2000,lb_m,bb_m, 1,/degree
```

```
;################ Sersic Bulge ###################
;openw,1, "function-lookup.txt"
openw, 12, "lookuptable.txt"
ss=n*(3-p)
r_s=randomu(s,nb)*max_bulge_rad
xx=b*(r_s/R_e)^(1/n); xx= r_ss
r_uni=igamma(ss, xx)
; uniform distrbution corresponding to the r_s values.
;this relation is used to obtain the r_s required values
; from a uniform distribution i.e. u_cdf
; uniform distribution to fetch values for r_s
; by looking at the relation between r_s and r_uni
u_cdf=randomu(s, nb)*1.0
norm_r_uni=r_uni/max(r_uni)
printf,12, " k,   index, norm_r_uni[index], u_cdf[k], r_s  error"
for k=0, nb-1 do begin
index=closest(norm_r_uni, u_cdf[k])
error=abs(u_cdf[k]-norm_r_uni[index])
printf,12, k,index, norm_r_uni[index], u_cdf[k], r_s[index], error
endfor
close, 12
file=rd_tfile('lookuptable.txt', /auto,/convert, /nocomment)
print, "error values :", max(file(5,*)), min(file(5,*))
rb_in=file(4,*)
rb_in=reform(rb_in)
```

```
; observer position
cos_theta_b=(randomu(s,nb)*2.0-1.) ; spherical
theta_b=acos(cos_theta_b)
phi_b=randomu(s,nb)*2.*pi ; spherical
print,"bulge radii:", max(rb_in), min(rb_in)

xb=rb_in*cos(phi_b)*sin(theta_b)
yb=rb_in*sin(phi_b)*sin(theta_b)
zb=rb_in*cos(theta_b)
Rb=sqrt(xb^2+yb^2+zb^2)

; rotation by u as an inclination angle
xb_sr=xb
yb_sr=cos(u)*yb-sin(u)*zb
zb_sr=sin(u)*yb+cos(u)*zb

xb_Mc=Tx1+xb_sr
yb_Mc=Ty1+yb_sr
zb_Mc=Tz1+zb_sr
Rb_Mc=sqrt(xb_Mc^2+yb_Mc^2+zb_Mc^2)
thetab_Mc=acos(zb_Mc/Rb_Mc)
phib_Mc=atan2(yb_Mc,xb_Mc)
lb_M=(phib_Mc)*deg
bb_M=(pi/2-thetab_Mc)*deg

;calculate ra and dec from l and b in 2000
tb1=sin((l_ncp-lb_M)/deg)*cos(bb_M/deg)
```

```
tb2=(cos(dec_ngp/deg)*sin(bb_M/deg))-(sin(dec_ngp/deg)
*cos(bb_M/deg)*cos((l_ncp-lb_M)/deg))
rab=(deg*(atan(tb1/tb2)+(ra_ngp/deg)))-180.
decb=deg*(asin((sin(bb_M/deg)*sin(dec_ngp/deg))+(cos(bb_M/deg)
*cos(dec_ngp/deg)*cos((l_ncp-lb_M)/deg))))
; shift to 0,0
netrab=rab-ra_c
netdecb=decb-dec_c
rab_r=cos(v)*(netrab)-sin(v)*(netdecb)
decb_r=sin(v)*(netrab)+cos(v)*(netdecb)
; final ra -dec plane
rab_n=rab_r+ra_c
decb_n=decb_r+dec_c
openw,2,'nova_pos.txt'
for i=0,n_elements(x_Mc)-1 do begin
printf,2,x[i],y[i],z[i],l_m[i], b_m[i]
endfor
close,2
openw,3,'nova_pos_b.txt'
for j=0,n_elements(xb)-1 do begin
printf,3,xb[j],yb[j],zb[j],lb_m[j],bb_m[j]
endfor
close,3
end
```

A.6 Uniform Nova Distribution

This program generates a nova distribution distributed uniformally in the cylindrical disk and spherically symmetric bulge

```
; Same parameters as in the previous program ;
;Uniform disk
t=randomu(s,nd)*100.
r_in=sqrt(2.*t)
print,"disk radii:", max(r_in), min(r_in)
phi_d=randomu(s,nd)*2.*pi ; cylindrical
x=r_in*cos(phi_d)
y=r_in*sin(phi_d)
z=randomu(s,nd)*0.5+randomu(s,nd)*(-0.5)
R=sqrt(x^2+y^2+z^2)


x_sr=cos(u)*x+sin(u)*z
y_sr=y
z_sr=-sin(u)*x+cos(u)*z
; shift to M31
x_Mc=Tx1+x_sr
y_Mc=Ty1+y_sr
z_Mc=Tz1+z_sr
R_Mc=sqrt(x_Mc^2+y_Mc^2+z_Mc^2)
theta_Mc=acos(z_Mc/R_Mc)
phi_Mc=atan2(y_Mc,x_Mc)
l_M=(phi_Mc)*deg
b_M=(pi/2-theta_Mc)*deg
```

```
; Convert from l and b for disk to ra and cdec
ra=(deg*(atan(t1/t2)+(ra_ngp/deg)))-180.
dec=deg*(asin((sin(b_M/deg)*sin(dec_ngp/deg))
+(cos(b_M/deg)*cos(dec_ngp/deg)*cos((l_ncp-l_M)/deg))))
v=42./deg
netra=(ra-ra_c)/deg;for radians
netdec=(dec-dec_c)/deg
; counterclockwise
ra_rot=cos(v)*(netra)+sin(v)*(netdec)
dec_rot=-sin(v)*(netra)+cos(v)*(netdec)
ra_n=ra_rot*deg+ra_c ; this is in degrees
dec_n=dec_rot*deg+dec_c ; this is in degrees
;Spherically Symmetric Bulge ;
rb_in=sqrt(2.*randomu(s,nb)*12.)
; observer position
cos_theta_b=randomu(s,nb)*2.-1
phi_b=randomu(s,nb)*2.*pi ; spherical
theta_b=acos(cos_theta_b)
xb=rb_in*cos(phi_b)*sin(theta_b)
yb=rb_in*sin(phi_b)*sin(theta_b)
zb=rb_in*cos(theta_b)
Rb=sqrt(xb^2+yb^2+zb^2)
; rotation by u as an inclination angle
xb_sr=xb
yb_sr=cos(u)*yb-sin(u)*zb
zb_sr=sin(u)*yb+cos(u)*zb
; translate to M31
```

```
xb_Mc=Tx1+xb_sr
yb_Mc=Ty1+yb_sr
zb_Mc=Tz1+zb_sr
Rb_Mc=sqrt(xb_Mc^2+yb_Mc^2+zb_Mc^2)
thetab_Mc=acos(zb_Mc/Rb_Mc)
phib_Mc=atan2(yb_Mc,xb_Mc)
lb_M=(phib_Mc)*deg
bb_M=(pi/2-thetab_Mc)*deg
;calculate ra and dec from l and b in 2000
rab=(deg*(atan(tb1/tb2)+(ra_ngp/deg)))-180.
decb=deg*(asin((sin(bb_M/deg)*sin(dec_ngp/deg))
+(cos(bb_M/deg)*cos(dec_ngp/deg)*cos((l_ncp-lb_M)/deg))))
; shift to 0,0
netrab=rab-ra_c
netdecb=decb-dec_c
rab_r=cos(v)*(netrab)-sin(v)*(netdecb)
decb_r=sin(v)*(netrab)+cos(v)*(netdecb)
rab_n=rab_r+ra_c
decb_n=decb_r+dec_c
glactc, ra_n,dec_n,2000,l_m,b_m, 1,/degree
glactc, rab_n,decb_n,2000,lb_m,bb_m, 1,/degree
openw,3,'nova_pos_b.txt'
for j=0,n_elements(xb)-1 do begin
printf,3,xb[j],yb[j],zb[j],lb_m[j],bb_m[j]
endfor
close,3
end
```

Appendix B Milky Way vs Andromeda

Table B.1. Milky Way vs Andromeda Comparison

Parameter	Milky Way	Reference	Andromeda	Reference
Global Properties				
Hubble Type	SbI-II	van den Bergh (1999)	SbI-II	van den Bergh (1999)
Total Mass $(10^{10} M_{\odot})$	5.0	Hammer et al. (2007)	5.9-8.7	Yin et al. (2009a)
K Luminosity $(10^{10} L_{K\odot})$	5.5	Kent et al. (1991)	$\sim$ 18.5	Shafter et al. (2000)
Nova Rate (yr^{-1})	35	Shafter (2002)	50	Shafter and Irby (2001)
Bulge Properties				
Stellar Mass $(10^{10} M_{\odot})$	1-2	Dehnen and Binney (1998)	3.2	Geehan et al. (2006)
Radius (kpc)	2.5	Yin et al. (2009a)	5	Courteau et al. (2011)
Disk Properties				
Scalelength				
R	2.3	Hammer et al. (2007)	5.3	Courteau et al. (2011)
K	2.3 - 2.8	Freudenreich (1998)	4.7	Courteau et al. (2011)
Total Mass $(10^{10} M_{\odot})$	3.7	Hammer et al. (2007)	$\sim$ 7	Klypin et al. (2002); Widrow et al. (2003)

Table B.1 (cont'd)

Parameter	Milky Way	Reference	Andromeda	Reference
Gas Mass ($10^{10} M_\odot$)	0.7	Yin et al. (2009a)	0.6	Yin et al. (2009a)
Stellar Mass ($10^{10} M_\odot$)	3	Zheng et al. (2001)	~ 6	Tamm et al. (2007)
SFR ($M_\odot/yr$)	3	Boissier and Prantzos (1999)	0.4	Barmby et al. (2006)
Dust Properties				
Dust Mass ($10^7 M_\odot$)	~ 60	Yin et al. (2009b)	4-5.4	Draine et al. (2014); Gordon et al. (2006)
Dust to Gas Ratio	0.01		0.005 - 0.026	Draine et al. (2014)
Disk Scale Length	2.26 kpc	Drimmel and Spergel (2001)	...	...
Disk Scale Height	134 pc	Drimmel and Spergel (2001)	...	...
Spiral Arm's Width	...	...	1.0-2.0	Ryden and Stark (1986)

Appendix C Kolmogorov Smirnov Test

It is non-parametric[1] statistical test to compare two datasets or a dataset to a theoretical distribution. The former case is called the 2-sample KS test and the latter one is known as the 1-sample KS test or KS-goodness of fit test. Andrey Nikolaevich Kolmogorov (1933) invented the goodness of fit test, while the two sample test was established by Vladimir Ivanovich Smirnov (1939). This test is applicable to any unbinned distribution which is a function of only one independent variable. It is based on the $null\ hypothesis$, H_0, which holds true if an unknown distribution, X is equal to another distribution (or function), Y. The alternative hypothesis, H_1 holds true if X $\neq$ Y.

C.1 The 1-Sample KS test

Suppose a set of N data points are located at x_i (i=1,..N), then S_N(x) represents the fraction of data points, which are placed at values $\leq$ x. In other words, this function would demonstrate the cumulative distribution of the given data. This function is plotted in Fig. C.1. This sample is then compared with a given theoretical distribution, Q(x), such that P(x) represents its cumulative distribution function. The K-S statistic is calculated based on the maximum distance between these two distributions:

$$D_N = max|S_N(x) - P(x)|$$

The significance of this calculated D is provided by a monotonic function (Press et al., 2007):

$$Q_{KS}(\lambda) = 2\Sigma_{j=1}^{\infty}(-1)^{j-1}e^{-2j^2\lambda^2}$$

[1] does not assume any underlying distribution for the data

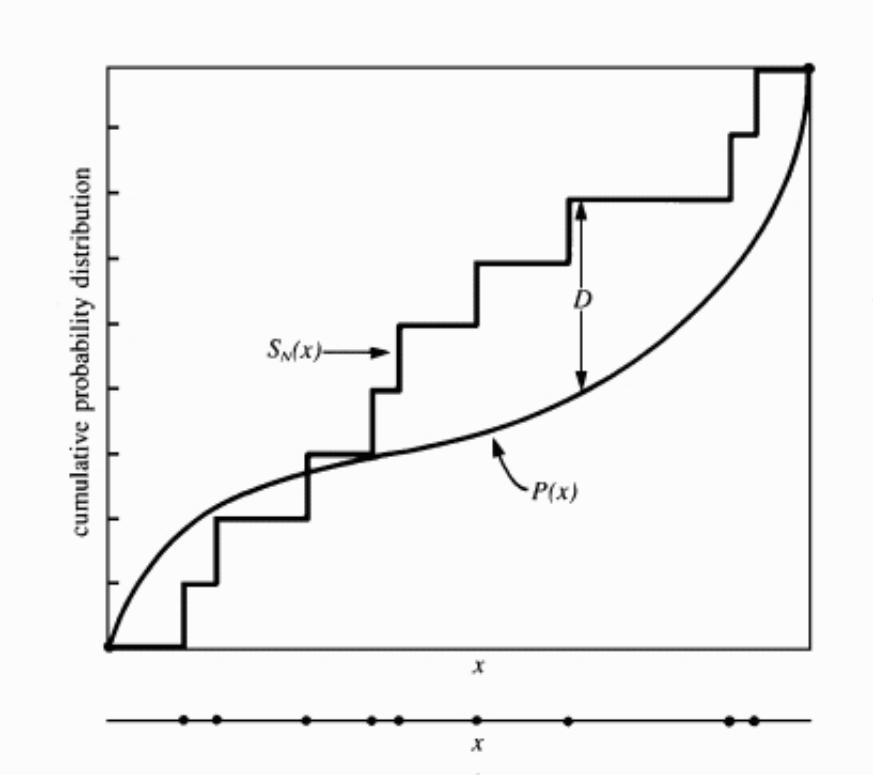

Figure C.1 The cumulative distribution (S_N(x)) for an unknown distribution with 9 data points (shown as dots under the x axis) is plotted against a theoretical distribution, whose CDF is given by P(x). The CDF of the unknown data is stepped up at every known data point. D is the greatest distance between the two distributions. (Adapted from Press et al. (2007))

such that $Q_{KS}(0) = 1$ and $Q_{KS}(\infty) = 0$. Based on this function, the probability that the distributions are different is given by:

$$p(D > D_{obs}) = Q_{KS}(\sqrt{N}D)$$

C.2 The 2-Sample KS test

This test was developed by Smirnov (1939) to compare two samples of size N1 and N2, by calculating the maximum difference between their CDFs as given below:

$$D_{N1,N2} = max|S_{N1}(x) - S_{N2}(x)|$$

The probability in the 2-sample case is provided by :

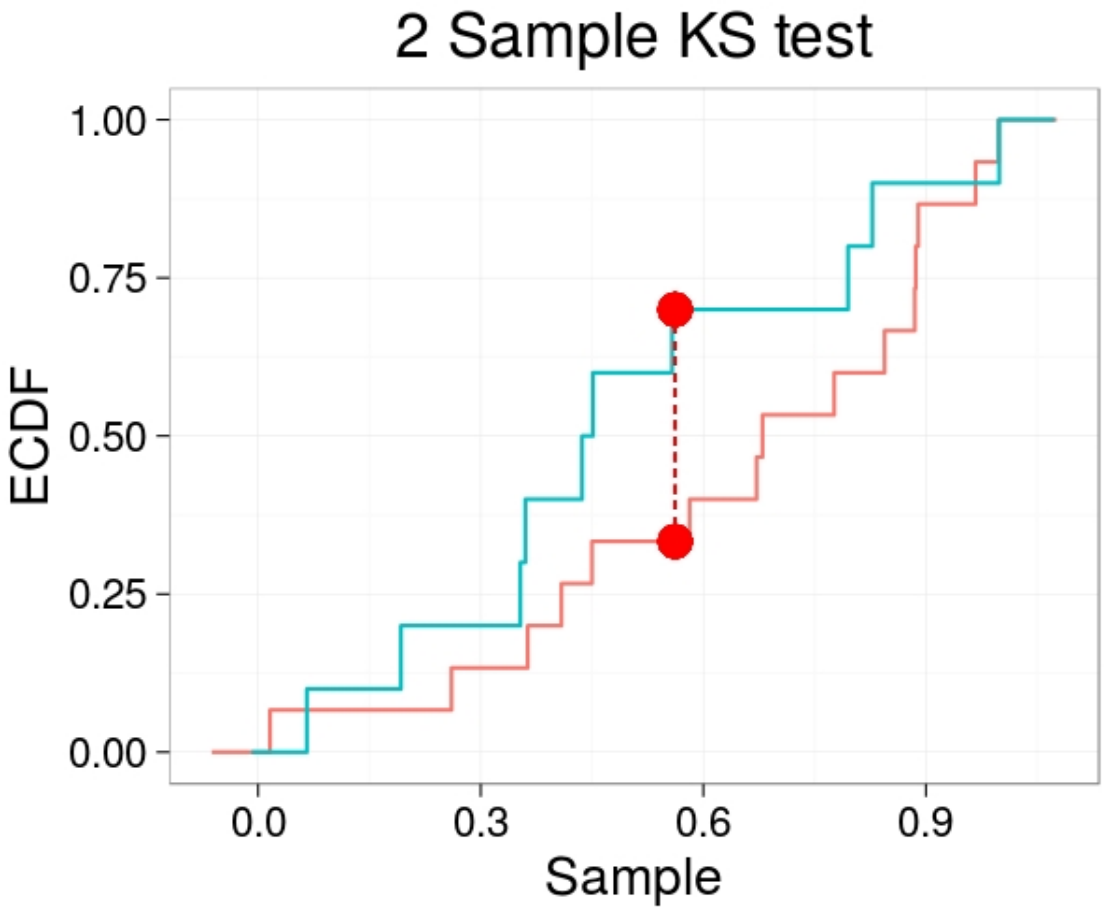

Figure C.2 The cumulative distribution ($S_{N1}(x)$) for an unknown distribution is plotted against another CDF, $S_{N1}(x)$. D is the greatest distance between the plotted data.

$$p(D > D_{obs}) = Q_{KS}(\sqrt{\frac{N1N2}{N1+N2}}D)$$

In the context of this work, we employed the `ks.test` routine from R[2].

[2]https://www.r-project.org/

Appendix D Observational Projects

D.1 The First Ultraluminous X-Ray Source in M31

Ultraluminous X-ray sources (ULXs) are associated with X-ray binaries, in which the accreting black hole displays X-ray luminosities greater than 10^{39} erg/s. The nature of the companion star and the accretion rate is not established yet. In particular, whether or not the accretion is super/sub Eddington is a mystery. Using the data obtained with XMM-Newton[D.1], $Swift-$XRT[D.2] and Chandra-HRC-I [D.3], we inferred that the underlying source for this ULX is a 13 $M_{\odot}$ black hole under the assumption that it is non-spinning. This details of this work can be found in Kaur et al. (2012).

We also constructed a simple disk plus bulge model to test its association with starlight and used IR images from Spitzer Space Telescope[D.4] to investigate its possible link to star formation. The combined study of X-ray properties and the spatial distribution suggested stellar mass black hole accreting at near Eddington rates from a high mass companion. The details of this work can be found in Kaur (2012).

D.2 Photometric Redshift Determinations for Fermi BL Lacs with Swift and GROND

Blazars represent a class of active galactic nuclei (AGNs) with the relativistic jets pointing along our line of sight (Blandford and Rees, 1978). Based on their optical spectra, they can be divided into two types : Flat Spectrum Radio Quasars (FSRQs), characterized by broad emission lines and BL Lacertae objects (BL Lacs), with no emission lines or narrow lines with equivalent width < 5 Å(Urry and Padovani, 1995). In this project, we

[D.1] http://sci.esa.int/xmm-newton/
[D.2] https://www.swift.psu.edu/xrt/
[D.3] http://cxc.harvard.edu/index.html
[D.4] http://www.spitzer.caltech.edu/

observed 25 BL Lacs discovered by Fermi-LAT[D.5] to determine their photometric redshifts using the $Swift$-UVOT and a 7 color imager, GROND at 2.2 m MPI [D.6] telescope, Chile. We found 5 high-z (z $>$ 1.3) sources, which would make a significant contribution to the existing extremely small sample of high-redshift BL Lacs, since only 16 BL Lacs with z $>$ 1.3 are known till date. This work utilizes the technique established by Rau et al. (2012) to calculate the photometric redshifts. The results of this work would be published in near future.

D.3 Cataclysmic Variables Observations with MDM

We employed 2.4 m Hiltner telescope, MDM observatory at Kitt Peak to obtain the spectroscopic (OSMOS[D.7]) and photometric observations of 19 new cataclysmic variables, which included supernovae, dwarf novae, AM CVns, Nova Like variables over a time period of 10 observing nights. This work was conducted under the guidance of Dr. R. M. Wagner (LBTO[D.8]) and Dr. Sumner Starrfield, Arizona State University. The details of these observations will be published in the near future.

D.4 Observations with SARA and WIYN

We obtained optical observations for GRB 130427A with 0.9 m SARA-N[D.9] telescope in 2013 and GRB 140423A with 3.5 m pODI/WIYN[D.10] telescope in 2014 and reported the results of our photometry in the Astronomer Telegrams. A recurrent nova in M31 (M31N 1963-09c) was observed with SARA-N in 2015 in the multi-band optical photometric observations. Another recurrent nova in the Local Magellanic Cloud, LMCN 1968-12a

[D.5] http://fermi.gsfc.nasa.gov/
[D.6] https://www.eso.org/sci/facilities/lasilla/telescopes/national/2p2.html
[D.7] http://www.astronomy.ohio-state.edu/MDM/OSMOS/
[D.8] http://www.lbto.org/
[D.9] http://saraobservatory.org/
[D.10] http://www.noao.edu/wiyn/ODI/

was followed up with 0.6m SARA-CT, Cerro Tololo, Chile. The photometric results of all these observations were reported in the Astronomer Telegram.

D.5 Refereed Journal Publications

The list of my publications with 49 total citations is as follows :

2016 BVRI photometry of the recurrent nova LMCN 1968-12a during the 2016 eruption with the SARA-CT telescope (A. Kaur, T. C. Hillwig, W. C. Keel, G. D. Henson, D. H. Hartmann, S. Starrfield, R. M. Wagner), *In The Astronomer's Telegram*, volume 8626, 2016.

2016 Ultraviolet, Optical and near-infrared photometric follow up of the transient source Fermi J1654-1055 with GROND and Swift-UVOT (A. Kaur, J. Bolmer, J. Greiner, A. Rau, P. Schady, M. Ajello, D. H. Hartmann), *In The Astronomer's Telegram*, volume 8743, 2016.

2015 Additional BVRI photometry of the recurrent nova M31N 1963-09c during the 2015 eruption (A. Kaur, M. Henze, W. C. Keel, D. H. Hartmann), *In The Astronomer's Telegram*, volume 8243, 2015.

2014 Identification of a New Candidate Outbursting AM CVn System from ASAS-SN (R. M. Wagner, A. Kaur, A. Porter, A. Wilber, C. E. Woodward, S. G. Starrfield, D. H. Hartmann, A. B. Davis, T. W.-S. Holoien, G. Simonian, K. Z. Stanek, C. S. Kochanek, B. J. Shappee, J. L. Prieto), *In The Astronomer's Telegram*, volume 6669, 2014.

2014 M 31 novae M31N 2012-06a and M31N 2014-02a detected in X-rays with XMM-Newton (M. Henze, R. Sturm, J.-U. Ness, J. Greiner, M. Della Valle, G. Sala, M. Her-

nanz, A. W. Shafter, K. Hornoch, M. Orio, D. H. Hartmann, A. Kaur, D. Hatzidimitriou, M. Middleton), *In The Astronomer's Telegram*, volume 6564, 2014.

2014 Spectroscopic Confirmation of Recent ASAS-SN Transients as Cataclysmic Variable Stars (A. Kaur, A. Porter, A. Wilber, R. M. Wagner, C. E. Woodward, S. G. Starrfield, D. H. Hartmann), *In The Astronomer's Telegram*, volume 6624, 2014.

2014 Spectroscopic Classification of ASASSN-14bf and ASASSN-14ca (J. L. Prieto, A. Porter, A. Kaur, A. Wilber, B. J. Shappee, T. W.-S. Holoien, K. Z. Stanek, C. S. Kochanek, A. B. Davis, J. Jencson, U. Basu, J. F. Beacom, D. Szczygiel, G. Pojmanski, J. Brimacombe, D. Bersier, C. E. Woodward, S. G. Starrfield, D. Hartmann), *In The Astronomer's Telegram*, volume 6249, 2014.

2014 ASAS-SN Discovery and Spectroscopic Classification of a Type Ia Supernova in SDSS J130814.58+620201.2 (T. W.-S. Holoien, R. M. Wagner, A. Kaur, A. Porter, A. Wilber, J. L. Prieto, B. J. Shappee, A. B. Davis, K. Z. Stanek, C. S. Kochanek, J. Jencson, U. Basu, J. F. Beacom, D. Szczygiel, G. Pojmanski, J. Brimacombe, D. Bersier, C. E. Woodward, S. G. Starrfield, D. Hartman), *In The Astronomer's Telegram*, volume 6219, 2014.

2014 ASAS-SN Discovery and Spectroscopic classification of Two Supernovae in UGC 05566 and SDSS J111840.97+250958.5 (A. B. Davis, R. M. Wagner, A. Kaur, A. Porter, A. Wilber, J. L. Prieto, T. W.-S. Holoien, B. J. Shappee, K. Z. Stanek, C. S. Kochanek, J. Jencson, U. Basu, J. F. Beacom, D. Szczygiel, G. Pojmanski, J. Brimacombe, D. Bersier, C. E. Woodward, S. G. Starrfield, D. Hartman), *In The Astronomer's Telegram*, volume 6196, 2014.

2014 Spectroscopic Classification of ASASSN-14bd (R. M. Wagner, A. Kaur, A. Porter, A. Wilber, J. L. Prieto, T. W.-S. Holoien, B. J. Shappee, K. Z. Stanek, C. S. Kochanek,

A. B. Davis, J. Jencson, U. Basu, J. F. Beacom, D. Szczygiel, G. Pojmanski, J. Brimacombe, D. Bersier, C. E. Woodward, S. G. Starrfield, D. Hartmann), *In The Astronomer's Telegram*, volume 6203, 2014.

2014 Spectroscopic Confirmation of ASASSN-14bq and ASASSN-14br as Cataclysmic Variable Stars (A. Wilber, A. Kaur, A. Porter, R. M. Wagner, C. E. Woodward, S. G. Starrfield, D. Hartmann), *In The Astronomer's Telegram*, volume 6275, 2014.

2014 GRB 140423A Third epoch pODI photometry. (D. Harbeck, A. Kaur, A. Delgado-Navarro, M. Orio, D. H. Hartmann), *In GRB Coordinates Network*, volume 16175, 2014.

2014 GRB 140423A pODI/WIYN afterglow photometry. (D. Harbeck, A. Kaur, A. Delgado-Navarro, M. Orio, D. H. Hartmann), *In GRB Coordinates Network*, volume 16165, 2014.

2014 GRB 140423A optical observations with pODI/WIYN at KPNO. (A. Kaur, A. Delgado-Navarro, D. Harbeck, M. Riabokin, M. Orio, D. H. Hartmann), *In GRB Coordinates Network*, volume 16144, 2014.

2013 H-alpha Confirmation of Nova Candidates in M31 (K. Hornoch, M. Orio, A. Kaur), *In The Astronomer's Telegram*, volume 5099, 2013.

2013 GRB 130427A: SARA-N optical observations. (A. Kaur, D. Hartmann, W. C. Keel), *In GRB Coordinates Network*, volume 14523, 2013.

2013 GRB 130427A: SARA-N detection. (W. C. Keel, D. Hartmann, A. Kaur), *In GRB Coordinates Network*, volume 14507, 2013.

2012 CXOM31 J004253.1+411422: the first ultraluminous X-ray transient in M 31 (A. Kaur, M. Henze, F. Haberl, W. Pietsch, J. Greiner, A. Rau, D. H. Hartmann, G.

Sala, M. Hernanz), *Astronomy and Astrophysics*, volume 538, pp. A49, 2012.

2011 Discovery and Follow-up of a Nearby Galaxy from the Arecibo Zone of Avoidance Survey (T. P. McIntyre, R. F. Minchin, E. Momjian, P. A. Henning, A. Kaur, B. Parton), *The Astrophysical Journal*, volume 739, pp. L26, 2011.

2011 Three new optical nova candidates in M 31 (W. Pietsch, M. Henze, V. Burwitz, A. Kaur, D. H. Hartmann, G. Williams, P. Milne), *In The Astronomer's Telegram*, volume 3409, 2011.

2011 New optical nova candidate in the outer disk of M 31 (W. Pietsch, M. Henze, V. Burwitz, A. Kaur, D. H. Hartmann, P. Milne, G. Williams), *In The Astronomer's Telegram*, volume 3175, 2011.

2011 Nova in M31: M31N 2011-01a (M. Henze, W. Pietsch, V. Burwitz, A. Kaur, D. H. Hartmann, P. Milne, G. Williams), *In Central Bureau Electronic Telegram*, volume 2631, 2011.

2010 New optical nova candidate in M 31 (W. Pietsch, M. Henze, V. Burwitz, A. Kaur, D. H. Hartmann, P. Milne, G. Williams), *In The Astronomer's Telegram*, volume 3076, 2010.

2010 Apparent Nova in M31: M31N 2010-12b (W. Pietsch, M. Henze, V. Burwitz, A. Kaur, D. H. Hartmann, P. Milne, G. Williams), *In Central Bureau Electronic Telegrams*, volume 2582, 2010.

2010 Apparent nova in M31: M31N 2010-12b. (W. Pietsch, M. Henze, V. Burwitz, A. Kaur, D. H. Hartmann, P. Milne, G. Williams), *In Central Bureau Electronic Telegrams*, volume 2582, pp. 2, 2010.

2010 M31N 1963-09c - Fourth recorded outburst of a recurrent nova in M 31 or a foreground U Gem system? (W. Pietsch, M. Henze, V. Burwitz, A. Kaur, D. H. Hartmann, P. Milne, G. Williams), *In The Astronomer's Telegram*, volume 3001, 2010.

2010 Supersoft X-ray transient leads to the discovery of the second optical nova in a M 31 globular cluster (M. Henze, W. Pietsch, V. Burwitz, J. Lloyd, K. Hornoch, K. Nishiyama, F. Kabashima, A. Kaur, D. H. Hartmann, P. Milne, G. Williams), *In The Astronomer's Telegram*, volume 3019, 2010.

2009 Optical Spectroscopy of the M31 nova M31N-2009-10b (F. Di Mille, S. Ciroi, H. Navasardyan, S. Lepine, L. von Zee, K. L. Barnes, D. H. Hartmann, S. D. Brittain, A. C. Updike, A. Kaur, G. G. Williams, W. Pietsch, A. Siviero, T. Saguner, M. Orio, P. Rafanelli, A. Bianchini), *In The Astronomer's Telegram*, volume 2248, 2009.

2009 Supernova 2009P in Pgc 34730 (U. K. Gurugubelli, G. C. Anupama, D. K. Sahu, A. Kaur), *In Central Bureau Electronic Telegrams*, volume 1687, 2009.

2008 Supernova 2008in in M61 (S. Chakraborti, T. Prabhu, G. C. Anupama, A. Kaur, G. Uday Kumar, A. Ray), *In Central Bureau Electronic Telegrams*, volume 1638, 2008.

Bibliography

Arp, H. C. (1956). Novae in the Andromeda nebula. *The Astronomical Journal*, 61:15.

Baade, W. and Zwicky, F. (1934). On Super-Novae. *Proceedings of the National Academy of Sciences*, 20(5):254–259.

Barmby, P., Ashby, M. L. N., Bianchi, L., Engelbracht, C. W., Gehrz, R. D., Gordon, K. D., Hinz, J. L., Huchra, J. P., Humphreys, R. M., Pahre, M. A., Pérez-González, P. G., Polomski, E. F., Rieke, G. H., Thilker, D. A., Willner, S. P., and Woodward, C. E. (2006). Dusty Waves on a Starry Sea: The Mid-Infrared View of M31. *The Astrophysical Journal*, 650(1):L45–L49.

Blandford, R. D. and Rees, M. J. (1978). Extended and Compact Extragalactic Radio Sources: Interpretation and Theory. *Physica Scripta*, 17(3):265–274.

Bode, M. (2010). The outbursts of classical and recurrent novae. *Astronomische Nachrichten*, 331(2):160–168.

Bode, . and Evans, . (2008). Classical Novae. *Classical Novae*.

Bohren, . and Huffman, . (1983). Absorption and scattering of light by small particles. *New York: Wiley*.

Boissier, S. and Prantzos, N. (1999). Chemo-spectrophotometric evolution of spiral galaxies – I. The model and the Milky Way. *Monthly Notices of the Royal Astronomical Society*, 307(4):857–876.

Capaccioli, M., della Valle, M., Rosino, L., and D'Onofrio, M. (1989). Properties of the nova population in M31. *The Astronomical Journal*, 97:1622.

Chen, H.-L., Woods, T. E., Yungelson, L. R., Gilfanov, M., and Han, Z. (2016). Modelling nova populations in galaxies. *Monthly Notices of the Royal Astronomical Society*, 458(3):2916–2927.

Ciardullo, R., Ford, H. C., Neill, J. D., Jacoby, G. H., and Shafter, A. W. (1987). The spatial distribution and population of novae in M31. *The Astrophysical Journal*, 318:520.

Ciardullo, R., Shafter, A. W., Ford, H. C., Neill, J. D., Shara, M. M., and Tomaney, A. B. (1990). The H-alpha light curves of novae in M31. *The Astrophysical Journal*, 356:472.

Courteau, S., Widrow, L. M., McDonald, M., Guhathakurta, P., Gilbert, K. M., Zhu, Y., Beaton, R. L., and Majewski, S. R. (2011). THE LUMINOSITY PROFILE AND STRUCTURAL PARAMETERS OF THE ANDROMEDA GALAXY. *The Astrophysical Journal*, 739(1):20.

Dalcanton, J. J., Fouesneau, M., Hogg, D. W., Lang, D., Leroy, A. K., Gordon, K. D., Sandstrom, K., Weisz, D. R., Williams, B. F., Bell, E. F., Dong, H., Gilbert, K. M., Gouliermis, D. A., Guhathakurta, P., Lauer, T. R., Schruba, A., Seth, A. C., and Skillman, E. D. (2015). THE PANCHROMATIC HUBBLE ANDROMEDA TREASURY. VIII. A WIDE-AREA, HIGH-RESOLUTION MAP OF DUST EXTINCTION IN M31. *The Astrophysical Journal*, 814(1):3.

Darnley, M. J., Bode, M. F., Kerins, E., Newsam, A. M., An, J., Baillon, P., Belokurov, V., Novati, S. C., Carr, B. J., Creze, M., Evans, N. W., Giraud-Heraud, Y., Gould, A., Hewett, P., Jetzer, P., Kaplan, J., Paulin-Henriksson, S., Smartt, S. J., Tsapras, Y., and Weston, M. (2006). Classical novae from the POINT-AGAPE microlensing survey of M31 - II. Rate and statistical characteristics of the nova population. *Monthly Notices of the Royal Astronomical Society*, 369(1):257–271.

Dehnen, W. and Binney, J. (1998). Mass models of the Milky Way. *Monthly Notices of the Royal Astronomical Society*, 294(3):429–438.

Della Valle, M. and Livio, M. (1998). The Spectroscopic Differences between Disk and ThickDisk/Bulge Novae. *The Astrophysical Journal*, 506(2):818–823.

della Valle, M., Rosino, L., Bianchini, A., and Livio, M. (1994). The nova rate in galaxies of different Hubble types. *Astronomy and Astrophysics (ISSN 0004-6361)*, 287:403–409.

Downes, R. A. and Shara, M. M. (1993). A catalog and atlas of cataclysmic variables. *Publications of the Astronomical Society of the Pacific*, 105:127.

Downes, R. A., Webbink, R. F., Shara, M. M., Ritter, H., Kolb, U., and Duerbeck, H. W. (2001). A Catalog and Atlas of Cataclysmic Variables: The Living Edition. *Publications of the Astronomical Society of the Pacific*, 113(784):764–768.

Draine, B. T. (1985). Tabulated optical properties of graphite and silicate grains. *The Astrophysical Journal Supplement Series*, 57:587.

Draine, B. T., Aniano, G., Krause, O., Groves, B., Sandstrom, K., Braun, R., Leroy, A., Klaas, U., Linz, H., Rix, H.-W., Schinnerer, E., Schmiedeke, A., and Walter, F. (2014). ANDROMEDA'S DUST. *The Astrophysical Journal*, 780(2):172.

Draine, B. T. and Li, A. (2007). Infrared Emission from Interstellar Dust. IV. The Silicate-GraphitePAH Model in the Post Spitzer Era. *The Astrophysical Journal*, 657(2):810–837.

Drimmel, R. and Spergel, D. N. (2001). Threedimensional Structure of the Milky Way Disk: The Distribution of Stars and Dust beyond 0.35 R Ł. *The Astrophysical Journal*, 556(1):181–202.

Duerbeck, H. (1987). A reference catalogue and atlas of galactic novae. *Space Science Reviews*, 45(1-2):1–212.

Duerbeck, H. W. (1981). Light curve types, absolute magnitudes, and physical properties of galactic novae. *Publications of the Astronomical Society of the Pacific*, 93:165.

Duerbeck, H. W. (1990). *Physics of Classical Novae*, volume 369 of *Lecture Notes in Physics*. Springer Berlin Heidelberg, Berlin, Heidelberg.

Freudenreich, H. T. (1998). A COBE Model of the Galactic Bar and Disk. *The Astrophysical Journal*, 492(2):495–510.

Fritz, J., Gentile, G., Smith, M. W. L., Gear, W. K., Braun, R., Roman Duval, J., Bendo, G. J., Baes, M., Eales, S. A., Verstappen, J., Blommaert, J. A. D. L., Boquien, M., Boselli, A., Clements, D., Cooray, A. R., Cortese, L., De Looze, I., Ford, G. P., Galliano, F., Gomez, H. L., Gordon, K. D., Lebouteiller, V., OHalloran, B., Kirk, J., Madden, S. C., Page, M. J., Remy, A., Roussel, H., Spinoglio, L., Thilker, D., Vaccari, M., Wilson, C. D., and Waelkens, C. (2012). The Herschel Exploitation of Local Galaxy Andromeda (HELGA). *Astronomy & Astrophysics*, 546:A34.

Gaposchkin, . (1957). The galactic novae. *Amsterdam*.

Geehan, J. J., Fardal, M. A., Babul, A., and Guhathakurta, P. (2006). Investigating the Andromeda stream – I. Simple analytic bulge–disc–halo model for M31. *Monthly Notices of the Royal Astronomical Society*, 366(3):996–1011.

Gordon, K. D., Bailin, J., Engelbracht, C. W., Rieke, G. H., Misselt, K. A., Latter, W. B., Young, E. T., Ashby, M. L. N., Barmby, P., Gibson, B. K., Hines, D. C., Hinz, J., Krause, O., Levine, D. A., Marleau, F. R., Noriega-Crespo, A., Stolovy, S., Thilker, D. A., and Werner, M. W. (2006). Sp i t zer MIPS Infrared Imaging of M31: Further Evidence for a Spiral-Ring Composite Structure. *The Astrophysical Journal*, 638(2):L87–L92.

Haas, M., Lemke, D., Stickel, M., Hippelein, H., Kunkel, M., Herbstmeier, U., and Mattila, K. (1998). Cold dust in the Andromeda Galaxy mapped by ISO. *Astronomy and Astrophysics*, 36:33–36.

Hachisu, I. and Kato, M. (2001). Recurrent Novae as a Progenitor System of Type Ia Supernovae. I. RS Ophiuchi Subclass: Systems with a Red Giant Companion. *The Astrophysical Journal*, 558(1):323–350.

Hagen, J. G. (1921). Die Ver{ä}nderlichen Sterne. Erster Abschnitt: Die Ausr{ü}stung des Beobachters. *Specola Astronomica Vaticana Pubblicazioni Serie Seconda*, 4.

Hammer, F., Puech, M., Chemin, L., Flores, H., and Lehnert, M. D. (2007). The Milky Way, an Exceptionally Quiet Galaxy: Implications for the Formation of Spiral Galaxies. *The Astrophysical Journal*, 662(1):322–334.

Hatano, K., Branch, D., Fisher, A., and Starrfield, S. (1997). New Insight into the Spatial Distribution of Novae in M31. *The Astrophysical Journal*, 487(1):L45–L48.

Hubble, E. P. (1929). A spiral nebula as a stellar system, Messier 31. *The Astrophysical Journal*, 69:103.

Kaur, A. (2012). Ultraluminous X-ray Sources in Andromeda Galaxy: Two Recent Discoveries and their Implications.

Kaur, A., Henze, M., Haberl, F., Pietsch, W., Greiner, J., Rau, A., Hartmann, D. H., Sala, G., and Hernanz, M. (2012). CXOM31 J004253.1+411422: the first ultraluminous X-ray transient in M 31. *Astronomy & Astrophysics*, 538:A49.

Kent, S. M., Dame, T. M., and Fazio, G. (1991). Galactic structure from the Spacelab infrared telescope. II - Luminosity models of the Milky Way. *The Astrophysical Journal*, 378:131.

Klypin, A., Zhao, H., and Somerville, R. S. (2002). ΛCDMbased Models for the Milky Way and M31. I. Dynamical Models. *The Astrophysical Journal*, 573(2):597–613.

Laor, A. and Draine, B. T. (1993). Spectroscopic constraints on the properties of dust in active galactic nuclei. *The Astrophysical Journal*, 402:441.

Lundmark, . (1927). Studies of Anagalactic Nebulae - First Paper. *Nova Acta Regiae Societatis Scientiarum Upsaliensis*.

Lundmark, . (1935). On the novae and their classification among the variable stars. *Meddelanden fran Lunds Astronomiska Observatorium Series II*, 74.

Marleau, F. R., NoriegaCrespo, A., Misselt, K. A., Gordon, K. D., Engelbracht, C. W., Rieke, G. H., Barmby, P., Willner, S. P., Mould, J., Gehrz, R. D., and Woodward, C. E. (2006). Mapping and Mass Measurement of the Cold Dust in NGC 205 with Spitzer. *The Astrophysical Journal*, 646(2):929–938.

McLaughlin, D. B. (1945). The space distribution of the novae. *The Astronomical Journal*, 51:136.

McLaughlin, D. B. (1946). An interpretation of the nova spectrum. *Publications of the American Astronomical Society*, 10:255.

McLaughlin, . (1960). The Spectra of Novae. *Stellar atmospheres. Edited by Jesse Leonard Greenstein. Supported in part by the National Science Foundation. Published by the University of Chicago Press*.

Press, W. H., Teukolsky, S. A., Vetterling, W. T., and Flannery, B. P. (2007). Numerical Recipes 3rd Edition: The Art of Scientific Computing.

Rau, A., Schady, P., Greiner, J., Salvato, M., Ajello, M., Bottacini, E., Gehrels, N., Afonso, P. M. J., Elliott, J., Filgas, R., Kann, D. A., Klose, S., Krühler, T., Nardini, M., Nicuesa Guelbenzu, A., E., F. O., Rossi, A., Sudilovsky, V., Updike, A. C., and Hartmann, D. H. (2012). BL Lacertae objects beyond redshift 1.3 UV-to-NIR photometry and photometric redshift for Fermi /LAT blazars. *Astronomy & Astrophysics*, 538:A26.

Rosino, . (1964). Novae in Messier 31 discovered and observed at Asiago from 1955 to 1963. *Annales d'Astrophysique*, 27:498–505.

Rosino, . (1973). Novae in M 31 discovered and observed at Asiago from 1963 to 1970. *Astronomy and Astrophysics Supplement*, 9.

Ryden, B. S. and Stark, A. A. (1986). Molecules in galaxies. I - CO observations in a spiral arm of M31. *The Astrophysical Journal*, 305:823.

Schlafly, E. F. and Finkbeiner, D. P. (2011). MEASURING REDDENING WITH SLOAN DIGITAL SKY SURVEY STELLAR SPECTRA AND RECALIBRATING SFD. *The Astrophysical Journal*, 737(2):103.

Sérsic, . (1963). Hydromagnetic stability of a plasma in a gravitational field. *Boletin de la Asociacion Argentina de Astronomia*, 5.

Shafter, A. W. (2002). The Galactic Nova Rate. In *AIP Conference Proceedings*, volume 637, pages 462–471. AIP.

Shafter, A. W., Ciardullo, R., and Pritchet, C. J. (2000). Novae in External Galaxies: M51, M87, and M101. *The Astrophysical Journal*, 530(1):193–206.

Shafter, A. W., Darnley, M. J., Hornoch, K., Filippenko, A. V., Bode, M. F., Ciardullo, R., Misselt, K. A., Hounsell, R. A., Chornock, R., and Matheson, T. (2011). A SPECTROSCOPIC AND PHOTOMETRIC SURVEY OF NOVAE IN M31. *The Astrophysical Journal*, 734(1):12.

Shafter, A. W. and Irby, B. K. (2001). On the Spatial Distribution, Stellar Population, and Rate of Novae in M31. *The Astrophysical Journal*, 563(2):749–767.

Shafter, ., Curtin, ., Pritchet, ., Bode, ., and Darnley, . (2014). Extragalactic Nova Populations. *Stella Novae: Past and Future Decades. ASP Conference Series*, 490.

Sharov, A. S. and Alksnis, A. (1991). Novae in M31 discovered with wide field telescopes in Crimea and Latvia. *Astrophysics and Space Science*, 180(2):273–286.

Shore, S. N. (2012). Spectroscopy of novae – a user's manual. *Bulletin of the Astronomical Society of India*.

Smirnov, N. (1939). On the deviation of the empirical distribution function. *Rec. Math.[Mathematicheskii Sbornik] NS*.

Smith, M. W. L., Eales, S. A., Gomez, H. L., Roman-Duval, J., Fritz, J., Braun, R., Baes, M., Bendo, G. J., Blommaert, J. A. D. L., Boquien, M., Boselli, A., Clements, D. L., Cooray, A. R., Cortese, L., de Looze, I., Ford, G. P., Gear, W. K., Gentile, G., Gordon, K. D., Kirk, J., Lebouteiller, V., Madden, S., Mentuch, E., OHalloran, B., Page, M. J., Schulz, B., Spinoglio, L., Verstappen, J., Wilson, C. D., and Thilker, D. A. (2012). THE HERSCHEL EXPLOITATION OF LOCAL GALAXY ANDROMEDA (HELGA). II. DUST AND GAS IN ANDROMEDA. *The Astrophysical Journal*, 756(1):40.

Snijders, ., Batt, ., Seaton, ., Blades, ., and Morton, . (1984). Nova Aquilae 1982 - A short report. *Monthly Notices of the Royal Astronomical Society (ISSN 0035-8711)*, 211.

Starrfield, S., Sparks, W. M., and Shaviv, G. (1988). A model for the 1987 outburst of the recurrent nova U Scorpii. *The Astrophysical Journal*, 325:L35.

Starrfield, S., Truran, J. W., Sparks, W. M., and Kutter, G. S. (1972). CNO Abundances and Hydrodynamic Models of the Nova Outburst. *The Astrophysical Journal*, 176:169.

Strope, R. J., Schaefer, B. E., and Henden, A. A. (2010). CATALOG OF 93 NOVA LIGHT CURVES: CLASSIFICATION AND PROPERTIES. *The Astronomical Journal*, 140(1):34–62.

Tamm, ., Tempel, ., and Tenjes, . (2007). Visible and dark matter in M31 - I. Properties of stellar components. *eprint arXiv:0707.4375*.

Terzić, B. and Graham, A. W. (2005). Density-potential pairs for spherical stellar systems with S{é}rsic light profiles and (optional) power-law cores. *Monthly Notices of the Royal Astronomical Society*, 362(1):197–212.

Urry, C. M. and Padovani, P. (1995). Unified Schemes for Radio-Loud Active Galactic Nuclei. *Publications of the Astronomical Society of the Pacific*, 107:803.

van den Bergh, S. (1999). The local group of galaxies. *Astronomy and Astrophysics Review*, 9(3-4):273–318.

Warner, . (2003). Cataclysmic Variable Stars. *Cataclysmic Variable Stars*.

Webbink, R. F., Livio, M., Truran, J. W., and Orio, M. (1987). The nature of the recurrent novae. *The Astrophysical Journal*, 314:653.

Widrow, L. M. (2008). Dynamical Models for Disk Galaxies with Triaxial Halos. *The Astrophysical Journal*, 679(2):1232–1238.

Widrow, L. M., Perrett, K. M., and Suyu, S. H. (2003). DiskBulgeHalo Models for the Andromeda Galaxy. *The Astrophysical Journal*, 588(1):311–325.

Williams, R. (2012). ORIGIN OF THE He/N AND Fe II SPECTRAL CLASSES OF NOVAE. *The Astronomical Journal*, 144(4):98.

Williams, R. E. (1992). The formation of novae spectra. *The Astronomical Journal*, 104:725.

Williams, R. E., Hamuy, M., Phillips, M. M., Heathcote, S. R., Wells, L., and Navarrete, M. (1991). The evolution and classification of postoutburst novae spectra. *The Astrophysical Journal*, 376:721.

Williams, S. J. and Shafter, A. W. (2004). On the Nova Rate in M33. *The Astrophysical Journal*, 612(2):867–876.

Xu, C. and Helou, G. (1996). High-Resolution IRAS Maps and Infrared Emission of M31. II. Diffuse Component and Interstellar Dust. *The Astrophysical Journal*, 456:163.

Yaron, O., Prialnik, D., Shara, M. M., and Kovetz, A. (2005). An Extended Grid of Nova Models. II. The Parameter Space of Nova Outbursts. *The Astrophysical Journal*, 623(1):398–410.

Yin, J., Hou, J. L., Prantzos, N., Boissier, S., Chang, R. X., Shen, S. Y., and Zhang, B. (2009a). Milky Way versus Andromeda: a tale of two disks. *Astronomy and Astrophysics*, 505(2):497–508.

Yin, J., Hou, J. L., Prantzos, N., Boissier, S., Chang, R. X., Shen, S. Y., and Zhang, B. (2009b). Milky Way versus Andromeda: a tale of two disks. *Astronomy and Astrophysics*, 505(2):497–508.

Yungelson, L., Livio, M., and Tutukov, A. (1997). On The Rate of Novae in Galaxies of Different Types. *The Astrophysical Journal*, 481(1):127–131.

Zheng, Z., Flynn, C., Gould, A., Bahcall, J. N., and Salim, S. (2001). M Dwarfs from Hubble Space Telescope Star Counts. IV. *The Astrophysical Journal*, 555(1):393–404.

Zwicky, F. (1936). Life-Luminosity Relation for Novae. *Publications of the Astronomical Society of the Pacific*, 48:191.